

Chain mobility in polymer systems : on the borderline between solid and melt

Citation for published version (APA):

Kurelec, L. (2001). *Chain mobility in polymer systems : on the borderline between solid and melt*. [Phd Thesis 1 (Research TU/e / Graduation TU/e), Chemical Engineering and Chemistry]. Technische Universiteit Eindhoven. <https://doi.org/10.6100/IR548856>

DOI:

[10.6100/IR548856](https://doi.org/10.6100/IR548856)

Document status and date:

Published: 01/01/2001

Document Version:

Publisher's PDF, also known as Version of Record (includes final page, issue and volume numbers)

Please check the document version of this publication:

- A submitted manuscript is the version of the article upon submission and before peer-review. There can be important differences between the submitted version and the official published version of record. People interested in the research are advised to contact the author for the final version of the publication, or visit the DOI to the publisher's website.
- The final author version and the galley proof are versions of the publication after peer review.
- The final published version features the final layout of the paper including the volume, issue and page numbers.

[Link to publication](#)

General rights

Copyright and moral rights for the publications made accessible in the public portal are retained by the authors and/or other copyright owners and it is a condition of accessing publications that users recognise and abide by the legal requirements associated with these rights.

- Users may download and print one copy of any publication from the public portal for the purpose of private study or research.
- You may not further distribute the material or use it for any profit-making activity or commercial gain
- You may freely distribute the URL identifying the publication in the public portal.

If the publication is distributed under the terms of Article 25fa of the Dutch Copyright Act, indicated by the "Taverne" license above, please follow below link for the End User Agreement:

www.tue.nl/taverne

Take down policy

If you believe that this document breaches copyright please contact us at:

openaccess@tue.nl

providing details and we will investigate your claim.

**Chain Mobility in Polymer Systems;
On the Borderline between Solid and Melt**

CIP-DATA LIBRARY TECHNISCHE UNIVERSITEIT EINDHOVEN

Corbeij-Kurelec, Lada

Chain mobility in polymer systems : on the borderline between solid and melt / by Lada Corbeij-Kurelec. - Eindhoven : Technische Universiteit Eindhoven, 2001.

Proefschrift. - ISBN 90-386-3032-8

NUGI 813

Trefwoorden: polymeren ; mechanische eigenschappen / kunstgewrichten / polyetheen ; UHMW-PE / faseovergang ; hexagonale fase / Raman spectra

Subject headings: polymers ; mechanical properties / artificial joints /

polyethylene ; UHMWPE / phase transition ; hexagonal phase / Raman spectra

© 2001, L. Corbeij-Kurelec

Printed by University Press Facilities, Eindhoven, The Netherlands

This research was financially supported by Dutch Polymer Institute (DPI)

Chain Mobility in Polymer Systems; On the Borderline between Solid and Melt

PROEFSCHRIFT

ter verkrijging van de graad van doctor aan de
Technische Universiteit Eindhoven, op gezag van de
Rector Magnificus, prof.dr. R.A. van Santen, voor een
commissie aangewezen door het College voor
Promoties in het openbaar te verdedigen
op dinsdag 30 oktober 2001 om 16.00 uur

door

Lada Corbeij-Kurelec

geboren te Zagreb, Kroatië

Dit proefschrift is goedgekeurd door promotoren:

prof.dr. P.J. Lemstra

en

prof.dr.ir. H.E.H. Meijer

Copromotor:

dr. S. Rastogi

Aan René
Mojim roditeljima

Contents

Summary	ix
Chapter 1 General Introduction	
1.1 Polyethylene; structure vs. properties	13
1.2 Processing of polymers: restrictions of the high molecular weight	15
1.3 Salient features concerning crystallisation of polyethylene	18
1.4 Nascent UHMW-PE	21
1.5 Scope of the thesis	22
1.6 References	23
Chapter 2 Phase transitions in polyethylenes, the influence of crystal dimensions	
2.1 Introduction	25
2.1.1 Size dependent phase stability; summary of the experimental observations on crystallisation of single crystals of polyethylene from the melt	25
2.2 Experimental	27
2.2.1 Materials and Sample Preparations	27
2.2.2 Pressure cell	28
2.2.3 Electron beam irradiation	28
2.2.4 In-situ wide angle X-ray diffraction (WAXS)	28
2.2.5 Small angle X-ray scattering (SAXS)	28
2.2.6 Transmission electron microscopy	28
2.3 Results and discussion	29
2.3.1 In-situ X-ray investigations of solution-crystallised film of UHMW-PE at elevated pressures and temperatures	29
2.3.2 In-situ X-ray investigations on irradiated solution-crystallised film of UHMW-PE at atmospheric as well as elevated pressures and temperatures	33
2.3.2.1 Observations at atmospheric pressure	33
2.3.2.2 Phase transformations of irradiated solution-crystallised films at elevated pressures	34
2.3.3 A thermodynamic explanation for the in-situ results	37
2.4 Conclusions	40
2.5 References	40

Chapter 3 Structure and Morphology of Nascent UHMW-PE

3.1 Introduction	43
3.2 Experimental Section	45
3.2.1 Materials	45
3.2.2 Compaction of nascent powders in the plate press	45
3.2.3 Wide Angle X-ray Scattering (WAXS) using the Guinier camera	45
3.2.4 Differential scanning calorimetry (DSC) and temperature modulated DSC (TMDSC)	46
3.2.5 Transmission electron microscopy (TEM)	46
3.3 Results and Discussion	47
3.3.1 Ductility of different grades of UHMW-PE below the α -relaxation temperature	47
3.3.2 Crystal dimensions of different grades of UHMW-PE powders before and after annealing at elevated temperatures	48
3.3.3 Dynamics of the reorganization process during heating UHMW-PE powder as revealed by TMDSC	51
3.3.3.1 TMDSC measurements on nascent UHMW-PE powder (laboratory scale Ziegler-Natta grade)	51
3.3.3.2 Reorganisation processes on heating different powders of UHMW-PE as revealed by TMDSC	59
3.4 Conclusions	62
3.5 References	63

Chapter 4 Phase transformations in nascent UHMW-PE powder at elevated pressure as revealed by in-situ Raman spectroscopy

4.1 Introduction	65
4.2 Scientific background-Raman spectroscopy of polyethylene	66
4.3 Experimental Section	68
4.3.1 Materials	68
4.3.2 Pressure cell	69
4.3.3 In-situ Wide Angle X-ray Scattering (WAXS)	69
4.3.4 In-situ Raman spectroscopy	69
4.4 Results and discussion	70
4.4.1 Raising the pressure at room temperature	70
4.4.2 Heating the sample at 4000 bar	74
4.5 Conclusions	83
4.6 References	84

Chapter 5 A novel route to sinter UHMW-PE nascent powders into homogeneous, grain boundary free, products

5.1 Introduction	85
5.2 Experimental section	87
5.2.1 Materials	87
5.2.2 Pressure cell with diamond windows (PCDW)	87
5.2.3 In-situ Wide Angle X-ray Scattering (WAXS)	87
5.2.4 Light microscopy (LM)	88
5.3 Results and Discussion	88
5.3.1 Melting of nascent powders via the hexagonal phase at pressures below the equilibrium triple point	88
5.3.2 Sintering of different nascent powders	90
5.3.2.1 Experimental observations on sintering behaviour of different nascent powders	90
5.3.2.2 Experimental evidence of the importance of the residence time in the hexagonal phase during sintering	96
5.3.2.3 Experimental evidence of the role of the “chain explosion” in the sintering of nascent powders	98
5.4 Conclusions	100
5.4 References	101

Chapter 6 Wear and fatigue resistance of fully sintered UHMW-PE products for medical applications like hip and knee joints

6.1 Introduction	103
6.1.1 Wear mechanism acting on UHMW-PE components in artificial hip and knee joints: a literature survey	104
6.2 Experimental section	106
6.2.1 Materials	106
6.2.2 Pin on ball wear machine	108
6.2.3 Crack propagation measurements	110
6.3 Results and Discussion	112
6.3.1 Wear results from pin on ball machine	112
6.3.2 Tension fatigue resistance of different types of polyethylene: influence of the grain boundaries	118
6.4 Conclusions	124
6.5 References	125

Chapter 7 High melting temperature of nascent powders, a kinetic approach

7.1 Introduction	129
7.2 Experimental Section	130
7.2.1 Materials	130

7.2.2 Differential Scanning Calorimetry (DSC)	130
7.3 Results and Discussion	131
7.4 Conclusions	133
7.5 References	133
Technology Assessment	135
Appendix 1	139
Appendix 2	143
Samenvatting	147
Acknowledgements	151
Curriculum Vitae	153

Summary

The properties and performance of synthetic polymeric materials depend not only on their chemical composition but also on the structure and morphology developed during processing. In this respect, polymers that intrinsically possess excellent mechanical properties might be difficult to use in practice, because they are difficult to process. A well-known example of such an intractable polymer is Ultra-High-Molecular-Weight Polyethylene (UHMW-PE), a linear polyethylene grade possessing a molecular weight $> 3 \times 10^3$ kg/mol, that possesses intrinsically excellent mechanical properties such as wear resistance and fatigue. These properties make UHMW-PE the material of choice in high demanding applications like bearing surfaces in hip and knee prosthesis. However the lifetime of such joints, where UHMW-PE is used as an inlay between a metal or ceramic countersurface and the human bone, shows insufficient lifetime and in most of the cases it is the UHMW-PE component that fails. This failure is partially due to problems that are a direct consequence of the high values of molecular mass, like the melting viscosity ($\eta_0 \sim M_w^{3.4}$). During the sintering of UHMW-PE (melt processing is not possible due to high melt viscosity) chains are unable to cross completely from one powder particle to another (due to long relaxation times) and, accordingly, products possess residues of the original powder particles, resulting in grain boundaries or fusion defects. This incomplete fusion of the original powder particles has been considered one of the main reasons for the insufficient lifetime of the polyethylene components in artificial joints. Considering the fact that worldwide approximately one million UHMW-PE components are implanted on a yearly basis, it is important to develop new routes to process UHMW-PE powder into products with improved performance.

In this thesis a novel route to process UHMW-PE into fully fused homogeneous (grain boundary free) products has been developed. The method makes use of a phenomenon called “chain explosion” which occurs upon melting of (fully) *disentangled* folded chain crystals. Upon melting single crystals an *instantaneous* increase in radius of gyration is observed, referred to as “chain explosion”. In the folded-chain crystal, the polymer chain possesses a compact conformation compared with its (equilibrium) random-coil conformation in the melt. Consequently, upon melting the chain conformation changes suddenly and drastically, entropy-driven. Since in practice we are dealing with an ensemble of chains, the ‘chain-explosion’ phenomenon upon melting, results into a fast interpenetration of chains, even across boundaries related to the original powder morphology. Consequently, fusion (sintering) making use of the ‘chain-explosion’ phenomenon, is facilitated.

A prerequisite for utilising the phenomenon of “chain explosion” to be effective upon melting, is to start from an initially (fully) disentangled state. A reduced number of entanglements in high molecular mass polymer can be obtained directly in the reactor if the temperature of synthesis is lower than the crystallisation temperature of the polymer chain in the reaction medium. Due to these synthesis conditions chains are unable to experience the random coil conformation since they crystallise immediately upon their creation, leading to a unique nascent morphology consisting of individual single crystals. A detailed study on nascent UHMW-PE powders has been performed in order to understand the morphological and structural characteristics of these powders. It is shown that the initial morphology, i.e. crystal size, topology and entanglement density, in the nascent powders highly depend on the synthesis conditions, notably synthesis temperature and type of the catalyst. Currently most commercial grades of UHMW-PE are synthesised with the help of Ziegler-Natta catalysts, which are shown to be unable to produce the fully disentangled state within nascent powder. This is associated to the fact that the active sites in such supported catalyst systems are too close to each other and that, consequently, neighbouring chains are prone to meet during their growth/crystallisation. In order to fuse these powders via the phenomenon of “chain explosion”, it is necessary to disentangle the system prior to melting. The feature of the enhanced chain mobility within the hexagonal phase in polyethylene (thermodynamically stable at $P > 4000$ bar and $T > 250^\circ\text{C}$) can be used as the route to disentangle the system. Due to the enhanced chain mobility in the c -direction, folded chain crystals thicken within the hexagonal phase and, as they thicken, the chains are pulled into a crystal leading to disentanglement of the total system. A practical problem encountered in using the hexagonal phase in commercial processing of polymers is that its thermodynamic equilibrium position requires high pressures and temperatures ($P > 4000$ bar and $T > 250^\circ\text{C}$). Therefore, an extensive study has been performed on phase transformations at elevated pressures of solution-crystallised films of UHMW-PE. With help of in-situ Wide Angle X-ray Scattering experiments, performed at European Synchrotron Radiation Facilities, an interesting phenomenon related to polymorphism induced by pressure has been found, indicating that the stability of different phases in polymer systems (notably polyethylene) can vary with size. The experiments confirmed that the stability of the hexagonal phase is dependent on the initial crystal size. Small crystals transform from the usual orthorhombic to the hexagonal phase, much below the thermodynamic critical point, Q_0 . These findings reveal that with the proper choice of the initial morphology, i.e. crystal size, it is possible to obtain the hexagonal phase at pressures ~ 1000 bar, a value that becomes feasible in polymer processing. The nascent powders used in this study consist of very small folded chain crystals, which are a consequence of specific synthesis conditions, where synthesis temperature is kept below 80°C . Therefore, based on the experimental findings related to the size dependent phase

stability, these nascent powders melt via the hexagonal phase at pressures much below the equilibrium triple point.

Subsequently it was confirmed that the intervention of the hexagonal phase at pressures below the equilibrium triple point influence the sintering characteristics of the nascent powders. Experiments with different grades suggest that, depending on the initial entanglement density, different residence times within the hexagonal phase are needed in order to obtain fully fused products of UHMW-PE. The hexagonal phase is hence used as a mean of disentanglement of the system which makes the phenomenon of “chain explosion” upon melting effective for the fusion process. Phase transformations were followed by in-situ Raman spectroscopy which proved to be a powerful tool to detect the different phases in polyethylene.

The intervention of the hexagonal phase could be overcome by creating the fully disentangled state already within the reactor. For this purpose a *single site* metallocene catalyst has been used, where chains are grown far from each other being unable to meet. Such initially disentangled powders could be fully fused upon melting, without prior disentanglement, e.g. via intervention of the hexagonal phase.

The new processing route was scaled-up and grain boundary free products were tested for mechanical properties, notably wear and fatigue, which are of the relevance in medical applications of UHMW-PE. It was shown that fully fused products possess superior fatigue resistance due to the absence of the internal defects, i.e. grain boundaries. This makes the material suitable not only for high demanding medical applications, but it also opens a whole new area for potential use.

Finally, this thesis sets a basis for some fundamental aspects related to the melting behavior of nascent crystals. It was shown that melting of nascent crystals is a kinetically driven process, which is highly dependent on the crystal topology, created during synthesis/crystallisation, as well as on its molecular weight.

Chapter 1

General introduction

1.1 Polyethylene; structure vs. properties

It is difficult to imagine life today without synthetic polymeric materials. They surround us wherever we go. Objects like computer and television cases, car dashboards and bumpers, liquid crystal displays, packaging products, textiles and constructing materials are only a small fraction of polymers that we encounter in every day life.

What are polymeric materials and what makes them so unique? Polymers are long chain molecules consisting of chemically bonded building blocks, referred to as monomers. The monomer units can be arranged in many different ways, from fully linear to highly branched systems, giving rise to different material properties. One of the main factors contributing to the popularisation of polymers is their ease of processing into complex shapes, low specific mass and large range of properties from soft rubbers to fibres stronger than steel. The final properties of polymeric materials are not only dependent on their chemical structure but also on the way of processing. The stiffness of most conventional polymeric materials is in the range of a few GPa, which does not make it superior to other materials like metals and ceramics. However, processing techniques have been developed in which long polymer molecules are aligned next to each other having moduli up to 150 GPa and strengths values approaching the theoretical strength of the covalent bonds (estimated value of E modulus for covalent bond is 180-340 GPa)^{1,2}. In order to tailor the desired polymeric material for certain applications it is not sufficient to chemically build the molecule within the reactor but also to choose a processing route which would enable a structure development leading to the desired end properties. It is therefore necessary to study polymeric materials interdisciplinary, i.e. to link the final product properties not only to the synthesis conditions but also to the structure development during processing into desired shapes³.

Polyethylene is the most simple synthetic polymer and is a well-known commodity plastic with many applications. In fact, the name polyethylene is only a generic one and a large number of various polyethylene types are produced nowadays which all differ in molecular characteristics,

including the length of the molecular chain (molecular weight), degree of chain-branching and comonomer content.

Due to its molecular simplicity polyethylene has served as a model system in studies related to synthesis, structure, morphology and properties. The knowledge gained in these studies was crucial in understanding polymer systems in general.

Polyethylene was synthesised for the first time in 1933 in the laboratories of ICI (Imperial Chemical Industries) where Fawcett and Gibson performed the reaction between ethylene and benzaldehyde in a high-pressure autoclave and reported that “a waxy solid was found in the reaction tube”⁴. The “waxy solid” was polyethylene, nowadays referred to as Low Density Polyethylene (LDPE). During this polymerisation reaction intra- and intermolecular chain transfer reactions occurred leading to short- and long-chain branches respectively. Due to the high content of the branches, the chains are unable to pack closely inside of crystals resulting in a material possessing a rather low density. This material is nowadays still extensively used, e.g. for packaging purposes, due to its ease of processing⁵. The polymerisation of ethylene under low pressure became feasible 20 years later, when Ziegler and Natta reported the importance of the stereoregulating catalyst in synthesis of various monomers at relatively lower pressures and low temperatures compared to the synthesis of LDPE⁶. The resulting ethylene based polymer, synthesised with the help of the novel stereoregulating catalyst system, was high density polyethylene (HDPE) which was shown to be much more linear and consequently possessed much higher density. The low pressure processes, using specific catalyst systems, were not restricted to the production of the linear polymer systems. Lower density products of polyethylene could be also obtained, by incorporating higher olefins like propylene, 1-butene, 1-hexene, 1-octene, etc., which led to chains possessing short-chain branches. The copolymers synthesised in this way are usually referred to as linear low density polyethylenes (LLDPE), or with increasing the comonomer content, very-low density polyethylene (VLDPE). The invention of the stereoregulating catalyst systems opened a whole new area of research, where lots of effort has been posed on synthesis of different organometallic complexes, which were able to produce various types of macromolecular architectures leading ultimately to different material properties. One of the major breakthroughs in polymer catalysis was made in the early seventies when metallocene compounds were found to be suitable to produce well defined polyolefins and its copolymers⁷. In the metallocene catalyst system, active species (transition metal ions) are sandwiched between two cyclopentadiene or its modifications, which provides for locking up of the active site on the molecular scale. Since these catalyst are homogeneous, molecular systems, the reactivity is much more uniform leading to polyolefins having much narrower molecular weight distribution in comparison with the heterogeneous Ziegler-Natta based

systems. The variety of modifications of cyclopentadiene rings leads to better accessibility of to the active metal ion and therefore better control of molecular architectures.

It has to be noted that this simple description of homogeneous metallocene-based catalyst vs. heterogeneous Ziegler-Natta catalysts is not the state-of-the-art since these novel homogeneous catalyst systems need often to be put on a support for handling in large scale reactors giving rise to less efficiency and selectivity. A detailed discussion is, however, outside the scope of the present thesis.

Properties of polymer materials do not only depend on the molecular architecture but also on the molecular weight. It is known that the properties like stiffness, toughness and wear increase with the molecular weight, while, on the other hand, processability becomes more difficult^{8,9}. Problems encountered in processing of high molecular weight polymers are addressed in the following section.

1.2 Processing of polymers: restrictions of the high molecular weight

Processing of synthetic polymers is often a compromise between ease of processing and desired product properties. Processing routes conventionally applied in polymer industry are injection moulding, extrusion and film blowing or blow molding³. All these routes start from a melt and the molten state is mostly affected by changes in the molecular weight. This is illustrated by the universal relationship between zero shear viscosity and molecular weight³ as given in the Figure 1.1.

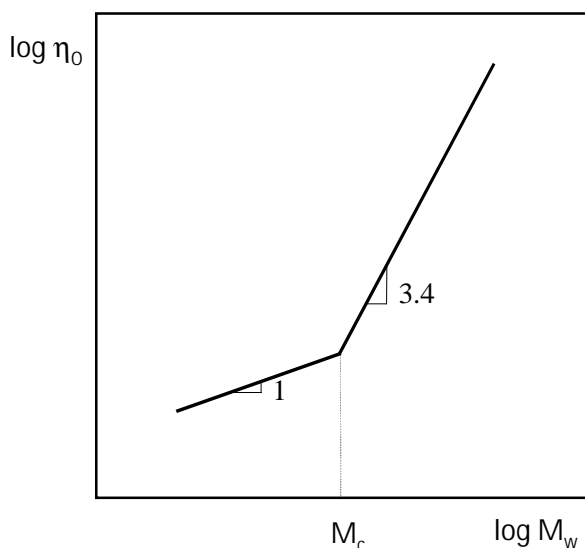


Figure 1.1: Universal relationship between zero shear viscosity (η_0) and molecular weight (M_w). M_c is the critical molecular weight, which is related to the onset of molecular entanglements⁹.

It can be inferred from Figure 1.1 that for relatively low molecular weight polymers ($M_w < M_c$), there is a simple proportionality between zero-shear viscosity and molecular weight. However, for polymers possessing higher molecular weight ($M_w > M_c$), the dependence becomes rather strong ($\eta_0 \sim M_w^{3.4}$). The difference is related to the ability of long chains to entangle, which imposes a restriction to the ease of flow. The motion of chains within a highly entangled melt is described by the reptation model, introduced by de Gennes^{10,11}. In this model the chain within the melt moves worm-like through a virtual tube, formed by the neighbouring chains. The time needed for the chain to renew its tube, i.e. to change its position within the melt and relax, is also highly dependent on molecular weight ($\tau_0 \sim M_w^3$). These fundamental restrictions make high molecular weight polymers rather intractable via conventional processing routes, which invoke a rather viscous melt. However, final properties like toughness, strength and wear increase with molecular weight. Such superior properties are necessary to meet requirements for the high demanding applications. An illustrative example, showing the discrepancy between intrinsic properties related to high values of molecular weight and insufficient product performance due to difficulties in processing, is found in ultrahigh molecular weight polyethylene (UHMW-PE). UHMW-PE is a linear grade of polyethylene, just like HDPE, but possessing a molecular weight above $3 \cdot 10^6 \text{ g mol}^{-1}$ (according to ASTM D4020). Due to its intrinsically good wear, fatigue and friction characteristics, originating from the high molecular weight, it has been selected as the material of choice in application like hip and knee joint prosthesis^{12,13}. In both types of the joints UHMW-PE is used as an inlay between the human bone and a metal or ceramic part which slides against the polyethylene component during normal gait, as illustrated in Figure 1.2.

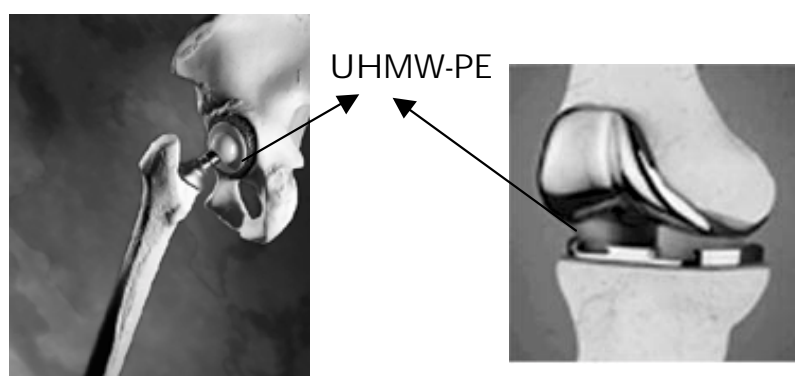


Figure 1.2: Photograph of the artificial (a) hip and (b) knee joint. The polyethylene part is used as the counter surface paired with metal or ceramics.

It has been recognised that such design of joint prostheses does not meet sufficient lifetime requirements and, in most of the cases, it is the polyethylene part that fails¹². In the case of

hip prosthesis hundreds thousands of (sub)-micron particles of polyethylene are released upon each gait leading to severe body reaction and ultimately loosening of the joint¹³. On the other hand, the polyethylene tibial component within a knee prosthesis undergoes macroscopical failure due to cyclic loading experienced by the knee joint.

Due to its intractability, UHMW-PE is usually processed via compression molding or ram-extrusion into simple shapes like rods, plates or sheets, which are subsequently machined into the desired products¹³. It has been found that all products of UHMW-PE possess residues of the original powder particles usually referred to as grain boundaries or fusion defects¹⁴. These flaws in the material are a consequence of the long diffusion time needed for molecular chain to cross from one powder particle to another.

Figure 1.3 shows light microscopy pictures made on thin slices cut from the UHMW-PE hip cups, as-received (Figure 1.3a) and retrieved from the body after 7 years (Figure 1.3b). In Figure 1.3a, the grain boundaries related to original UHMW-PE powder particles can be observed and they become much more pronounced in the used UHMW-PE cup, Figure 1.3b. Similar grain boundaries have been also reported for the UHMW-PE components used in knee-joints, where even more dramatic failure is observed after joint retrieval. Here, crack is shown to propagate through the improper fused grains, causing delamination on the macroscopical level¹⁵.

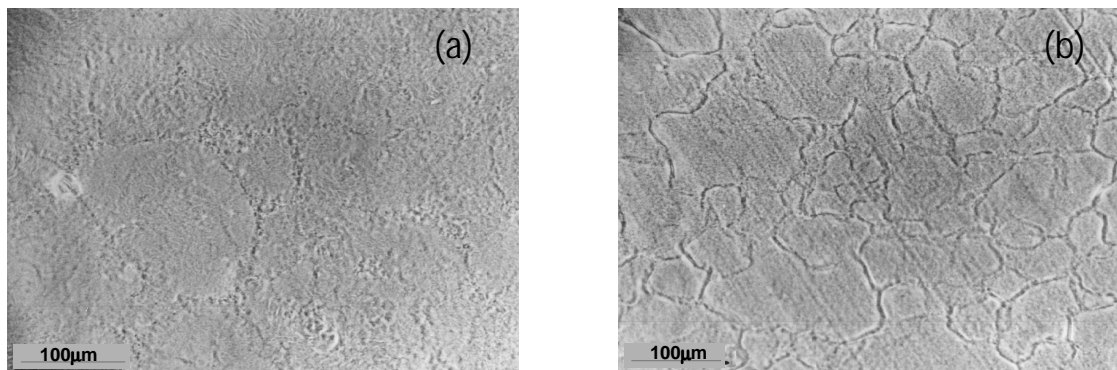


Figure 1.3: *Light microscopy of thin sections cut from (a) the as-produced hip cup and (b) the hip cup retrieved from the human body after 7 years. The grain boundaries become more pronounced after usage¹⁶.*

Fusion defects within the material have always been considered as one of the reasons for the insufficient lifetime of the artificial joints. Therefore, an improvement of the processability of UHMW-PE is important in order to meet the ultimate properties anticipated for materials with such high values of the molecular weight.

A major breakthrough in processing of UHMW-PE was achieved in the early eighties when solution-spinning of UHMW-PE into high modulus/high strength fibres was developed¹⁷⁻²⁴.

In this process, UHMW-PE is dissolved at elevated temperatures and the semi-dilute solution is spun into filaments, which could subsequently be drawn to high drawing ratios (above 30), at temperatures close to but below melting point^{22,25}. Thus obtained fibres possess a tensile strength of 3 GPa and a Young's modulus of 150 GPa, which approaches the theoretical value for the fully extended polyethylene chain. However, UHMW-PE crystallised from the melt, could not be drawn more than 5-10 times resulting in fibres possessing poor mechanical properties^{26,27}. These results suggested that the entanglement density plays a prominent role in the process of drawing and obtaining fully aligned chains in the drawing direction^{22,25}. In the case of melt-crystallised UHMW-PE, entanglements are trapped upon crystallisation and they act as semi-permanent crosslinks in a physical network, which hinders solid state drawability. On the other hand, upon crystallisation from semi-dilute solutions a much less entangled system can be obtained leading to ultradrawability of the system. Experimental results, however, showed that highly disentangled solution-crystallised films of UHMW-PE, drawable below the melting temperature, lose their drawability immediately upon melting^{21,25,28}. This has been associated with the phenomenon of "chain explosion", experimentally assessed by Barham and Sadler²⁹. With the help of in-situ neutron scattering experiments they observed that chains of highly disentangled folded chain crystals of polyethylene increase their radius of gyration instantaneously upon melting. Consequently the chains entangle immediately upon melting which causes the sudden loss in solid state drawability once the sample has been molten. These results were rather disappointing, since they imply that disentangled state can not be preserved once the sample has been melted suggesting it is impossible to benefit from the initially disentangled state once a system is melted.

These experimental findings show that the fundamental restrictions related to the strong dependence of the zero-shear viscosity on molecular weight can not be easily overcome. Simple disentanglement of the chains prior to melting will not lead to a less entangled melt and accordingly it can not be used to improve melt-processing of UHMW-PE.

1.3 Salient features concerning crystallisation of polyethylene

One of the prominent features of regular chains of polyethylene is their ability to crystallise. Linear polyethylene has been considered a model system in studies on polymer crystallisation³⁰⁻³². It has been recognised that upon crystallisation from solution, long flexible chains formed platelet (lamellar) single crystals, the thickness was found to be in the range of 10-30 nm, which is much smaller than the length of a fully extended chain. Formation of such crystals invoked one of the most important findings in the area of crystallisation of the long linear polymer chains which was pioneered by Keller³³ and Fisher³⁴

in the early fifties and is known as *chain folding*. Detailed studies demonstrated that the crystallisation temperature, viz. the degree of supercooling, plays a prominent role in determining the lamellar thickness of solution-crystallised single crystals³⁵. Moreover the melting temperature of single crystals is shown to be dependent on the lamellar thickness^{36,37}. The formation of folded chain crystals is thermodynamically unfavorable (due to high surface/volume ratio) and the process is hence driven kinetically^{36,37}. That means that such folded chain crystals are metastable and will tend to approach a more thermodynamically stable state (extended chain crystals) by reducing its basal surface area, which is possible if the lamellae increases its thickness. Since the thickening of the crystal would lead to thermodynamically more stable state this process will be prone to happen if the chains are given sufficient mobility. The increase of fold length on annealing or heating is one of the most remarkable properties of chain folded polymer crystals and it plays an important role in understanding crystallisation of polymer systems³⁰. Such perfecting of already formed crystals is usually termed *secondary thickening or secondary growth*.

Most of the crystallisation theories were postulated based on the experimental results found for polyethylene crystallised from a dilute solution^{36,37}. Crystallisation from the melt is much more complex. Polymer chains in the melt are highly entangled (depending on molecular weight) which means that folding of the chains during the crystallisation process is hindered. A model has been proposed which invokes reeling-in of chains from the melt on the crystal surface³⁸. This can be regarded as a disentangling process from a virtual tube based on the concept of reptation. Crystallisation from the polymer melt results in the formation of spherical crystal aggregates, the so-called spherulites. The origin of spherulitic growth is still not very well understood despite of extensive studies performed in this direction³⁹.

To bridge the gap between single crystal growth (crystallisation from dilute solutions) and growth into spherulitic structures (crystallisation from the melt), crystallisation studies on linear polyethylenes at elevated pressures and temperatures are important, since single crystals can be grown directly in the melt and the observations on their growth can be compared with the nucleation and growth of spherulites at ambient pressures⁴⁰.

The morphology of polyethylene crystallised at elevated pressures (above 4000 bar), is rather different from the one observed upon crystallisation at atmospheric pressure. Instead of usual folded chain crystals, polyethylene crystallises into large entities having a thickness up to a few microns⁴¹. The morphological difference between the two types of crystals obtained under different crystallisation conditions is associated to the appearance of the intermediate hexagonal phase⁴², thermodynamically stable above 4000 bar and 250°C⁴³, as shown in p-T phase diagram in Figure 1.4.

One of the most prominent features of the hexagonal phase is enhanced chain mobility in the chain direction, which originates from more open lattice and thus weak Van der Waals interactions between the neighbouring chains^{44,45}. The enhanced chain mobility allows crystal thickening up to the full extension of the chain, which is the thermodynamically most preferable state of polymer crystals. The crystals obtained within the hexagonal phase possess a characteristic tapered shape suggesting that the crystallisation, even within the hexagonal phase, begins by chain folding, due to kinetic reasons⁴⁶. Such an initially small folded chain crystal is able to thicken within the hexagonal phase, which leads to simultaneous crystal growth along the lateral and thickness direction. The chain extension upon crystal growth is still recognised as a part of the primary crystal growth and is termed “*thickening growth*”^{44,45}. This is in contrast to the conventional understanding of crystallisation, as revealed from experiments at ambient pressure, where the lamellae are shown to grow only laterally with unaltered crystal thickness (usually referred to as lamellar growth).

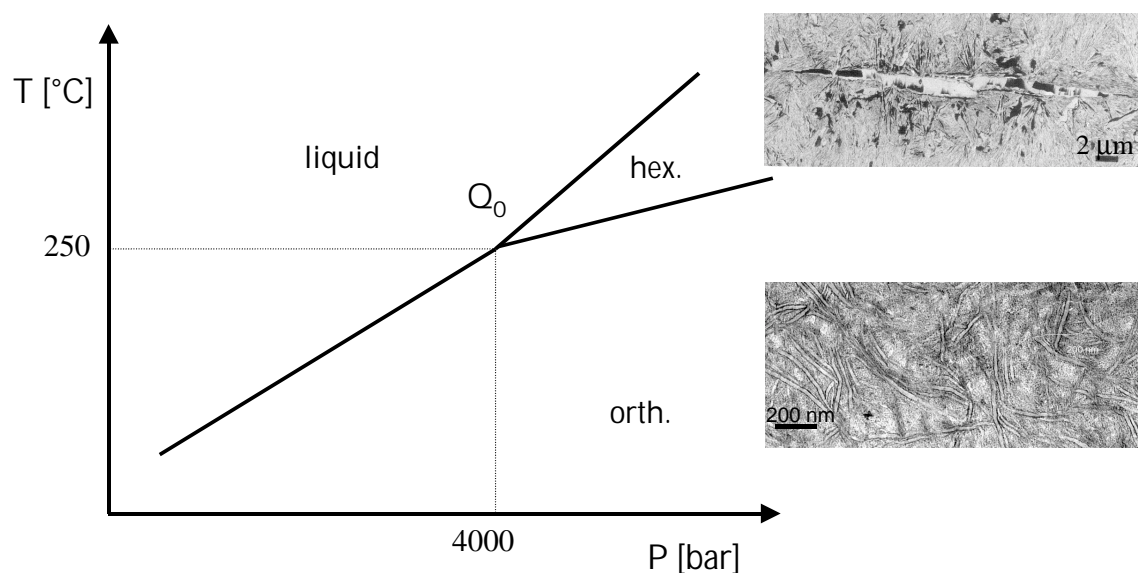


Figure 1.4: Schematic pressure-temperature phase diagram of polyethylene. Q_0 , the equilibrium triple point is the intersection of orthorhombic to hexagonal, hexagonal to liquid, and orthorhombic to liquid transition lines. Transmission electron micrographs show two different morphologies created upon crystallisation of polyethylene at pressures below triple point (folded chain lamellar crystals) and above triple point (extended single crystals).

Extensive studies on crystallisation of linear polyethylene at elevated pressures revealed that crystallisation of this material proceeds via the hexagonal phase even in the thermodynamically stable region of the orthorhombic phase where, by definition, the hexagonal phase is metastable (at pressures below the equilibrium triple point; $P < 4000$ bar)^{46,47}. The crystals, initially in the hexagonal phase, grow both in lateral and thickness direction (the latter leading towards chain extension) but at certain crystallisation time, a transformation from the hexagonal to the orthorhombic phase takes place and all growth

stops or slows down drastically. These findings drew attention to the role played by the finite crystal size in the field of polymer crystallisation³¹, which will be treated in detail in Chapter 2.

Interesting features related to the initial stage of spherulite formation during crystallisation from the melt (at ambient pressure) have been obtained by a detailed study of the morphological characteristics of the crystals formed in the hexagonal phase, at pressures below the equilibrium triple point, i.e. within the thermodynamically stable region of the orthorhombic phase⁴⁰. The observations of multilayering in the hexagonal phase and the overgrowth of crystals on newly transformed crystals in the orthorhombic phase are believed to be a precursor in formation of the spherulites at atmospheric pressure. These results confirm the wide generality of the generic Ostwald's stage rule⁴⁸ which states that the stable state will always be achieved via the metastable one.

1.4 Nascent UHMW-PE

Polyolefins produced in large-scale reactors are produced in the form of (reactor) powders. Usually, these polymer powder particles are compounded with numerous additives and sold to the processor in the form of particulate granules. In the case of UHMW-PE compounding is not feasible due to the excessive melt viscosity and, consequently, UHMW-PE is provided to the processor in the form of powder.

For UHMW-PE, the polymerisation temperature is relatively low in order to obtain the high molar mass⁴⁹⁻⁵¹. Such synthesis conditions allow for successive polymerisation and crystallisation of a polymeric chain at the surface of the catalyst⁵²⁻⁵⁴, leading to rather specific structural and morphological characteristics of thus obtained powders⁵⁵⁻⁵⁸.

Nascent powders of UHMW-PE have drawn attention after it had been recognised that some specific as-polymerised powders could be drawn at temperatures below the melting point into filaments possessing a modulus comparable to the one obtained by solution spun fibres⁵⁹⁻⁶³ ($E_{\text{gel-spun}}=100-150\text{GPa}$). The high drawability of some nascent powders in the solid state was associated to a reduced number of entanglements. Once the nascent powder was molten, the drawing characteristics were lost²⁸, which was a rather disappointing result, because disentangled state was believed to be also beneficial for standard processing of UHMW-PE. Lots of effort was put in realising solid state processing of nascent powders on an industrial scale^{59,64,65}, but only the two-stage solid state process of Kanamoto et al.⁶⁰, in which the compressed and shaped powder is drawn into tapes below the melting temperature, has been scaled up to a pilot scale plant having a capacity of 25 tons per year⁶⁶. Though the remarkable idea of solvent-free solid state processing of UHMW-PE into high modulus products apparently lacked industrial significance, the structure and morphology of nascent UHMW-

PE powders stayed until now unclear and might need some elucidation. Due to specific crystallisation conditions (during synthesis), not all the phenomena observed in nascent powders can be explained by the classical theories developed on the basis of the experimental finding on crystallisation from melt or solution⁶⁷. An example of such controversy is the unusually high melting point of the nascent powders which will be treated in details in Chapters 3 and 7.

1.5 Scope of the thesis

The prime objective of this thesis is to explore novel processing routes making use of transient meso-phases on the borderline between solid and melt.

In this thesis the problem of intractability of high molecular weight polymers is discussed taking UHMW-PE as an example. For this purpose, UHMW-PE is studied from its “birth” on the surface of a catalyst up to its structure development in the final products. Such multidisciplinary approach is treated in the following steps.

In *Chapter 2* an extensive work on meso-phases in polymer systems is discussed, based on the experimental results obtained on morphologically well defined solution-crystallised UHMW-PE.

In *Chapter 3* structural and morphological characteristics of nascent UHMW-PE powders, assessed by different experimental techniques, are reported for powders obtained under different synthesis conditions.

In *Chapter 4* some interesting results related to the phase transformations of nascent powders at elevated pressures are addressed. It is shown that Raman spectroscopy is a powerful technique to distinguish between different phases in polyethylene.

Combining the knowledge gained in the studies mentioned so far, a novel route has been developed to process UHMW-PE into homogeneous products which is discussed in detail in *Chapter 5*. The choice of processing conditions is shown to be dependent on the initial powder morphology.

The novel route has been scaled-up and the mechanical properties relevant for applications of UHMW-PE in the hip and knee prostheses, like wear and fatigue, are tested. These results are presented in *Chapter 6*.

Finally, in *Chapter 7* a new kinetic approach for melting of the nascent powders is proposed.

1.6 References

1. Tashiro, K.; Kobayashi, M.; Tadakoro, M. *Macromolecules* **1978**, *10*, 194
2. Salem, D.R. *Structure Formation in Polymer Fibres*, Hanser Publisher: Munich, **2000**
3. Cahn, R.W.; Haasen, P.; Kramer, E.J. *Materials Science and Technology, Vol 18, Processing of Polymers*, VCH: Weinheim, **1997**
4. *Golden Jubilee Conference, Polyethylenes 1933-83: Past Present and Future*, Plast. Rubber Inst.: London, **1983**
5. Stoiljkovic, D.; Bogdanovic, V.; Eles-Ljubic, V. *Polimeri* **1984**, *5*, 301
6. Moore, E.P. *The Rebirth of Polypropylene: Supported Catalyst: how the people from Mentedison laboratories revolutionized the PP industry*, Hanser Publishers; Munich, **1998**
7. Scheirs, J.; Kaminsky, W. *Metallocene-based polyolefins: preparation, properties and technology*, Wiley: Chichester, **2000**
8. Ferry, J.D. *Viscoelastic Properties of Polymers*, John Wiley & Sons: Toronto, **1980**
9. Gedde, U.W. *Polymer Physics*, Chapman&Hall: London, **1995**
10. de Gennes, J. *Chem. Phys.* **1971**, *55*, 572
11. Doi, M.; Edwards, S.F. *The Theory of Polymer Dynamics*; Oxford Press: Oxford, **1986**
12. Li, S.; Burstein, A.H. *J. Bone and Joint Surg.* **1994**, *76A*, 1080
13. Kurtz, S.M.; Muratoglu, O.K.; Evans, M.; Edidin, A.A. *Biomaterials* **1999**, *20*, 1659
14. Jenkins, H.; Keller, A. *Macromol. Sci. Phys. B* **1975**, *11*, 301
15. Bartel, D.L.; Bicknell, V.L.; Wright, T.M. *J. Bone Joint Surg.* **1986**, *26A*, 1041
16. Rastogi, S.; Kurelec, L.; Lemstra P.J. *Macromolecules* **1998**, *31*, 5022
17. Smith, P.; Lemstra, P.J. *UK Patent 2,051,661*, **1979**
18. Smith, P.; Lemstra, P.J. *Macromol. Chem.* **1979**, *180*, 2983
19. Smith, P.; Lemstra, P.J.; Kalb, B.; Pennings, A.J. *Polym. Bull.* **1979**, *1*, 733
20. Lemstra, P.J.; van Aerle N.A.J.M.; Bastiaansen, C.W.M. *Polym. J.* **1987**, *19*, 85
21. Lemstra P.J.; Bastiaansen, C.W.M.; Meijer, H.E.H. *Angew. Macromol. Chem.* **1986**, *145/146*, 343
22. Smith P.; Lemstra, P.J.; Booij H.C. *J. Polym. Sci. Polym. Phys.* **1981**, *19*, 877
23. Smith, P.; Lemstra, P.J. *J. Mater. Sci.* **1980**, *15*, 505
24. Lemstra, P.J.; Kirschbaum, R. *Polymer* **1985**, *26*, 1372
25. Bastiaansen, C.W.M. *Ph.D. thesis*, Eindhoven University of Technology, **1991**
26. Capaccio, G.; Ward, I.M. *Polymer* **1974**, *15*, 233
27. Capaccio, G.; Ward, I.M. *Polymer* **1975**, *16*, 243
28. Bastiaansen C.W.M.; Meijer, H.E.H.; Lemstra, P.J. *Polymer* **1990**, *31*, 1435
29. Barham, P.; Sadler, D.M. *Polymer* **1991**, *32*, 393
30. Wunderlich, B. *Macromolecular physics*; Academic Press: New York, **1976**; vol.2
31. Keller, A.; Hikosaka, M.; Rastogi, S.; Toda, A.; Barham, P.J.; Gooldbeck-Wood, G. *J. Mater. Sci.* **1994**, *29*, 2579; *Philos. Trans. R. Soc. London* **1994**, *A348*, 3
32. Wunderlich, B.; Grebowicz, J. *Adv. Polym. Sci.* **1984**, *60/61*, 1
33. Keller, A. *Philos.Mag.* **1957**, *2*, 1171

34. Fischer, E.W. *Nature* **1957**, *12a*, 753
35. Organ, S.J.; Keller, A. *J. Polym. Sci., Part B, Polymer Physics* **1986**, *24*, 2319
36. Frank, C.F.; Tosi, M. *Proc. R. Soc.* **1961**, *A263*, 323
37. Hoffman, J.D.; Guttman, C.M.; di Marzio, E.A. *Discuss. Farady Soc.* **1979**, *68*, 177
38. Klein, J.; Ball, R.C. *Discuss. Farady Soc.* **1979**, *68*, 198
39. Abo el Maaty, M.I.; Hosier, I.L.; Bassett, D.C. *Macromolecules* **1998**, *31* 153
40. Rastogi, S.; Kurelec, L. *J. Mater. Sci.* **2000**, *35*, 5121
41. Basset, D.C.; Khaifa, A.; Turner, B. *Nature (London)* **1972**, *239*, 109; *ibid* **1972**, *240*, 146
42. Basset, D.C.; Block, S.; Piermarini, G.J. *J. Appl. Phys.* **1974**, *45*, 4146
43. Hikosaka, M.; Tsukijama, K.; Rastogi, S; Keller, A. *Polymer* **1992**, *33*, 2502
44. Hikosaka, M. *Polymer* **1987**, *28*, 1257
45. Hikosaka, M. *Polymer* **1990**, *31*, 458
46. Hikosaka, M.; Rastogi, S.; Keller, A.; Kawabata, H.J. *Macromol. Sci.-Phys.* **1992**, *B31(1)*, 87
47. Rastogi, S.; Hikosaka, M.; Kawabata, H.J.; Keller, A. *Macromolecules* **1991**, *24*, 9384
48. Ostwald, W. *Z. Physik.Chem.* **1897**, *22*, 286
49. Mackie, P.; Berger, M.N.; Grieveson, B.M.; Lawson, D. *Polym. Lett.* **1967**, *251*, 563
50. Chanzy, H.D.; Revol, J.F.; Marchessault, R.H.; Lamande, A. *Kolloid Z.Z. Polymere* **1973**, *251*, 563
51. Keller, A.; Willmouth, F.M. *Macromol. Chem.* **1969**, *121*, 42
52. Chanzy, H.D.; Day, A.; Marchessault, R.H. *Polymer* **1967**, *8*, 567
53. Chanzy, H.D; Marchessault, R.H. *Macromolecules* **1969**, *2*, 108
54. Chanzy, H.D; Bonjour, E.; Marchessault, R.H. *Colloid Polym. Sci.* **1974**, *252*, 8
55. Munoz-Escalona, A.; Parada, A. *J. Crystal. Growth.* **1980**, *48*, 250
56. Munoz-Escalona, A.; Hernandez, J. G.; Gallardo, J.A.; Sustic, A. *Advances in Polyolefins*, Plenum Press: New York, **1987**
57. Kakugo, M.; Sadatoshi, H.; Sakai, J.; Yokoyama, M. *Macromolecules* **1989**, *22*, 3172
58. Hutchinson, R.A.; Chen, C.M.; Ray, W.H. *J. Appl. Polym. Sci.* **1992**, *44*, 1389
59. Zacharaiades, A.E.; Watts, M.P.C.; Kanamoto, T.; Porter R.S. *J. Polym. Sci.: Polym. Lett. Ed.* **1984**, *22*, 133
60. Kanamoto, T.; Ohama, T.; Tanaka, K.; Takeda, M.; Porter, R.S. *Polymer* **1987**, *28*, 1517
61. Smith, P.; Chanzy, H.D.; Rotzinger, B.P. *Polym. Com.* **1985**, *26*, 258
62. Smith, P.; Chanzy, H.D.; Rotzinger, B.P. *J. Mater. Sci.* **1987**, *22*, 523
63. Rotzinger, B.P.; Chanzy, H.D.; Smith, P. *Polymer* **1989**, *30*, 1814
64. Kanamoto, T; Sherman, E.S.; Porter, R.S. *Polym. J.* **1979**, *11*, 497
65. Kanamoto, T; Tsuruta, A.; Tanaka, K.; Takada, M. *Polym. J.* **1984**, *16*, 85
66. Otsu, O.; Yoshida, S.; Kanamoto, T.; Porter, R.S. *Proceedings PPS-14* **1998**, G7-19
67. Tervoort-Engelen, Y.M.T.; Lemstra, P.J. *Polym Com.* **1991**, *32*, 345

Chapter 2

Phase transitions in polyethylenes, the influence of crystal dimensions

2.1 Introduction

Some fundamental features related to crystallisation of polyethylene have been presented in Chapter 1. It has been discussed that upon crystallisation at elevated pressures, above the equilibrium triple point of polyethylene ($P_Q > 4000$ bar and $T_Q > 250^\circ\text{C}$ ¹; Figure 1.3, Chapter 1), the formation of extended chain single crystals becomes feasible due to intervention of the hexagonal phase²⁻⁵. One of the most prominent features of the hexagonal phase is enhanced chain mobility in the chain direction, which originates from the more open lattice, and thus weaker van der Waals interactions between neighbouring chains³. Due to this reason, initially folded chains within the hexagonal phase are able to thicken to full extension, which is thermodynamically the most favourable state of polymer crystals⁶⁻⁸. This implies that in the hexagonal phase crystals grow simultaneously along the lateral and thickness direction, leading to characteristic tapered shape crystals^{3,9,10}.

With help of in-situ light microscopy, it has been found further that crystallisation of linear, sharply fractionated polyethylene, always starts in the hexagonal phase, even at the pressures below the equilibrium triple point, i.e. in the thermodynamically stable region of the orthorhombic phase (shaded region in the Figure 1.3)¹¹. From these experimental results some new considerations in polymer crystallisation have been invoked, and these will be shortly addressed in the following section¹².

2.1.1 Size dependent phase stability; summary of the experimental observations on crystallisation of single crystals of polyethylene from the melt

An extensive work on isothermal crystallisation of polyethylene at elevated pressures below the equilibrium triple point ($P_Q = 4000$ bar and $T_Q = 250^\circ\text{C}$)¹ revealed that crystallisation of polyethylene proceeds via the hexagonal phase, even in the thermodynamically stable region of the orthorhombic phase¹. The crystals, initially in the hexagonal phase, grow both in lateral

Reproduced in part from:

Rastogi, S; Kurelec, L.; Lemstra, P.J. *Macromolecules* **1998**, *31*, 5022-5031

Rastogi, S. Kurelec, L. *J. Mater. Sci.* **2000**, *35*, 1-18

and thickness direction (the latter leading towards chain extension) but, at some stage of growth, a transformation from the hexagonal to the orthorhombic phase takes place and all growth stops or slows down drastically⁶. The residence time of the crystals within the hexagonal phase depends on the supercooling and pressure at which the isothermal experiment is performed¹³. After certain crystallisation time, at isobaric and isothermal conditions, two different types of crystals could be observed – one in the hexagonal phase which continued to grow and the other which had already transformed into the thermodynamically stable orthorhombic phase and subsequently stopped growing^{6,11}. Upon melting such a sample, the hexagonal crystals melt at a lower temperature than the orthorhombic ones, which is contrary to the findings above the thermodynamic triple point. It has been anticipated, based on the experimental observations summarised above, that in the initial state of crystallisation, the chains are in the folded chain form (due to kinetic reasons) even within the hexagonal phase¹². Such initial crystallites possess relatively small dimensions, which causes a shift of the thermodynamically stable region of the hexagonal phase to lower pressures and temperatures. Once the crystal is in the hexagonal phase, it will thicken and, subsequently, the transition from the hexagonal to the orthorhombic phase will take place. This transition is anticipated to occur due to the shift of the phase diagram back to its equilibrium position (related to the increase in the crystal dimensions).

In order to introduce the size parameter in the considerations of phase behaviour of polymer systems, the pressure-temperature phase diagram has been extended by introducing a third axis containing the crystal size¹². Such a three-dimensional phase diagram (P, T, 1/l) is usually termed the phase stability diagram. For simplicity the three dimensional diagram will be discussed two dimensionally, at two different pressure regimes, below and above the equilibrium triple point pressure (P_Q) as shown in Figure 2.1.

For pressures above the equilibrium triple point pressure ($P > P_Q$) there is always a temperature interval for all values of crystal thicknesses where the hexagonal phase is thermodynamically stable (Figure 2.1a). On the contrary, for pressures below the equilibrium triple point pressure ($P < P_Q$) the hexagonal phase becomes stable only for a sufficiently low crystal size, as seen in Figure 2.1b. This means that the stability regions of the hexagonal and the orthorhombic phases cross over with lamellar thickness, i.e. the transition from the orthorhombic phase into the hexagonal phase is dependent on the lamellar thickness. It is, therefore, obvious that sufficiently thin crystals will be stable in the phase different from that of ultimate stability, as defined by equilibrium thermodynamics for infinite size crystals. When considering polymer systems, this phenomenon is rather unique since the size dependence can vary with crystal growth, i.e. the crystal size increases with crystallisation time as shown above for polyethylene. This means that the phase, which is initially

thermodynamically stable, may no longer be stable after a certain time of growth and, therefore, passes through a metastable state before a thermodynamically stable phase intervenes. The latter will be a nucleation controlled phenomenon¹⁴.

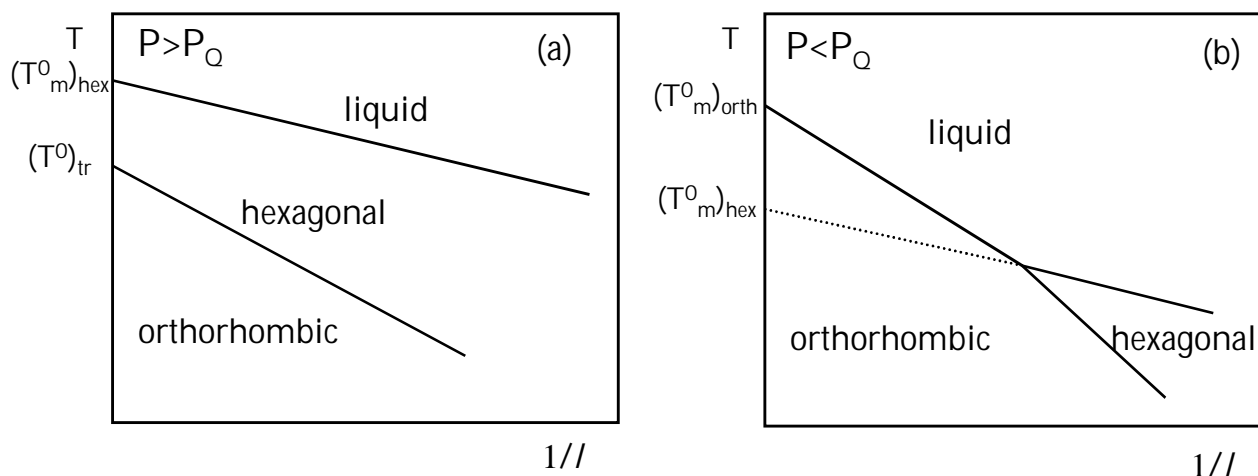


Figure 2.1: Section of $P, T, 1/l$ -phase stability diagram at constant pressures. (a) for $P > P_Q$ (b) for $P < P_Q$. At a pressure $P > P_Q$ there is always a temperature region of ultimate stability of the hexagonal phase, independent of the crystal size. At $P < P_Q$ the stability region of the hexagonal phase exists only for a limited crystal size. Notations T_m^0 and T_{tr}^0 are related to the equilibrium state (defined for an infinite crystal size)¹².

All theoretical considerations related to the size dependent phase stability were based on in-situ observations made with the help of light microscopy during crystallisation of polyethylene below and above the triple point. In this chapter, the experimental evidence of the size dependent stability of the hexagonal phase will be experimentally confirmed on very well defined system of solution-crystallised UHMW-PE film as a model system.

2.2 Experimental

2.2.1 Materials and Sample Preparations

The material used is UHMW-PE, Hostalen GUR-4130 supplied by Hoechst Ruhrchemie. Solution-crystallized films were prepared by dissolving 1% UHMW-PE powder by weight in xylene at elevated temperature ($\sim 125^\circ\text{C}$). To avoid air bubbles, the solution was degassed under vacuum and the homogeneous solutions were poured into aluminium trays and left to dry for about a week. A thin film (0.5 mm) was obtained by slow evaporation of the solvent.

2.2.2 Pressure cell

A piston-cylinder type of pressure cell has been used¹⁵, with a maximum attainable pressure of 5000 bar, and a temperature range between room temperature and 300°C. A sample is sandwiched in between two diamond windows which enables in-situ X-ray and optical studies. The pressure on the sample is generated hydrostatically by a precise movement of two pistons, provided by a pressure-regulated flow of nitrogen gas. The smooth motion of the pistons allowed for a maintenance of a constant pressure during any volume change related to phase transformations.

2.2.3 Electron beam irradiation

Irradiation of the samples was performed with a 3MeV "Van de Graaf" accelerator at the Interuniversitair Reactor Instituut, Delft. Solution cast films were mounted on aluminium plates and placed in a heating box with windows inert for the electron beam. The box was flushed with nitrogen gas, before and during irradiation, to prevent oxidative degradation (chain scission). The films were irradiated at room temperature with a dose of 2000 kGy.

2.2.4 In-situ wide angle X-ray diffraction (WAXS)

Monochromatic X-rays of wavelength 0.968 Å and a high flux, available on beam line ID11-BL2 at European Synchrotron Radiation Facility (ESRF) in Grenoble, were used to follow the kinetics of phase transformations at elevated pressures and temperatures. The experiments were performed with the pressure cell described before. The high energy requirements for the beam were also necessary to overcome the X-ray absorption by the diamond windows on the pressure cell.

Diffraction patterns were recorded on a two dimensional Princeton CCD-detector. Integration and data analysis of the diffraction patterns were performed with the help of the Fit2D program provided by ESRF, Grenoble.

2.2.5 Small angle X-ray scattering (SAXS)

In-situ SAXS experiments were performed at atmospheric pressure using Synchrotron Radiation at station 8.2 CLRC, Daresbury, UK with a X-ray wavelength of 1.54 Å.

2.2.6 Transmission electron microscopy (TEM)

The morphology of unannealed and annealed solution-crystallised films was examined using a JEOL 2000FX transmission electron microscope operating at 80 kV. The films were trimmed at -140°C and subsequently etched during 16h at 25°C with a ruthenium tetroxide solution to enhance contrast between the amorphous and crystalline regions. Finally thin sections (70 nm) were obtained using a Reichert Ultracut E microtome.

2.3 Results and discussion

UHMW-PE solution-crystallised films have been subject of several investigations related to chain mobility^{16,17}. A TEM micrograph of such a film viewed edge-on is displayed in Figure 2.2.

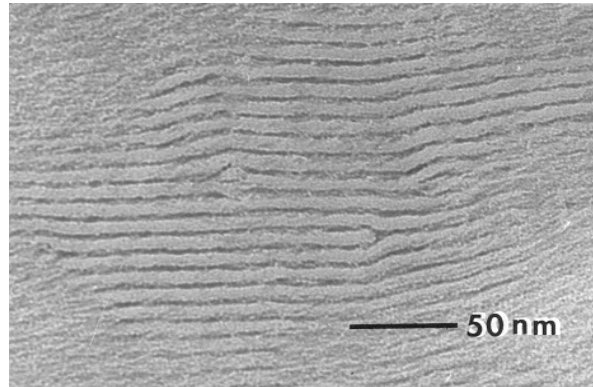


Figure 2.2: Transmission electron micrograph of solution-crystallised UHMW-PE; edge-on view of stacked lamellae of approximately 12 nm thickness

The TEM micrograph recorded edge-on along the film thickness shows that the solution-crystallised film of UHMW-PE consists of well-stacked lamella possessing a uniform thickness of about 12 nm. Due to uniformity as well as regular stacking of the lamella this material has been selected as a model system in study of size dependence phase stability.

2.3.1 In-situ X-ray investigations of solution-crystallised film of UHMW-PE at elevated pressures and temperatures

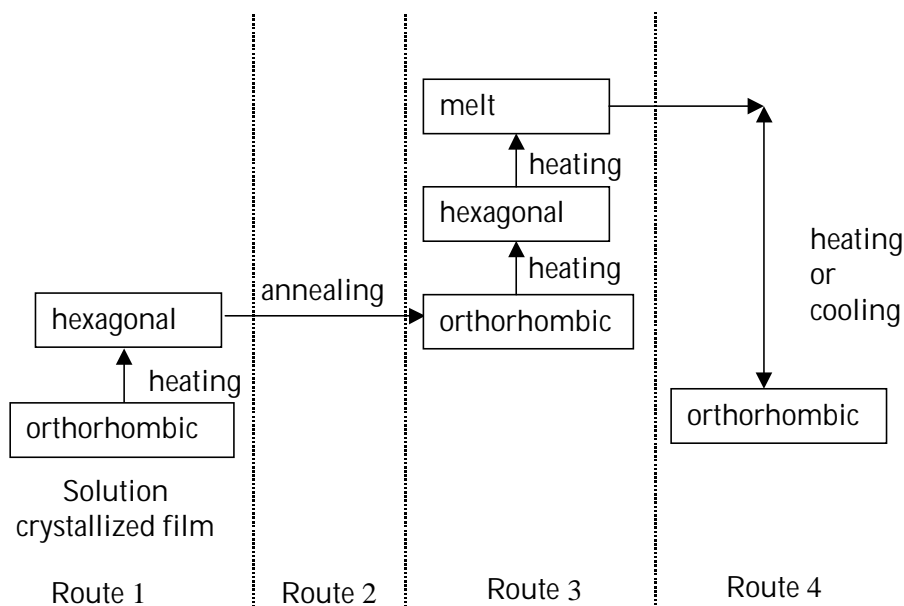


Figure 2.3: Schematic drawing of the experimental routes followed during in-situ X-ray experiments performed on solution-crystallised UHMW-PE at a constant pressure of 1600 bar.

In-situ WAXS measurements at a pressure of 1600 bar have been performed following the routes shown in Figure 2.3. *It has to be noticed that the pressure at which the experiments have been performed is much below the equilibrium triple point for polyethylene ($P_Q=4000$ bar, $T_Q=260^\circ\text{C}$)¹.*

Route 1. Isobaric heating (Figure 2.4a)

A solution-crystallised UHMW-PE sample was heated at a fixed pressure of 1600 bar, which is in fact much below the equilibrium triple point of polyethylene. X-ray diffraction patterns at lower temperatures show the characteristic orthorhombic (110) and (200) reflections. Upon heating, the (100) reflection of the hexagonal phase ($2\theta=13.42$) appears at approximately 195°C , next to the (110) reflection of the orthorhombic phase. These results confirm that for an initially small crystal size the hexagonal phase intervenes at pressures much below the equilibrium triple pressure.

Route 2. Isothermal and isobaric annealing (Figure 2.4b)

Upon annealing at 204°C at a pressure of 1600 bar (route 2 in Figure 2.3), the (100) reflection of the hexagonal phase slowly disappears whereas the orthorhombic reflections gain in intensity. These results suggest that after certain residence time within the hexagonal phase, the crystals transform back to the orthorhombic phase.

Route 3. Isobaric heating (Figure 2.4c)

During isobaric heating at a rate of $2^\circ\text{C}/\text{min}$ (route 3 in Figure 2.3), the hexagonal phase re-appears, and before final melting at 220°C , the characteristic (100) reflection of the hexagonal phase gains intensity at the expense of the (110) and (200) reflections of the orthorhombic phase.

Route 4. Isobaric cooling (Figure 2.4d)

Upon cooling from the melt at the same constant pressure of 1.6 kbar, only the orthorhombic phase is visible on crystallisation. If the sample is heated once again to the melting temperature, the hexagonal phase is no longer observed (route 4 as shown in Figure 2.3).

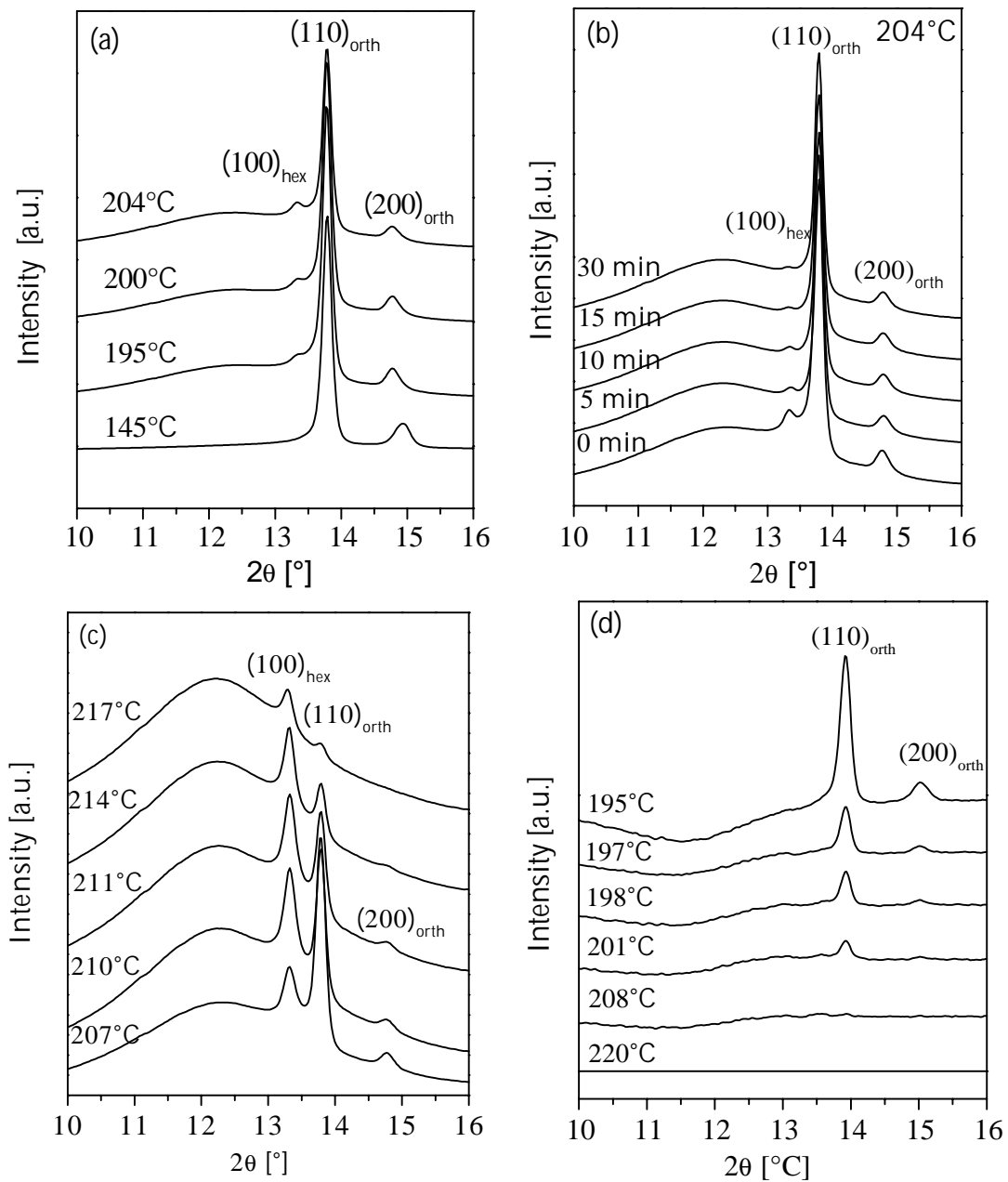


Figure 2.4: *In-situ* WAXS patterns of solution-crystallised film at 1600 bar upon (a) heating at 2°C/min, (b) annealing isobarically at 204°C, (c) further heating up to the melt and (d) cooling from the melt at 2°C/min. In order to observe the very initial stage stage of crystallisation at frame (d) each diffraction pattern is subtracted with the diffuse melt pattern.

From this set of experiments, it can be concluded that melting of the lamellar crystals of approximately 12 nm (initial) thickness, proceeds via the hexagonal phase much below the equilibrium triple point and thus within the region of the thermodynamically stable orthorhombic phase. After complete melting and upon re-crystallisation from the melt, the appearance of the hexagonal phase could not be observed again. During heating and annealing of initially small crystals of the solution-crystallized samples, the thickness of the lamellar crystals increases, especially in the mobile hexagonal phase^{6,7,11,18}. However, at a certain stage of the thickening process, the hexagonal crystals (during annealing) transform back to the thermodynamically stable orthorhombic phase suggesting strongly that the position of the hexagonal phase at pressures below the triple point is determined by the lamellae thickness. Due to the small initial crystal thickness, the hexagonal phase intervenes at much lower pressures and temperatures than usually anticipated. Upon annealing within the hexagonal phase, initially small crystals thicken and subsequently, the stability region of the hexagonal phase shifts back to higher pressures and temperatures, approaching its equilibrium position. At that stage, crystals initially in the hexagonal phase transform into the orthorhombic phase. Such a phenomenon of isothermal phase reversal, due to the changes in the crystal size upon annealing within the mobile phase, has also been reported for trans-1,4-polybutadiene at atmospheric pressure¹⁹. Crystallisation from the melt, however, usually leads to much thicker lamellar crystals compared to solution-crystallised samples, and consequently no crystals in the hexagonal phase are observed on cooling or subsequent heating at the same pressure and temperature. These findings maybe in disagreement with the earlier in-situ observations by optical microscopy, discussed in the introduction. Such a disagreement can be a result of a difference in pressures used for optical microscopy (always above 2800 bar)¹¹ and the one used for the current in-situ X-ray measurements (pressure always below 1600 bar). Further, it is necessary to consider the experimental limitations of the two different techniques. With optical microscopy observations are made on single crystals, while X-ray studies have been recorded on bulk samples of 0.4 mm thickness.

In order to confirm that the phenomenon of isothermal phase reversal is indeed caused by the changes in the crystal thickness upon heating/annealing, the same set of the experiments have been performed on the irradiated solution-crystallised films. It is believed that the chain mobility along the *c*-axis can be suppressed by crosslinking the amorphous zone between the lamellae by irradiation.

2.3.2 In-situ X-ray investigations on irradiated solution-crystallised film of UHMW-PE at atmospheric as well as elevated pressures and temperatures

2.3.2.1 Observations at atmospheric pressure

If the irradiation dose is sufficiently high, the lamella thickening process can be completely suppressed²⁰. For this purpose solution-crystallised films were irradiated with a dose of 2000 kGy. In order to be sure that the selected irradiation dose did not affect the crystalline core, but only caused sufficient crosslinking within the intercrystalline amorphous zone, which would disable the thickening process during annealing, in-situ SAXS experiments have been performed at atmospheric pressure, see Figure 2.5.

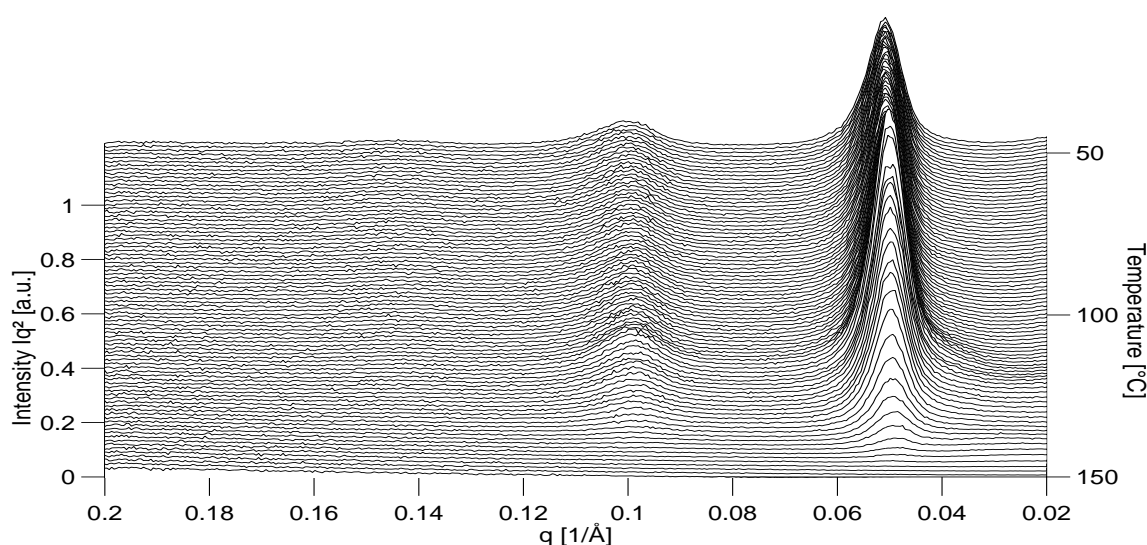


Figure 2.5: SAXS pattern of an irradiated solution-crystallised UHMW-PE film during heating at atmospheric pressure. $q=2\pi/l$ where l is the lamellar thickness.

For the initial state (at room temperature) a first-order maximum is observed at $q=0.052 \text{ \AA}^{-1}$ and the second-order maximum at $q=0.104 \text{ \AA}^{-1}$, which satisfies the Bragg's condition for a long period of 12 nm for well-stacked lamellar crystals. This result coincides with the crystal thickness found for the unirradiated sample¹⁶. Upon heating of the irradiated sample, the first order peak does not shift to the lower angles, as indeed observed in the unirradiated solution-crystallised films¹⁶, suggesting that the irradiation dose used for crosslinking was sufficient to prevent lamellar thickening during heating. Therefore, such samples can be used for further investigations of isothermal phase reversal which is anticipated to be guided by the increased chain mobility within the hexagonal phase leading to crystal thickening. The results of the in-situ WAXS experiments on the phase transformations in the irradiated films is given in the following section.

2.3.2.2 Phase transformations of irradiated solution-crystallised films at elevated pressures

The results of the in-situ WAXS experiments on irradiated solution-crystallised films at 1800 bar are given in the Figure 2.6.

The same experimental route has been followed as given in the Figure 2.3. However the results obtained for irradiated samples are strikingly different and will be summarised below:

Route 1. Isobaric heating (Figure 2.6a)

At pressure of 1800 bar and relatively low temperatures the WAXS pattern is characterised by the typical orthorhombic (110) and (200) reflections together with the relatively intense reflection $2\theta=12.53$. This reflection is associated with the monoclinic phase in polyethylene²¹ and it is usually related to shear during compression. Some features of this phase will be addressed in more details in Chapter 4. Upon heating the sample at a fixed pressure of 1800 bar the monoclinic crystals transform into the orthorhombic one which is accompanied by an increase in intensity of the orthorhombic (110) and (200) reflections. When the temperature is increased further, the (100) reflection of the hexagonal phase appears at the same angle as for the unirradiated sample ($2\theta=12.42$). Again, just like in the unirradiated solution-crystallised film the hexagonal phase intervenes at pressures much below the equilibrium triple point. The intensity of the hexagonal (100) peak increases with increase in temperature, which is also the same as observed for the unirradiated sample.

Route 2. Isothermal and isobaric annealing (Figure 2.6b)

Upon annealing at 172°C at a pressure of 1800 bar (route 2 in Figure 2.3), the intensity of the (100) reflection of the hexagonal phase does not change which is in contrast with the observations found for the unirradiated sample.

Route 3. Isobaric heating (Figure 2.6c)

During further isobaric heating at a rate of 2°C/min (route 3 in Figure 2.3), the crystals that still exist in the orthorhombic phase, fully transform into the hexagonal phase just before their final melting at 200°C. That means that melting of the crystals proceeds via the hexagonal phase, at pressures below the equilibrium triple point.

Route 4. Isobaric cooling (Figure 2.6d)

Contrary to the observations found for the unirradiated solution-crystallised films (Figure 2.4d), the irradiated sample crystallises primarily into the hexagonal phase. On further cooling the (110) orthorhombic reflection appears and slowly gains in the intensity. If the sample is heated again, melting will occur via the hexagonal phase at

the same constant pressure of 1800 bar, similar to the observations above the equilibrium triple point.

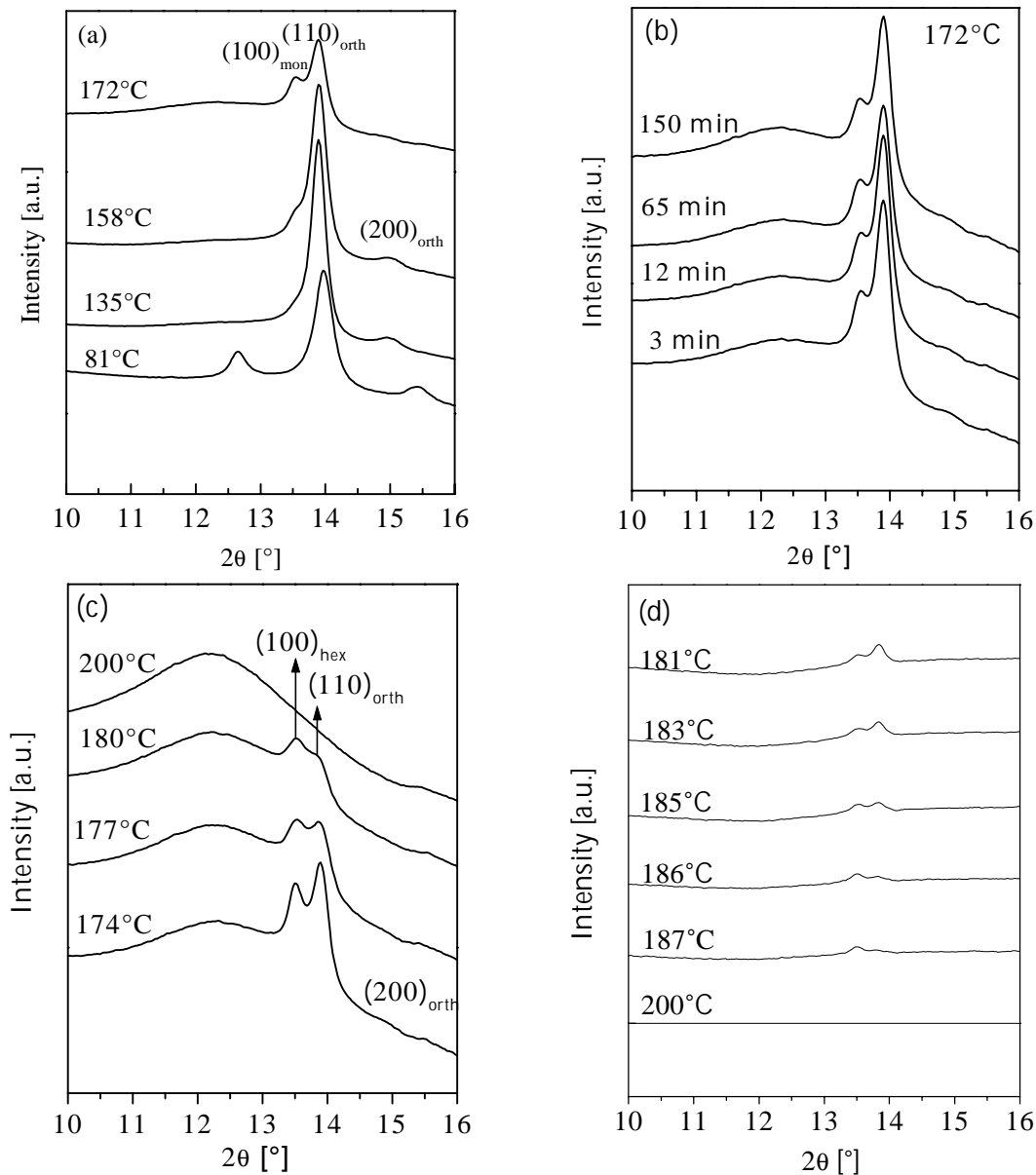


Figure 2.6: *In-situ WAXS pattern of a solution-crystallised film irradiated with 2000 kGy. The experiment is performed at 1800 bar upon (a) heating at 2°C/min, (b) annealing isobarically at 172°C, (c) further heating up to the melt and (d) cooling from the melt at 2°C/min. In order to observe the very initial stage of crystallisation at frame (d) each diffraction pattern is subtracted with the diffuse melt pattern.*

These findings differ substantially from the results obtained for the unirradiated solution-crystallised films. Once the transformation from the orthorhombic to the hexagonal phase occurs, no phase reversal from the hexagonal to the orthorhombic phase during annealing

under isobaric and isothermal conditions could be observed. Moreover, on heating the irradiated sample, crystals not only transform into the hexagonal phase but also melt via the hexagonal phase at pressures below the equilibrium triple point. The observed melting behaviour is very similar to the one anticipated above the triple point, thus confirming the thermodynamic stability of the hexagonal phase for small crystals in the thermodynamically stable region of the orthorhombic phase for crystals having an infinite lamellar thickness.

From the results related to both, irradiated and unirradiated, solution-crystallised films, it can be concluded that true thermodynamic stability conditions can invert with size. Specifically for a polyethylene crystal that is small enough, the hexagonal phase can be the thermodynamically stable phase, even in a pressure-temperature regime where the orthorhombic phase is thermodynamically stable for an infinite crystal-size, as shown in Figure 2.7 by the dashed lines. The triple point Q , related to the size dependent phase stability is located below Q_0 , denoting the equilibrium triple point. When this is the case, it is not the metastability which needs to be invoked for the observation of a metastable phase appearing first. In fact, here the metastable phase with its very small dimensions, will be the thermodynamically stable phase with an inversion of phase stability on growth, i.e. Q moves towards Q_0 with thickening of lamellae.

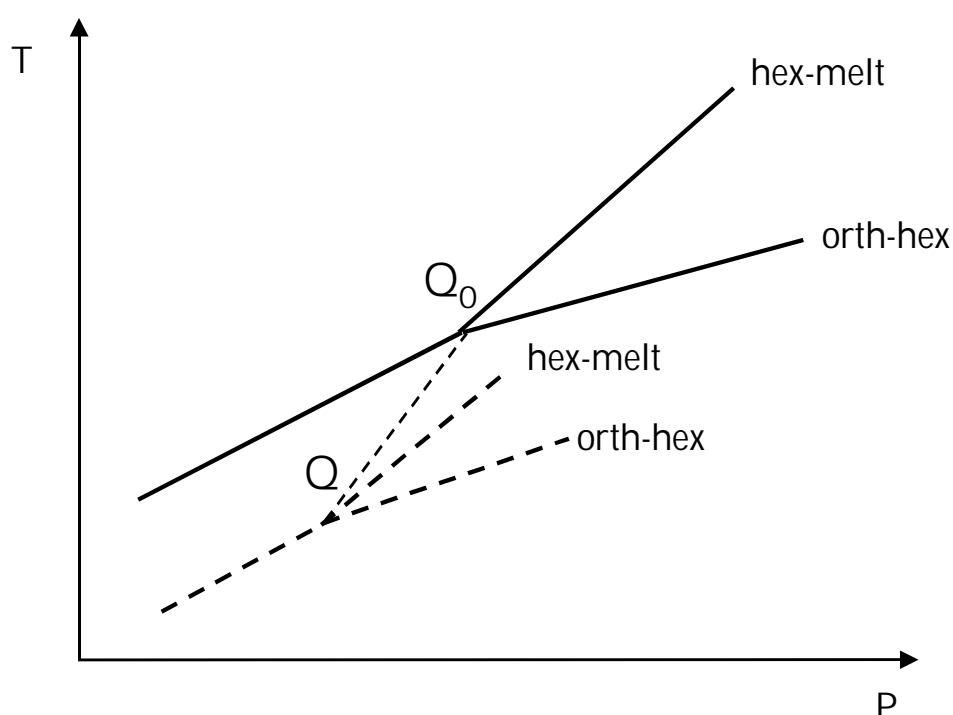


Figure 2.7: Schematic drawing of the shift of the triple point from Q^∞ to Q due to a small initial lamellar thickness. Full lines represent the equilibrium phase diagram for an infinite crystal size. The dashed lines represent a shifted phase diagram due to a reduced crystal size.

2.3.3 A thermodynamic explanation for the in-situ X-ray results

The phenomenon of size dependent phase stability is well known in phase transformations of condensed matter in general. It manifests itself by a depression of the phase transition temperature, as described by the Gibbs-Thompson equation²², which relates the transition temperature to phase dimensions. For polymer systems, this relation has been modified by Hoffman and Weeks who related the melting temperature T_m to the lateral and thickness dimensions of the folded chain crystals.

$$T_m = T_m^0 \left[1 - \frac{2\sigma_e}{l \cdot \rho \cdot \Delta H_m} - \frac{2\sigma}{A \cdot \rho \cdot \Delta H_m} - \frac{2\sigma}{B \cdot \rho \cdot \Delta H_m} \right] \quad (2.1)$$

In Equation 2.1 T_m is the experimentally determined melting point, T_m^0 is the equilibrium melting point for infinite perfect crystals (141.5°C for polyethylene)²³, σ_e is the surface free energy of the fold planes, σ is the surface free energy of the lateral planes, l is crystal thickness in the chain direction (fold length), ΔH_m is the heat of fusion, A and B are the lateral crystal dimensions and ρ is the crystal density. Normally, the last two terms are ignored due to relatively big lateral dimensions of melt and/or solution-crystallised samples (in the order of a few microns) and consequently the melting temperature is only related to the lamellar thickness, l . If l approaches infinity, T_m approaches T_m^0 , which is the equilibrium melting temperature.

The ratio $\frac{\sigma_e}{\Delta H}$ for orthorhombic crystals is larger than for hexagonal crystals¹²

$$\left(\frac{\sigma_e}{\Delta H} \right)_{\text{prth.}} = 3.5 \cdot \left(\frac{\sigma_e}{\Delta H} \right)_{\text{hex.}} \quad (2.2)$$

This implies that for a folded-chain crystal of the same average lamellar thickness l the difference ($T_m^0 - T_m$) is larger for orthorhombic crystals than for hexagonal crystals. Equivalently, the Gibbs free energy for a lamellar crystal with thickness l is closer to the equilibrium Gibbs free energy G^0 in the case of a hexagonal crystal structure. Based on these experimental facts, a Gibbs free energy diagram (Figure 2.8), can be constructed to account for the experimental results described in Figure 2.4 and 2.6. *For sake of simplicity, the Gibbs free energy functions are drawn in Figure 2.8 as straight lines, which is in fact an oversimplification, but not an essential requirement, for the present discussion.*

Figure 2.8 schematically gives, the Gibbs free energy at pressure $P < P_Q$ as a function of temperature T , for orthorhombic and hexagonal crystals. Below the equilibrium triple-point, the Gibbs free energy of a perfect (extended-chain) orthorhombic crystal, G_{orth}^0 , is lower than that

of a perfect (extended-chain) hexagonal crystal, G_{hex}^0 . The Gibbs free energy of folded-chain crystals is higher due to the contribution of the surface free energy. Assuming, for the present discussion, that the free energy curves for folded-chain crystals are parallel with the free energy of extended-chain crystals, and taking into account, as discussed above, that for a given lamellar thickness l the free energy is closer to equilibrium for hexagonal crystals, the various curves in Figure 2.8 become self explanatory.

If an orthorhombic folded-chain crystal with thickness l_2 , the dotted line in Figure 2.8, is heated at a constant pressure $P < P_Q$, the corresponding free energy curve crosses the free energy curves of hexagonal folded-chain crystals (the dashed-dotted line in Figure 2.8). At the crossing point A_1 , the crystal can transform from an orthorhombic into a hexagonal crystal structure since the decrease in free energy with increasing temperature, (dG/dT) , is faster in the case of hexagonal crystals. This situation is encountered during isobaric heating (see Fig.2.4a). Upon annealing at temperature T , Figure 2.4b, the hexagonal crystals thicken in order to decrease the Gibbs free energy towards the equilibrium value. However, during annealing and thickening at temperature T , the driving force $(G_{\text{hex}}^0 - G_{\text{hex}})$ becomes smaller and the thickening process slows down and finally is arrested, for example at point A_2 . The driving force $(G_{\text{orth}}^0 - G_{\text{orth}})$ at temperature T and point A_2 is higher than $(G_{\text{hex}}^0 - G_{\text{hex}})$ and, consequently, the crystal could transform back into the orthorhombic crystal structure. Upon further heating, Figure 2.4c, once again, the Gibbs free energy curve corresponding to the orthorhombic crystals crosses the Gibbs free energy curves of hexagonal folded-chain crystals. Consequently, a transformation from orthorhombic to hexagonal crystals can appear again before final melting.

In the case of irradiated samples, thickening during heating and annealing is hindered by the crosslinks present in the amorphous region of the lamellar morphology. Nevertheless, the transformation from the orthorhombic into the hexagonal phase during heating at pressures below the equilibrium triple point will occur at the crosspoint A_1 (Figure 2.8), because the decrease of free energy with an increase in temperature is faster for hexagonal than for orthorhombic crystals. However, during isothermal and isobaric annealing, thickening in the mobile phase is arrested, and melting proceeds via the same line corresponding to the free energy of the hexagonal folded chain crystals having a thickness l_3 . Due to the absence of lamellar thickening, the triple point of the P-T phase diagram stays “arrested” at lower values of pressure and temperature (position Q_0 in Figure 2.7), implying that the shift in the triple point is related to the crystal size.

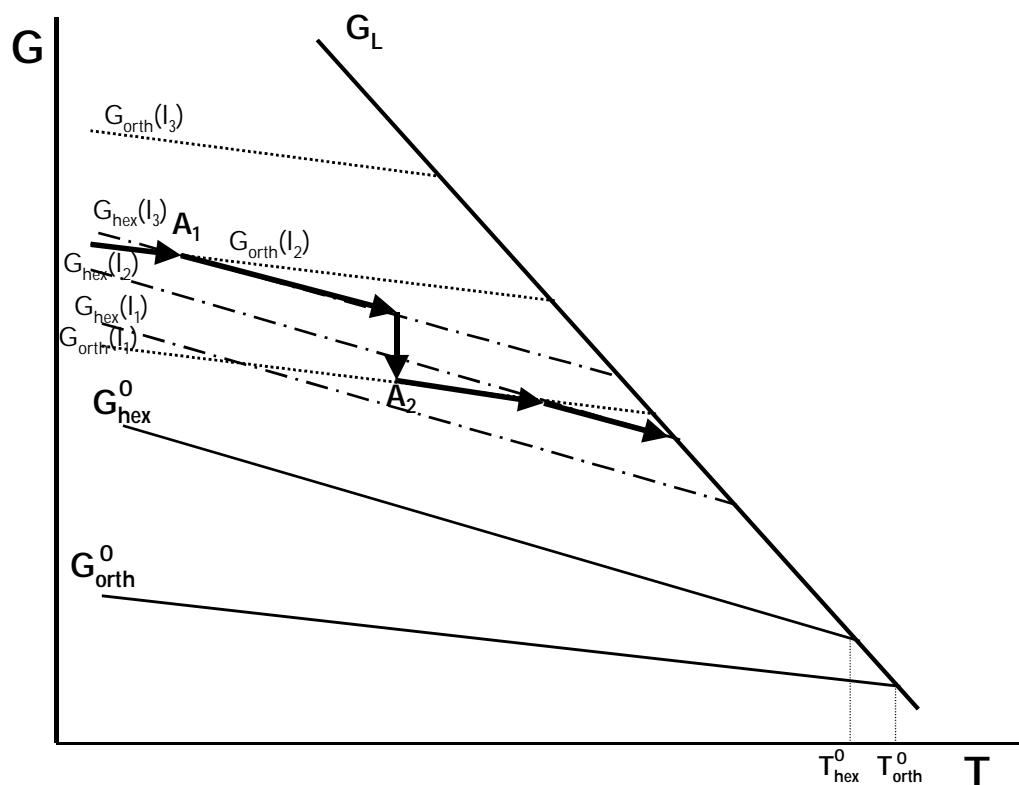


Figure 2.8: A thermodynamic explanation for the experimental observations made during heating and annealing at a pressure below the equilibrium triple point. Black bold lines are equilibrium free energy lines for extended chain orthorhombic and hexagonal crystals; (.....) are the free energy lines for folded-chain orthorhombic crystals possessing different thicknesses $l_1 > l_2 > l_3$; (-·-·-·-·-·-·-) are the free energy lines for folded-chain hexagonal crystals possessing different thicknesses $l_1 > l_2 > l_3$. For sake of simplicity the Gibbs free energy functions are drawn as straight lines.

The above explanation refers only to thermodynamic parameters. The rate of transformation from orthorhombic into hexagonal crystals, and vice versa, depends however on kinetic barriers between the two crystal structures¹⁴. The transformation from an orthorhombic into a hexagonal crystal structure involves nucleation and growth²⁴ and, consequently, the occurrence of a metastable hexagonal phase and the rate of transformation from an orthorhombic into a hexagonal crystal structure, and vice versa, depends on parameters like the initial morphology, (i.e crystal thickness), molar mass and pressure. In fact, the experiments on other solution-crystallised polyethylene samples, possessing a M_w of 32 kg mole^{-1} and a molecular weight distribution of 1.11, showed that a metastable hexagonal phase appeared at even lower pressures, for example as low as 1000 bar^{14} .

2.4 Conclusions

Isothermal phase reversal from the orthorhombic to the hexagonal phase and vice versa is, for solution-crystallised UHMW-PE, related to the limited thickness of the initial crystals. Initially small folded-chain crystals in the orthorhombic phase transform into the hexagonal phase at much lower pressures than the equilibrium triple point. During heating and isothermal annealing, initially small folded-chain crystals thicken and, as they thicken, the position of the triple point is shifting toward its equilibrium position. If thickening of the lamellar crystals is hindered, as it is in irradiated samples, the shift of the triple point, as well as a isothermal phase reversal, can not longer be observed. Melting, as well as re-crystallisation from the melt, occurs directly via the hexagonal phase.

The significance of these phenomena is not only fundamental. The idea to process UHMW-PE via the mobile hexagonal phase becomes now of practical interest, since the hexagonal phase can be obtained at much lower pressures and temperatures than usually associated with this phase. It will be shown in Chapter 3 that nascent powders of UHMW-PE consist of very small folded chain crystals, which melt via the hexagonal phase even at pressures around 1000 bar. This feature will be essential in the development of a novel processing route to obtain fully fused products of UHMW-PE, as elaborated more in detail in Chapter 5.

2.5 References

1. Hikosaka, M.; Tsukijima, K.; Rastogi, S.; Keller, A. *Polymer* **1992**, *33*, 2502
2. Basset, D.C.; Khaifa, A.; Turner, B. *Nature (London)* **1972**, *106*, 239; **1972**, *240*, 146
3. Basset, D.C. *Polymer* **1976**, *17*, 460
4. Basset, D. C.; Block, S.; Piermarini, G. J. *J. Appl. Phys.* **1974**, *45*, 4146
5. Wunderlich, B. *Macromolecular Physics Vol. 2*, Academic Press: New York, **1976**
6. Rastogi, S.; Hikosaka, M.; Kawabata, H.; Keller, A. *Macromolecules* **1991**, *24*, 9384
7. Wunderlich, B.; Grebovich, J. *Adv. Polym. Sci.* **1984**, *60/61*, 1
8. Hikosaka, M. *Polymer* **1987**, *28*, 1257; **1990**, *31*, 458
9. Wunderlich, B. *Macromolecular Physics Vol. 1*, Academic Press: New York, **1973**
10. Hikosaka, M.; Amano, K.; Rastogi, S.; Keller, A. *J. Mater. Sci.* **2000**, *35*, 5157
11. Hikosaka, M.; Rastogi, S.; Keller, A.; Kawabata, H. *J. Macromol. Sci.-Phys.* **1992**, *B31(1)*, 87
12. Keller, A.; Hikosaka, M.; Rastogi, S.; Toda, A.; Barham, P.J.; Gooldbeck-Wood, G. J. *J. Mater. Sci.* **1994**, *29*, 2579; *Philos. Trans. R. Soc. London* **1994**, *A348*, 3
13. Hikosaka, M.; Okada, H.; Toda, A.; Rastogi, S.; Keller, A. *J. Chem. Soc. Faraday Trans.* **1995**, *91*, 2573
14. Rastogi, S.; Kurelec, L. *J. Mater. Sci.* **2000**, *35*, 5121

15. Hikosaka, M.; Seto, T. *Jpn. J. Appl. Phys.* **1982**, *21*, L332
16. Rastogi, S.; Spoelstra, A.B.; Goossens, J.G.P.; Lemstra, P.J. *Macromolecules* **1997**, *30*, 7880
17. Loos, J.; Tian, M.; Rastogi, S.; Lemstra, P.J. *J. Mater. Sci.* **2000**, *35*, 5157
18. Maxwell, A.S.; Unwin, P.; Ward, I.M. *Polymer* **1996**, *37*, 3293
19. Rastogi, S.; Ungar, G. *Macromolecules* **1992**, *25*, 1445
20. Bair, H.E.; Salovey, R.; Huseby, T.W. *Polymer* **1967**, *8*, 9
21. Hay, I.L.; Keller, A. *J. Polym. Sci.* **1970**, *30*, 289
22. Hoffman, J.D.; Weeks, I.J. *J. Chem. Phys* **1965**, *42*, 1965
23. Wunderlich, B. et al. ATHAS databank. <http://web.utk.edu/~athas>
24. Hikosaka, M.; Amono, K.; Rastogi, S.; Keller, A. *Macromolecules* **1997**, *30*, 2067

Chapter 3

Structure and morphology of nascent UHMW-PE

3.1 Introduction

Most of the modern industrial processes used for synthesis of polyolefins, viz. polyethylenes and polypropylenes, use heterogeneous Ziegler-Natta catalyst systems¹. The mechanism of polymer growth at the surface of a catalyst particle has been studied extensively and several conceptual models have been envisaged over the years to explain the particle growth in olefin polymerisation^{2,3}. One of the most quoted models is the “multigrain model”² in which a catalyst particle (5-100 μm) is made up of several much smaller fragments (0.001-0.5 μm). A monomer diffuses into the particle and polymerises on the surface of the fragments forming microparticles. The growing microparticles remain connected to each other and together they form the macroparticle, which expands progressively. At the end of polymerisation, the polymer particle has a size in order of 100 μm ⁻¹ mm, while the catalyst concentration drops to a few parts per million. In general, replication of the catalyst, i.e. resemblance between an original catalyst particle and a final polymer particle, is observed both at the microparticle and macroparticle levels.

Another type of catalyst system, which is introduced only recently for industrial production of polyolefins, is the single site homogeneous catalyst, generally referred to as the metallocene type⁴. In this type of catalyst, the active sites are available on a molecular scale which provides for their equal accessibility to the monomer molecules and consequently better control over molecular architecture. It has to be realised, however that in practice, for the purpose of handling and powder morphology control, the metallocene-based catalysts have to be supported.

The powders thus obtained, independent of the type of catalyst used for their synthesis, are usually referred to as nascent or virgin powders, as already discussed in Chapter 1. The specific polymerisation conditions, where synthesis temperatures are below the crystallisation temperature of a polymer chain in the reaction medium⁵⁻⁷, lead to unique morphological and structural characteristics of nascent powders⁸⁻¹⁵. As mentioned in Chapter 1 nascent powders of UHMW-PE have drawn lots of attention after it had been recognised that such as-polymerised powders could be drawn at temperatures below the melting point into filaments

possessing a modulus comparable to those obtained for solution-spun fibres¹⁶⁻²⁰ ($E_{\text{gel-spun}}=100-150$ GPa). The high drawability of nascent powders in the solid state was associated to a reduced number of entanglements. The extent to which the nascent powder is disentangled highly depends on polymerisation conditions, notably a type of a catalyst and its activity, synthesis temperature and ethylene pressure⁶³. However, once the nascent powder is molten, the drawing characteristics are lost²¹, which was a rather disappointing result since the initially disentangled state was thought to be also beneficial for standard processing of usually intractable UHMW-PE.

Another interesting feature of nascent powders is their specific crystal morphology, which, due to unique crystallisation conditions (upon polymerisation), does not always follow the classical rules postulated for melt and/or solution-crystallised samples.

One of the striking characteristic of nascent crystals is their high melting temperature (T_m), which surpasses the value of the equilibrium melting point of polyethylene ($T_m^0=141.5^\circ\text{C}^{22}$). In the classical approach, which relates melting temperature to crystal thickness³³, the high values of the melting temperature were associated with the formation of extended chain crystals at the surface of a catalyst^{51,52,54,62}. However Engelen et al.²³ showed, by transmission electron microscopy, that nascent powders of UHMW-PE consist of irregularly stacked, small, folded chain crystals, which upon heating are prone to fast annealing/reorganisation. The reorganisation process during heating has been considered the reason for the high melting point observed in DSC. Many detailed studies, using different experimental techniques, have been performed in order to obtain more insight into the nascent powder morphology and their melting behaviour, yet the results remain rather vague^{13,24-26}. Most of those studies used techniques like irradiation or acid etching, in order to assess the initial morphology of the original powders. Although these techniques are rather well established and widely used²⁷ the probability of affecting the crystalline core remains and the results could be questionable.

In this chapter some prominent features of the nascent powder morphology will be discussed as a function of the catalyst type and the synthesis conditions. Next to the different types of Ziegler-Natta grades, a laboratory grade synthesised with help of a single-site metallocene catalyst will be discussed in terms of initial entanglement density and crystal size. Special attention will be paid to the processes taking place upon heating samples close to, but below, the melting point. Temperature modulated DSC (TMDSC) is shown to be a rather powerful technique to study dynamic processes in nascent UHMW-PE.

3.2 Experimental Section

3.2.1 Materials

Three different types of nascent powders of UHMW-PE were used. They differ in synthesis conditions and catalyst type. Two different grades based on Ziegler-Natta catalysts were selected: (i) a commercial grade 1900CM of Montell, which proved to give the similar results as commercial grades of UHMW-PE grades of DSM and Ticona, and (ii) a laboratory scale Ziegler-Natta powder (ES 1733/35) provided by DSM. The grade synthesised with the help of homogeneous metallocene catalyst was (iii) BW 2601-95 grade also provided by DSM. The molecular characteristics of the powders used in this study are given in Table 3.1.

Table 3.1: Listed details of the nascent UHMW-PE powder grades that were examined in this study.

Grade name	Producer	com./lab.	M_w [g mol ⁻¹]	M_w/M_n	$T_{\text{synthesis}}$ [°C]
1900CM	Montell	commercial	$4.5 \cdot 10^6$	Unavailable	60-80°C
ES (1733/35)	DSM	laboratory scale	$\sim 3.6 \cdot 10^6$	5.65	50°C
BW (2601-95)	DSM	laboratory scale	$\sim 3.6 \cdot 10^6$	2.95	25°C

3.2.2 Compaction of nascent powders in the plate press

All powders were placed between aluminium foil and compacted at 50°C at a maximum pressure of 200 bar. The coherence of the films obtained was only determined by optical inspection.

3.2.3 Wide Angle X-ray Scattering (WAXS) using the Guinier camera

X-ray patterns were obtained with a high resolution Guinier camera having a radius of 57 mm using Cu-K_{α1}-radiation with $\lambda=0.15405$ nm. For quantitative analysis, the intensities from the photographic patterns on the films were converted into numerical values with the aid of a microdensitometer (Joyce, [Leubl@Co.](#), Ltd.) and a data acquisition system. A pattern possessing 12 reflections of polyethylene was obtained. The overlapping reflections were separated by a computer fit program (GRAMS 386). The mean crystal size was obtained from line width analysis, using the method of Wilke et al.²⁸. This method offers the separation of two different contributions to the line width of the X-ray reflections of semicrystalline systems - lattice distortion and mean crystal size. The detailed procedure is given in Appendix 1.

3.2.4 Differential scanning calorimetry (DSC) and temperature modulated DSC (TMDSC)

For conventional DSC as well as TMDSC, samples of 2.5 – 3.5 mg mass were weighted with a precision balance and encapsulated in standard (crimped) Al-pans of well known (and always the same) mass. Almost identical empty pans were used in the reference side and for the zeroline run. Nitrogen was used as purge gas at a rate of 25 ml min⁻¹.

Some basic features of the TMDSC are given in Appendix 2. For TMDSC measurements an underlying heating rate of 0.1 or 0.5 K min⁻¹ was used, which was proved to be low enough to ensure influence on the modulated part of the signal. Time dependent measurements, were performed at different frequencies ranging between 2.5 and 125 mHz. The temperature amplitude T_A was kept low enough to ensure a linear response and in such a way that the heating rate was kept constant for the different frequencies ($\omega \cdot T_A = \text{constant}$). This was done to exclude possible influences of a changed heating rate on the processes in the sample and the measurements. Before further evaluation, the empty pan run (taking the same measuring parameters and phase position) was subtracted from the curve of the sample in order to reduce surroundings and apparatus influences.

Calculation of the apparent heat capacity (magnitude and phase) from the measured heat flow rate was done with a the mathematical procedure described in Reference 29. The proper (frequency dependent) calibration factor for the magnitude of heat capacity, needed to correct for errors caused by heat transfer influences³⁰, was determined by comparing the calculated heat capacity in the liquid state with the respective value from literature²².

3.2.5 Transmission electron microscopy (TEM)

Transmission Electron Microscopy was performed using a Jeol JEM 2000 FX microscope, operated at 80 kV. The powders were embedded at low temperature in Lowicryl resin using a cryosubstitution unit. After embedding, the specimens were trimmed at low temperature (-130°) and, subsequently, treated during 18 hours with a rutheniumtetraoxide(RuO₄)-solution prepared according to Montezinos et al.³¹. During preparation of the staining solution, an exothermal reaction takes place and the temperature can rise fast. The samples were therefore put in the solution cooled to room temperature. Ultrathin sections were obtained at -140°C using a Reichert Ultracut E microtome.

3.3 Results and Discussion

3.3.1 Ductility of different grades of UHMW-PE below the α -relaxation temperature

One of the most prominent features of nascent powders is their ductility below the melting temperature^{61,62}. As already discussed in the introduction, this extraordinary property of nascent powders has been associated with the reduced number of entanglements, which is highly dependent on the synthesis conditions (synthesis temperature and monomer pressure) as well as the type of catalyst⁶³. An indirect method, suitable to qualitatively assess the extent of initial (dis)entanglement of the nascent material, is simple compaction of the powder at low temperatures and subsequent observation of the coherence of the obtained film⁶³. The compaction temperature has been chosen below α -transition temperature ($T_{\alpha} \sim 80^{\circ}\text{C}$), i.e. below temperature of any reorganisation within the crystalline core. The results of compaction of three different powders at 50°C are shown in Figure 3.1.

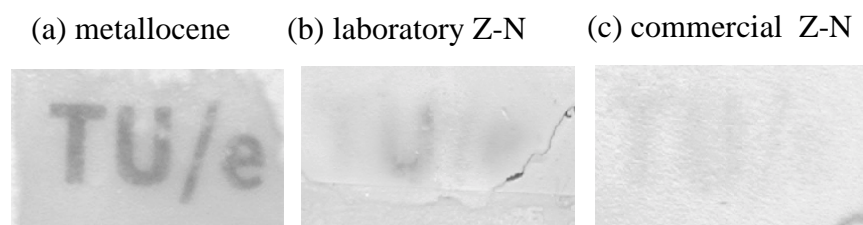


Figure 3.1: *Compaction results of different nascent powders at 50°C .*

It is rather obvious from Figure 3.1a that upon compaction of the metallocene powder a nearly transparent film is obtained suggesting very low initial entanglement density. In the case of the Ziegler-Natta laboratory scale powder (Figure 3.1b) a certain coherence of the compacted film is obtained, though the transparency is much less than in the case of the metallocene grade. The results obtained for commercial grade of Ziegler-Natta powder show no observable coherence, as the compacted powder stayed fully “powdery”. These results can be explained by differences in the catalyst type as well as synthesis conditions. The major difference between supported Ziegler-Natta and homogeneous metallocene catalyst system is that the former possesses a high density of active sites compared to the latter. In case of the Ziegler-Natta catalyst system chains grow relatively close to each other which enable them to “meet” and subsequently entangle. The extent to which chains can entangle highly depends on the catalyst activity and the synthesis conditions (temperature, monomer pressure)²⁰. Commercial grades are known to be synthesised with help of highly active catalysts having high yields. In that case, huge quantities of polymer are produced per gram catalyst (20-100 kg polymer/g catalyst¹) leading to a higher number of initial entanglements. In the case of the laboratory scale samples, which are synthesised with help of a moderately active catalyst, the chains grow slower, and further from each other, leading to initially less entangled systems.

On the other hand, in single-site metallocene catalyst, the active sites are available on a molecular scale and only one polymer chain can be produced per active site. This implies that the chains grow far from each other not having a strong probability of entangling. In this case the possibility of formation of an initially fully disentangled state becomes feasible. In the extreme of producing one single chain per active site, monomolecular crystals could eventually be produced.

N.B.: The author is fully aware that the description giving above might not be the state-of-the-art in terms of modern knowledge concerning polymer catalysis, but it serves the purpose only to make this complex field available for reading this thesis for non-experts.

3.3.2 Crystal dimensions of different grades of UHMW-PE powders before and after annealing at elevated temperature

Crystal dimension and lattice distortions were calculated from the width of the X-ray reflections, obtained by WAXS measurements using a high resolution Guinier camera. The evaluation method of Wilke et al.²⁸ was used for data analysis (Appendix 1). The results for different powder grades recorded at room temperature are given in Table 3.2.

Table 3.2: *Crystal size and lattice distortions as revealed from the calculations of the width of the WAXS reflections obtained with the help of a Guinier camera; for notations see Appendix 2.*

grade	D ₁ [Å]	D ₂ [Å]	D ₃ [Å]	φ [°]	g ₁₁ [%]	g ₂₁ [%]	g ₃₁ [%]	g ₂₂ [%]	g ₁₂ [%]	g _{av} [%]
metallocene	210	93	98	43	0.5	1.5	0.5	0	1.4	0.78
laboratory Ziegler-Natta	211	90	130	36	1.75	1.0	1.3	0.5	0	0.91
commercial Ziegler-Natta	167	127	165	63	0.01	0	0	0	0	0.002

These results show that all nascent powders consist of crystallites having rather small dimensions in the chain direction (fold length, D₃) as well as laterally (D₁ and D₂). However, there are rather significant variations in the parameters obtained for the different types of powders. These differences can be related to the synthesis temperature (T_{synth.}), which is in the case of nascent powders also the crystallisation temperature (T_c) and differs for different grades used in this study (Table 3.1). As expected, the lower the T_c (T_{synth.}) the smaller the crystal dimensions³². From Table 3.2 it can be seen that there is also a difference in percentage of lattice distortions (g_{av}) between the different samples. The metallocene and laboratory scale Ziegler-Natta grade possess rather disordered crystals, while the commercial grade is characterised by very low percentage of crystal distortions. Basically, crystallisation during polymerisation is rather different compared to crystallisation from solution or melt. In

the case of crystallisation during polymerisation, one end of the growing chain is attached to the catalyst surface and consequently, only one end is free. Consequently, the crystal morphology thus created is strongly influenced by the rate of polymerisation and rate of crystallisation.

The results on crystal dimensions obtained by WAXS were confirmed by transmission electron microscopy (TEM). From the TEM micrographs, shown in Figure 3.2, it can be seen that indeed nascent powder consists of small irregularly stacked folded chain crystals having dimensions which correspond to the dimensions obtained from X-ray measurements.

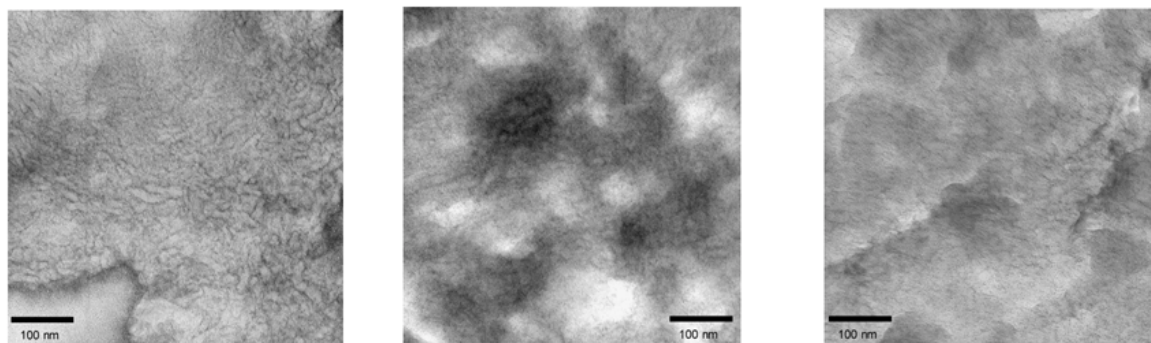


Figure 3.2: TEM micrographs of different grades of nascent powders: (a) metallocene grade, (b) laboratory scale Z-N, (c) commercial Z-N.

These results confirm the ambiguity concerning the high melting point of nascent UHMW-PE ($T_m=141\pm 1^\circ\text{C}$). According to the classical approach, the melting point of folded chain crystals is dependent on crystal dimensions, as shown by Gibbs-Thompson³³ equation (Eq. 2.1; Chapter 2). As already stated in Chapter 2 the last two terms (related to the lateral dimensions) are normally ignored due to relatively large lateral dimensions of melt and/or solution-crystallised samples (in the order of a few microns). However in the case of nascent powders, which consist of crystals having lateral dimensions in the range of few tens of nanometers, as shown in Table 3.2, the last two terms could not be ignored. This means that an even stronger melting point depression would be expected for nascent crystals. The high melting temperatures observed for the nascent powders suggest that these materials are morphologically rather unique and do not obey the classical relationship between T_m and crystal size, as discussed in more detail in Chapter 7.

It has been suggested in literature that the high melting point ($141\pm 1^\circ\text{C}$ for heating rate $1-100^\circ\text{C min}^{-1}$) is a consequence of the fast reorganisation of the small metastable folded chain crystals during heating²³. If the originally low T_m of the initially small crystals is shifted to the higher values due to a reorganisation process during heating, there must be an enormous thickening taking place which will finally lead to crystals having a thickness close to the extended chain crystals. In order to assess this thickening process upon heating, WAXS measurements using Guinier camera have been performed on samples which have been

annealed at 120°C for 20 minutes and 36 hours. The results of crystal dimensions and lattice distortions are shown in Table 3.3.

Table 3.3: *Crystal size and lattice distortions of annealed powders as revealed from the calculations of the width of the WAXS reflections obtained with help of Guinier camera. The WAXS patterns have been recorded at room temperature after indicated annealing time at 120°C.*

metallocene	D ₁ [Å]	D ₂ [Å]	D ₃ [Å]	φ [°]	g ₁₁ [%]	g ₂₁ [%]	g ₃₁ [%]	g ₂₂ [%]	g ₁₂ [%]	g _{av} [%]
20' @ 120°C	225	140	210	49	0.4	0.6	0.5	0	0.0	0.3
36h @ 120°C	270	165	265	60	0	0	0	0	0	0

laboratory Ziegler-Natta	D ₁ [Å]	D ₂ [Å]	D ₃ [Å]	φ [°]	g ₁₁ [%]	g ₂₁ [%]	g ₃₁ [%]	g ₂₂ [%]	g ₁₂ [%]	g _{av} [%]
20' @ 120°C	240	110	180	44	0.7	0.8	0.9	0	1	0.68
36h @ 120°C	210	120	240	58	0	0	0	0	0	0

commercial Ziegler-Natta	D ₁ [Å]	D ₂ [Å]	D ₃ [Å]	φ [°]	g ₁₁ [%]	g ₂₁ [%]	g ₃₁ [%]	g ₂₂ [%]	g ₁₂ [%]	g _{av} [%]
36h @ 120°C	250	190	190	60	0.01	0	0	0	0	0.002

It is rather obvious that the reorganisation does take place leading to thicker and more perfect crystals. However, the thickening process does not lead to crystals whose dimensions would approach the dimensions of the extended chain crystals and therefore it could not contribute to the extensive increase in the measured T_m . Figure 3.3 shows TEM micrographs of the nascent powders after annealing at 120°C. The crystal dimensions found on the TEM micrographs match the dimensions obtained with the help of X-ray measurements.

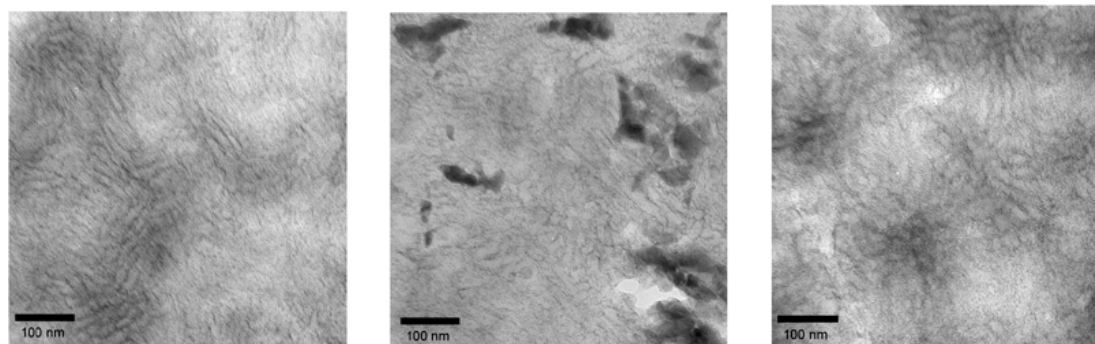


Figure 3.3: *TEM micrograph of the different powders annealed at 120°C for 30 hour: (a) metallocene grade, (b) laboratory scale Z-N, (c) commercial Z-N.*

3.3.3 Dynamics of the reorganization process during heating UHMW-PE powder as revealed by TMDSC

TMDSC is rather a new method which offers a possibility to study dynamic (time-dependent) processes occurring inside of the sample upon small temperature fluctuations. Some fundamental facts on this method are given in Appendix 2. In this section an interesting features related to the “reorganisation process” taking place while heating nascent materials will be described in terms of the results obtained by this technique. For clarity reasons the discussion will be divided into two parts. In the first one, the treatment of the TMDSC results on one powder grade will be discussed in detail in order to exhibit the ability of the method to assess valuable information on the kinetics of the process taking place on heating the nascent material. In the second part of this section TMDSC results of different grades will be presented and mutually compared which will lead to interesting and rather unique observations related to the initial morphology of the different powders.

3.3.3.1 TMDSC measurements on nascent UHMW-PE powder (laboratory scale Ziegler-Natta grade; ES 1733/35)

In the following discussion the periodic part of the TMDSC signal will be only considered in terms of the magnitude (modulus, absolute value) of the apparent (related to the modulation) complex heat capacity (c_p magnitude). The phase of the complex heat capacity will not be taken into account because the precise calibration of this quantity is still a problem and it can therefore lead to misplaced conclusions. All the results within this section are related to the laboratory scale Ziegler-Natta grade of the nascent powder.

In Figure 3.4 the c_p magnitude of the nascent UHMW-PE is plotted together with the c_p plot calculated from the heat flow obtained by conventional DSC measurements. Literature values²² of the static (thermodynamic) c_p of the 100% amorphous and 100 % crystalline phase of polyethylene are also included in the figure.

In accordance with Eq. A2.6 the excess heat capacity is defined as the difference between the static c_p and measured c_p curves. From this figure it is rather obvious that the c_p magnitude signal of the nascent material shows a rather large excess heat capacity in the temperature region above 80°C. In this region the c_p magnitude curve is much above the conventional DSC curve, suggesting that there is an extra process taking place upon heating nascent material which can only be detected by the the modulated part of the heat flow signal.

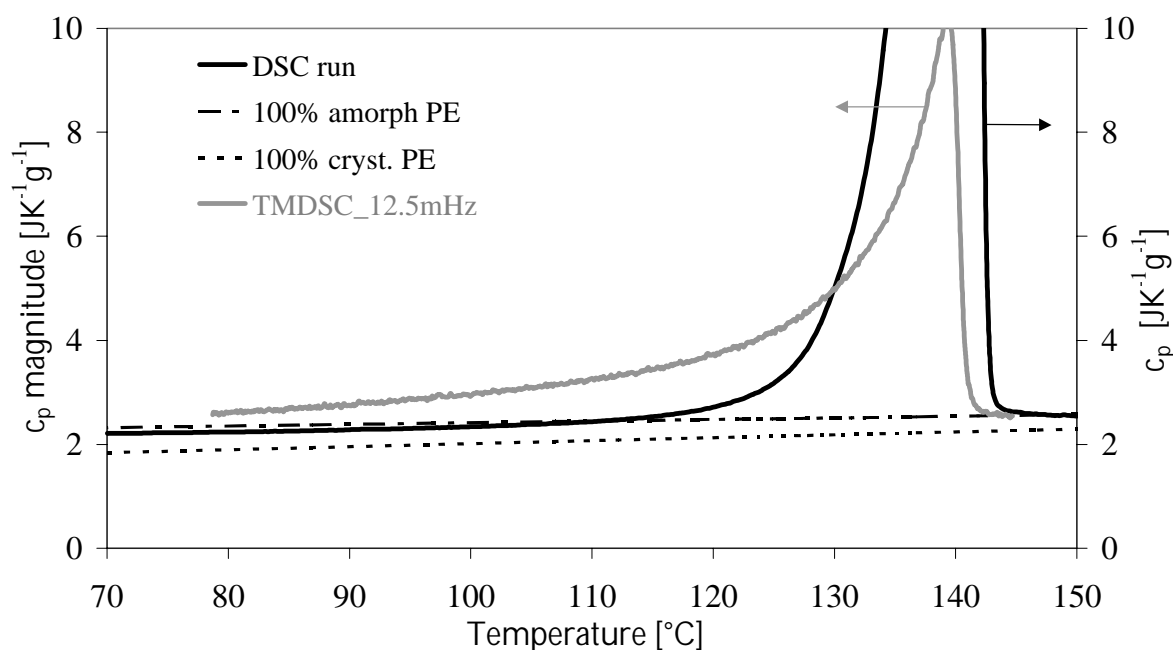


Figure 3.4: c_p magnitude curve of the nascent powder (Ziegler-Natta laboratory grade) upon 1st heating run (frequency: 12.5mHz, amplitude: $T_A=53$ mK, underlying heating rate: 0.5 K min^{-1}) together with the c_p plot of the conventional DSC (heating rate: 10 K min^{-1}) and literature²² values of static c_p for 100% crystalline and 100% amorphous polyethylene.

These results are rather remarkable because normally on heating melt-crystallised semicrystalline samples the c_p magnitude signal lays always below or on the top of the underlying curve (or conventional DSC curve) in the temperature region below melting as well as within the melting itself³⁴⁻³⁶. This means that in the “pre-melting region” (temperature region below T_m) of melt-crystallised samples there is no kinetic process taking place which would be able to follow temperature fluctuations and respond in the terms of excess heat flow. The melting process itself is rather fast and therefore unable to follow the oscillatory changes of the temperature, which makes the c_p magnitude signal always under the underlying one within the melting region of the polymers. This feature characteristic for melt-crystallised samples can even be seen for the second heating run of the same UHMW-PE grade, as shown in Figure 3.5.

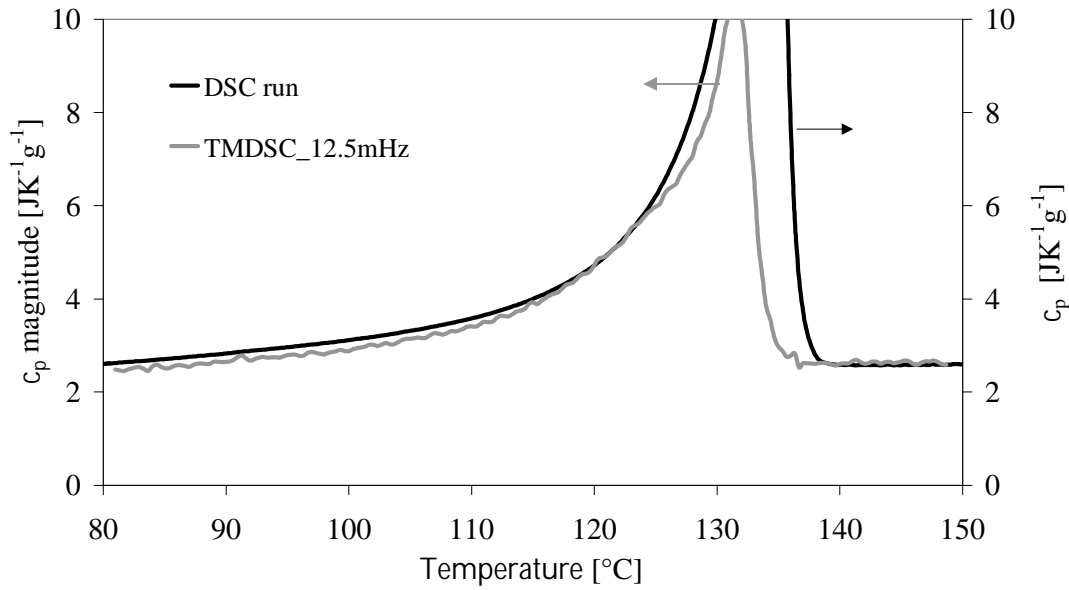


Figure 3.5: c_p magnitude of 2nd run of the nascent powder (frequency: 12.5 mHz, amplitude: $T_A=53$ mK, underlying heating rate: 0.5 K min^{-1}) together with c_p calculated from the 2nd run of the conventional DSC (underlying heating rate: 0.5 K min^{-1}).

These observations suggest that the excess heat capacity observed in the first heating run of the nascent material is something rather genuine for the nascent morphology and therefore stimulated further experiments using TMDSC in order to gain more information on the additional effect seen in TMDSC.

The main condition required to observe the signal in TMDSC is that the process is time dependent and that it reacts on temperature changes. In order to study kinetics of this process, frequency dependent measurements have been performed. The results of these measurements are shown in Figure 3.6. It can be seen that with increasing frequency the excess heat capacity drops to the value of the underlying curve which suggests that the process in question is time dependent. From these measurements the time scale of the process can be obtained.

The time law for a simple relaxation reads as follows³⁷:

$$C_p^{\text{ex.}} = C_{p,0}^{\text{ex.}} \cdot e^{-\frac{t}{\tau}} \quad (3.1)$$

where $C_{p,0}^{\text{ex.}}$ is the start value at $t=0$ and τ relaxation time.

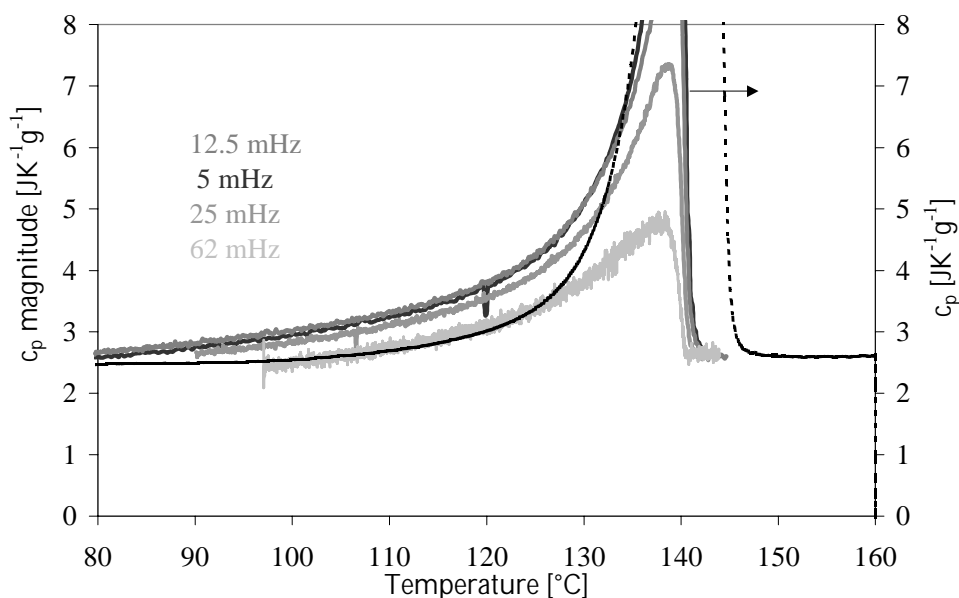


Figure 3.6: c_p magnitude curves of nascent UHMW-PE on 1st heating at different frequencies together with the c_p curve obtained by the conventional DSC at 10 K min^{-1} (underlying heating rate of modulated measurements: 0.5 K min^{-1}).

In order to obtain the time constant of the process the difference between the underlying c_p obtained by conventional DSC and the c_p magnitude (Δc_p) has been plotted against frequency. In this treatment not the real excess values (difference between the c_p magnitude signal and the static c_p ; as in eq. A2.6) have been taken as a measure of the process but the differences between conventional DSC and magnitude signal. This has been done in order to relate this phenomenon only to the quantity of the excess c_p which is genuine for the additional kinetic process visible only in the periodic part of the TMDSC signal of the first run.

Figure 3.7 shows frequency dependence of the process at two different temperatures. From the $\log\omega$ - $\log\Delta C_p$ plot, by extrapolating the asymptotes from very low and very high frequency, it is possible to obtain the intersection point ω_0 , which will give the reciprocal of time constant τ . The time constant of this process at 110°C is $5.4 \pm 0.5\text{ s}$ ($\omega_0 = \frac{1}{\tau} = 0.18\text{ s}^{-1}$). By entering the value of the so-called corner frequency, f_0 ($f_0 = \omega_0/2\pi$) and temperature into activation diagram of polyethylene it can be seen that the process in question fits exactly to the α_2 -process of polyethylene (Figure 3.8).

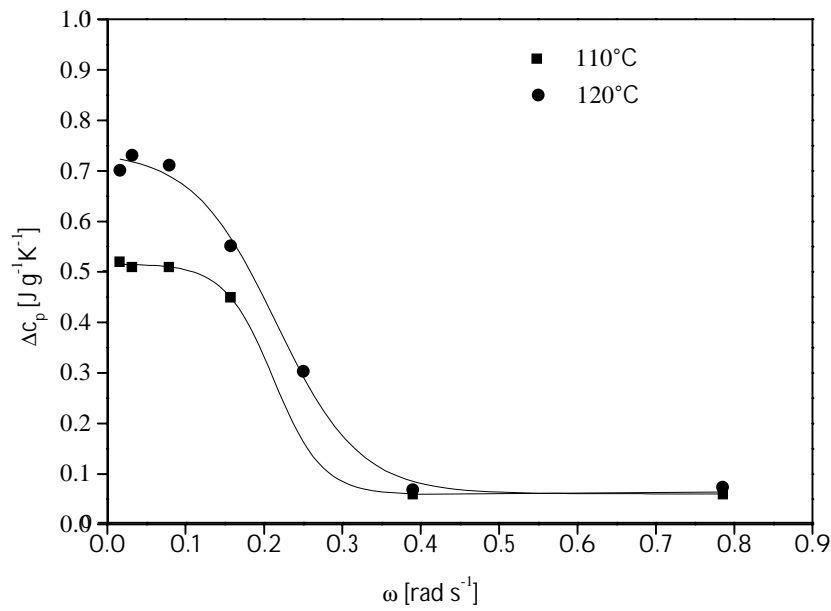


Figure 3.7: Change of the excess heat capacity (in this case difference between c_p magnitude of modulated and c_p calculated from the conventional DSC measurement) with frequency for two different temperatures (110°C and 120°C). Sigmoidal fit similar to the one used in ref 37 has been applied..

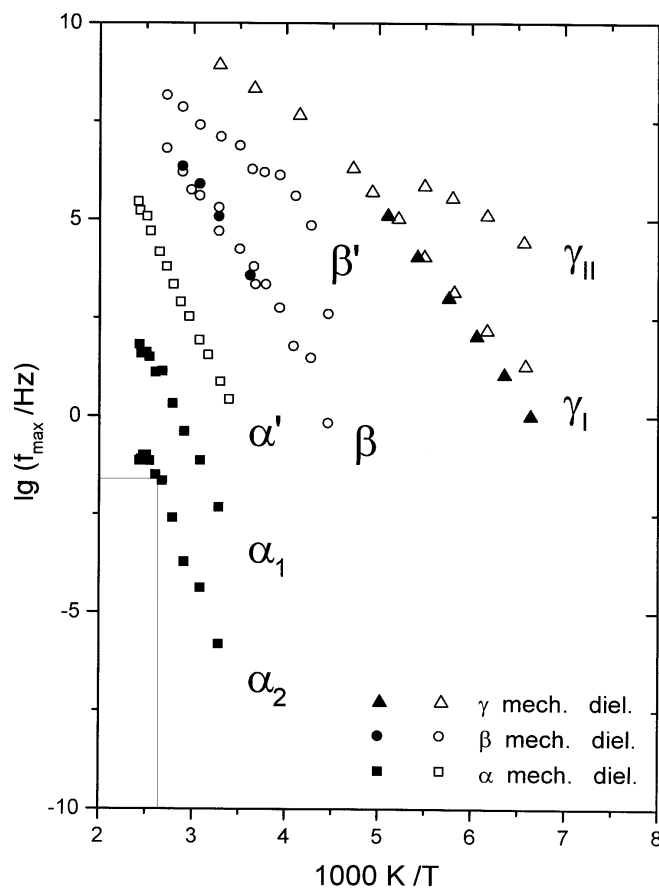


Figure 3.8: Activation diagram of the relaxation process in polyethylene³⁸.

As already stated above, the process in question has to be time dependent and has to react on temperature changes in order to be visible in TMDSC. Temperature dependence can be assessed by performing quasi-isothermal experiments at different temperatures in the temperature region of interest ($>80^{\circ}\text{C}$). In these experiments underlying heating rate is kept zero while small temperature fluctuations occur around the chosen isotherms. The results are shown in Figure 3.9.

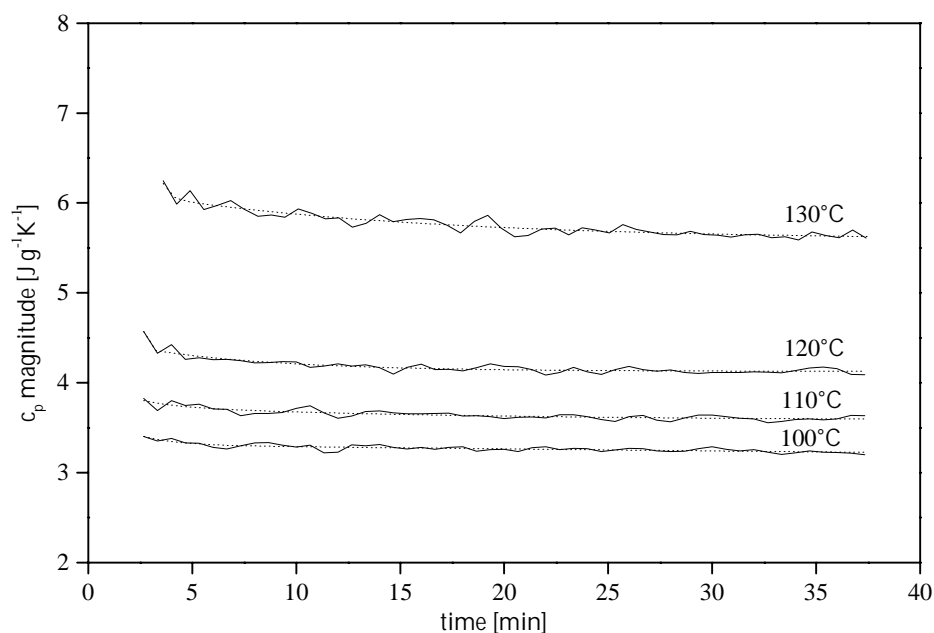


Figure 3.9: c_p magnitude curves from quasi-isothermal TMDSC measurements of nascent UHMW-PE at different temperatures together with the fit (dotted) of two exponential curves with values in Table 3.4.

Obviously the excess heat capacity changes with temperature and in time. With a proper mathematical fitting program the curves have been further analysed. For the 130°C measurement it was found, that a sum of two exponential functions with different time constants is able to describe the measured curves within the limits of our measurement accuracy (which of course are somewhat noisy) (see Figure 3.9). The same procedure has been used for the other temperatures as well and the results are listed in Table 3.4.

Table 3.4: Evaluation of the curves from Fig. 3.9 as a sum of two exponential functions

Temperature [$^{\circ}\text{C}$]	Total change of excess c_p [$\text{J g}^{-1} \text{K}^{-1}$]		Time constants [min]	
	90	0.6	1.1	5
100	0.4	1.1	1.5	610
110	0.4	1.0	2.5	510
120	0.4	1.1	3.5	360
130	0.1	1.1	4	165

Because of the rather small (but nevertheless significant) changes of the amplitude within the relatively short measuring time these values are not fully accurate ($\pm 10\%$), but they surely show clear tendency. The first exponential (with the shorter time constant) may be connected with the heat transfer from the apparatus to the sample. On every sudden change from ambient to the isothermal measuring temperature the DSC needs some time to come to equilibrium conditions. This time constant depends on the measuring and initial conditions of the DSC (and the temperature step width from load to isothermal condition) rather than on the measuring temperature in question. These conditions were not kept identical for all experiments what may have caused the unsystematic scatter of this time constant. The DSC used in this study needs some minutes after starting a run to come to steady state conditions (even for conventional runs). Therefore the first decrease of the measured magnitude can not be related to a relaxation process taking place in the sample. This is further supported by the finding that such an exponential has been found even for a sapphire sample, which surely does not contribute with a time dependent heat capacity.

The second time constant characterises undoubtedly a time dependent process occurring in the sample itself. As it can be seen from Table 3.4 this time constant depends significantly on temperature. The related total change of excess c_p is the change of excess heat capacity (for infinite times) connected with the exponential decay of this process (Table 3.4) and it can be written as follows:

$$c_p^{\text{ex}} - c_{p,\infty}^{\text{ex}} = (c_{p,0}^{\text{ex}} - c_{p,\infty}^{\text{ex}}) \cdot e^{-\frac{t}{\tau}} \quad (3.2)$$

This quantity is obviously independent of temperature which means that the relaxation of the process always occurs within the same absolute range of the c_p magnitude. This result suggests that the process in question can not be related to melting or pre-melting because the total change of excess c_p would in that case highly depend on temperature. Of course that also means that this process can not be related to possible reversible melting which exhibits similar effects upon quasi-isothermal experiments, as reported extensively in literature^{39,40}. In order to assess the information on irreversibility of the process, samples which were annealed at different temperatures (during quasi-isothermal experiments), were subsequently heated in TMDSC. Results of these measurements are shown in Figure 3.10.

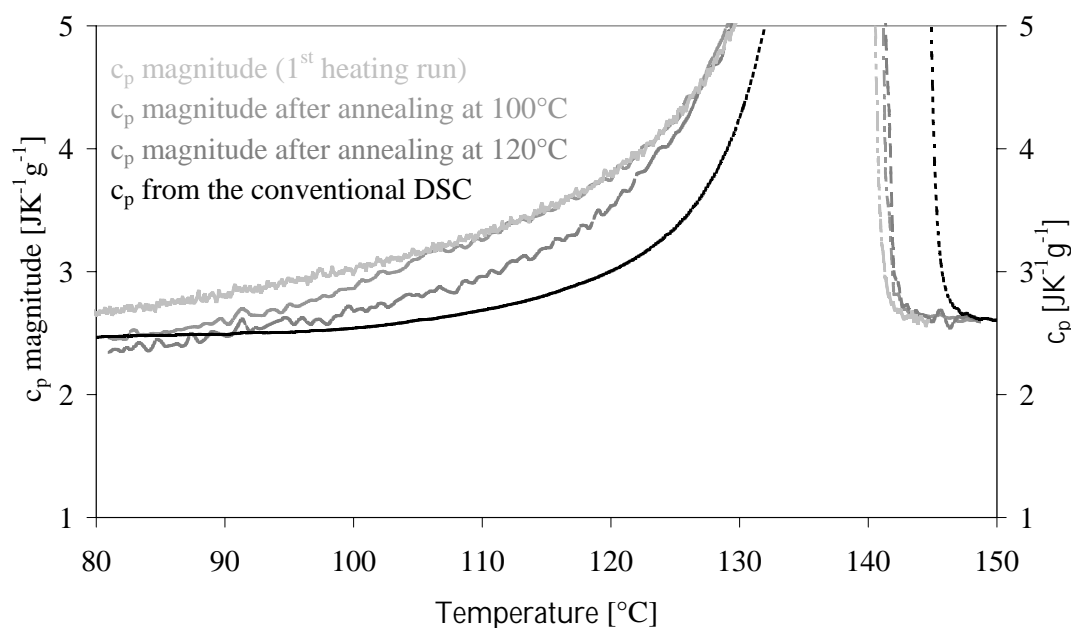


Figure 3.10: c_p magnitude of the 1st heating run together with the TMDSC runs of the samples which have been annealed at 100°C, 110°C and 120°C (frequency: 12.5 mHz, amplitude: $T_A=53$ mK, underlying heating rate: 0.5 K/min). The c_p calculated from the conventional DSC signal is also plotted.

It can be seen that the excess heat capacity of the annealed samples is much lower for the temperature region below than above the corresponding annealing temperature. Up to the temperatures below the annealing temperature the c_p magnitude of the annealed sample lies below the TMDSC signal of the first run. At temperatures above the corresponding annealing temperatures all curves (1st heating run as well as heating runs after quasi isothermal experiments) come together possessing excess heat capacity identical to the first heating run. It should not be forgotten that the annealing times in these experiments were much shorter than the calculated relaxation times, which explains the still visible excess values of c_p present in the annealed sample below the annealing temperatures. Therefore it can be concluded that the temperature dependent process is irreversible and fully genuine to the initial nascent morphology.

If we assume that the temperature dependence of the relaxation time follows the simple Arrhenius law ($\tau = \tau_0 \cdot e^{\frac{E_a}{RT}}$), which should be valid for thermally activated processes, it is possible to obtain the activation energy of the process by plotting $\log\tau$ against $1/T$. From the slope of the straight line the value for an activation energy (E_a) of roughly 40 kJ/mol could be obtained for the process which takes place on annealing the sample at the chosen temperatures.

From the activation diagram of polyethylene, on the other hand, an activation energy of 46 kJ/mol has been obtained. From this we can conclude that the process visible in TMDSC is related to the α_2 process in polyethylene.

A question that arises now is what makes the α_2 -process visible in TMDSC with nascent material and not in the melt-crystallised counterpart. The α_2 -relaxation process, which is connected with the chain diffusion through the crystal, is always present in polyethylene in the temperature region above 80°C. In order to be able to relate this phenomenon to the nascent morphology, TMDSC measurements have been performed for all three grades of UHMW-PE and will be compared in the following section.

3.3.3.2 Reorganisation processes on heating different powders of UHMW-PE as revealed by TMDSC

Figure 3.11 shows the c_p magnitude at different frequencies for (a) the metallocene grade and (b) Montell grade together with the corresponding conventional DSC curves.

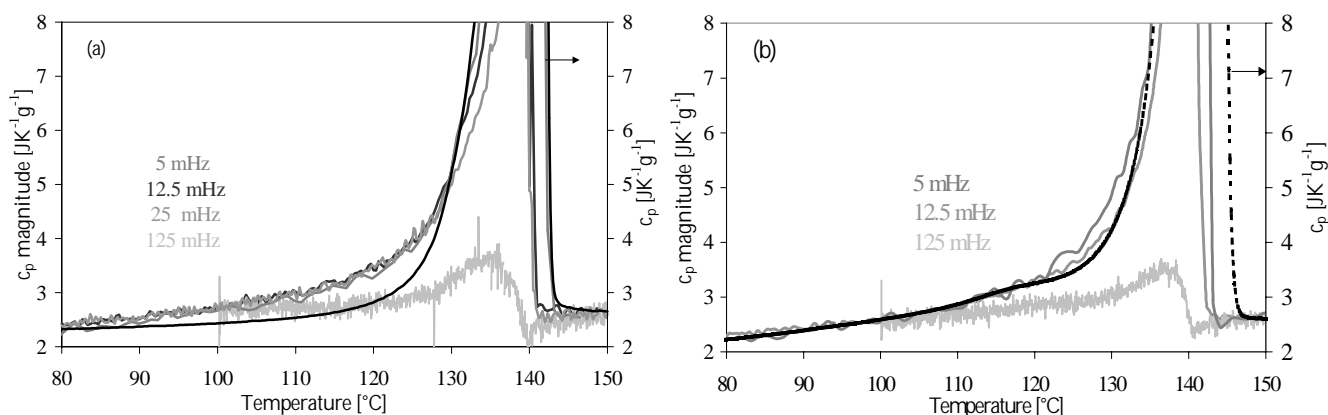


Figure 3.11: c_p magnitude of (a) the metallocene grade and (b) Ziegler-Natta commercial grade at different frequencies as indicated at the figure. c_p obtained by conventional DSC (heating rate 10°C/min) is also plotted for each sample.

There is rather obvious difference in the effects observable in TMDSC signal between these two samples in the temperature region between 80°C and 125°C. For the metallocene grade excess heat capacity is comparable to the one of the Ziegler-Natta laboratory scale sample presented in Figure 3.6. For the commercial Ziegler-Natta grade the excess heat capacity within the whole temperature region of interest is negligible, which makes it comparable with the effects seen in the melt-crystallised samples displayed in Figure 3.5. The morphological differences between different grades in the terms of initial entanglement density and crystal size have been already discussed in the Section 3.3.1 and 3.3.2. It has been found in Section 3.3.2 that the laboratory scale Ziegler-Natta and metallocene grades possess highly distorted small folded chain crystals which slightly thicken and order upon heating (Table 3.3). The

thickening process itself does not necessarily involve any enthalpy change, which obviously does not occur since the net heat flow as measured in the conventional DSC is almost zero. This means that the excess heat capacity observable by TMDSC can not be associated with a net enthalpy change. However, disappearance of the defects (distortions) from the crystal would lead to a decrease in enthalpy which means that this process is connected to the heat flow and could be visible in the modulated signal. It has been suggested in the previous section that the process observable in the TMDSC signal corresponds to the α_2 -relaxation process of polyethylene.

The question that arises is what is the connection between the α_2 -relaxation process and the disappearance of the crystal defects. If the α -process is regarded as diffusion of dislocations in chain direction⁴¹ one can imagine that this process would lead to disappearance of the defects of any kind if there is “space” enough for this transport. Therefore the α_2 -relaxation process can in that respect be considered as a process through which the defects (dislocations) can “escape” from the crystal. Such a process should be easier in the case of highly disentangled systems. Perfectioning of the crystals upon annealing is rather known and well established phenomenon in the field of material science. For polymer systems, however, creation of distortion free crystal upon annealing is rather difficult⁴². It has been reported in literature⁴³ that for the melt-crystallised as well as solution-crystallised polyethylene the number of crystal distortions after annealing at elevated temperatures decreases substantially but it never leads to crystals fully free of distortions. Creation of distortion free crystals in the case of nascent material is rather unique in polymer systems and it can be related to the unprecedented initial morphology created during crystallisation on the catalyst surface during synthesis at low temperatures. For commercial grade powder (Montell), which is initially almost fully free of distortions (Table 3.2), no excess heat capacity could be measured during the first run since there were no distortions left to be removed upon heating. These results show that the additional, time dependent process, which occurs in the laboratory scale nascent powders upon heating is perfectioning of the crystals through the α_2 relaxation process which becomes feasible due to the absence of constraints (entanglements).

When discussing the TMDSC results it should not be disregarded that the c_p magnitude is an absolute quantity which does not provide the information if the process is endothermic or exothermic. The c_p calculated from the net heat flow (conventional DSC signal) is in the case of nascent powders rather low. On comparing Figures 3.4 and 3.5 it can be seen that in the case of melt-crystallised samples the difference between static c_p and c_p of the conventional DCS signal in pre-melting region is much higher than in the case of the nascent powder upon 1st heating run. This implies that for the nascent material the total net heat balance upon 1st heating run is zero (or close to zero), suggesting that there is at least one endothermic and one

exothermic process taking place. It has been suggested above that the process detected by TMDSC is disappearance of the distortions from the crystal with the help of the α_2 process. This process of distortions removal is expected to lead to exothermic effects. The question that arises is can we detect something of exothermic process by conventional DSC as well, since the effects are relatively high in TMDSC. Precise experiments using conventional DSC have been performed in the temperature region before melting. The samples were heated to 125°C (just below the onset of the melting), cooled down to 30°C and heated up again to 125°. The results of these measurements for three different grades are shown in Figure 3.12.

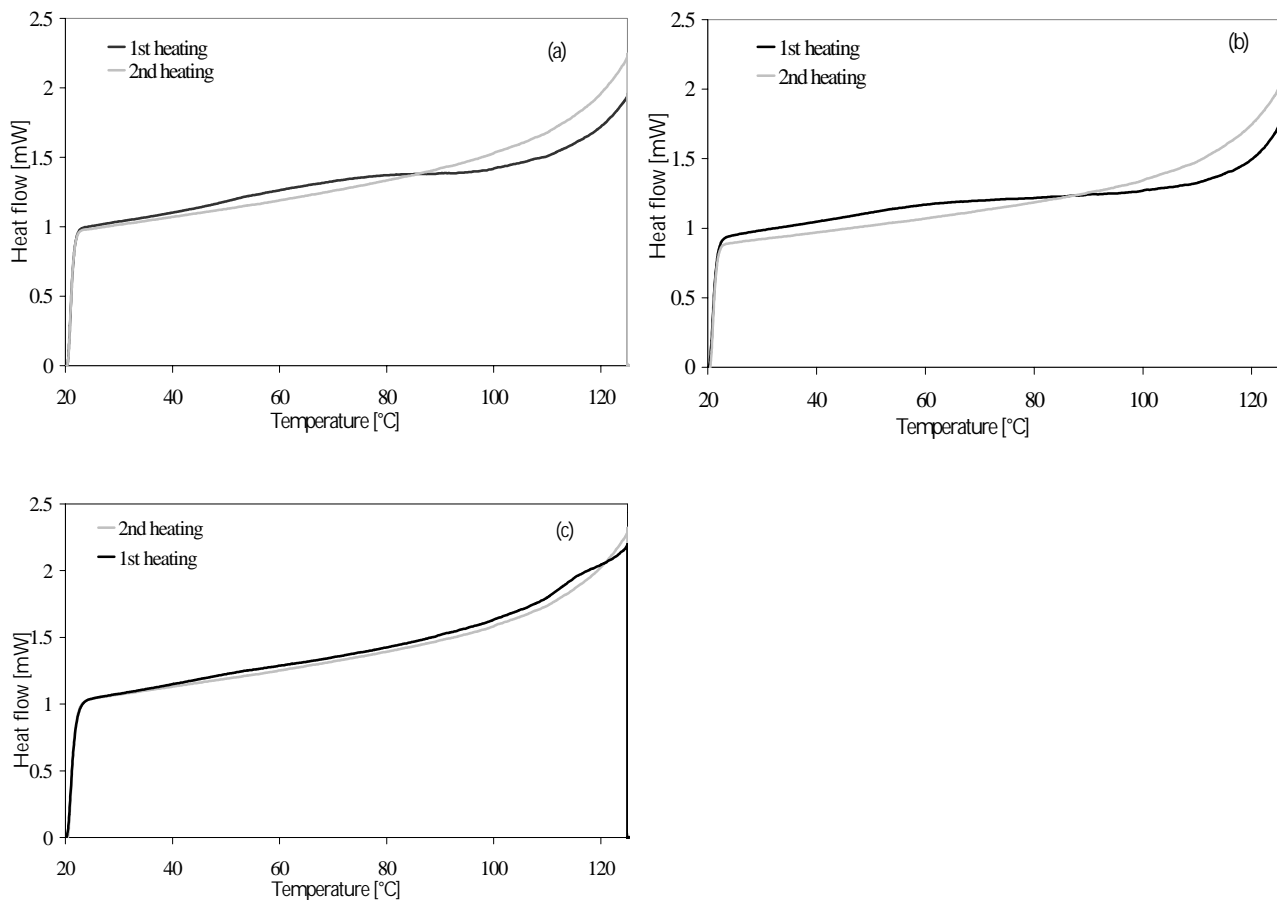


Figure 3.12: Conventional DSC of three different grades of UHMW-PE: (a) laboratory scale Ziegler-Natta, (b) metallocene grade and (c) commercial grade of UHMW-PE. Samples were heated up to 125°C at 10°C min⁻¹ (1st run), cooled and heated again up to same temperature of 125°C (2nd run).

It can be seen that for laboratory scale Ziegler-Natta and metallocene grade there is a very small exotherm observable during 1st heating compared to the 2nd run in the temperature region between 80°C and 125°C. This process is not visible for the commercial Ziegler-Natta grade. The observable exotherm is irreversibly genuine to the initial nascent morphology and therefore it can be associated to the process of reducing crystal defects like discussed above.

3.4 Conclusions

In this chapter the unique features of the nascent morphology have been investigated for different powder grades of UHMW-PE obtained by different catalysis. It has been shown that initial morphology of the nascent powders highly depends on synthesis conditions as well as on the type of the catalyst. A single site metallocene catalyst produces highly disentangled nascent powders, which upon compaction below α relaxation temperature form uniform transparent film, indicating that the powder is rather ductile. For supported Ziegler-Natta grades the number of initial entanglements will depend on the reaction temperature and catalyst activity. The lower the synthesis temperature and catalyst activity the lower the initial entanglement density. All nascent powders investigated in this study consist of folded chain crystals having very small dimensions in thickness direction as well as laterally. Powders synthesised at lower temperatures (laboratory scale Ziegler-Natta and metallocene grade) possess rather high percentage of lattice distortions. Such small metastable crystals are able to thicken and perfection upon heating as revealed by WAXS measurements using Guinier camera. After annealing nascent powders at elevated temperature (still below melting temperature) it has been shown that the crystals thicken not more than twice of the initial crystal size which means that the crystal dimensions stay relatively small. These results contradict the concept that the high melting temperature usually observed for the nascent powders is consequence of the fast thickening process during heating. The reorganisation process occurring upon heating UHMW-PE has been studied in details by temperature modulated DSC (TMDSC), which has been shown to be powerful in kinetic study of dynamic processes taking place upon heating nascent material. The excess value of the magnitude of apparent (related to the modulation) heat capacity (c_p magnitude) has been observed during 1st heating run in TMDSC which suggested that there is an extra process taking place in the nascent material which is irreversible and rather unique for the nascent morphology. The process in question has been identified as the α_2 relaxation process of polyethylene. The α_2 process enables the chain diffusion within the crystal along the chain axis and it is intrinsic to all polyethylene as long as crystallinity is sufficiently high. The fact that the α_2 relaxation process is visible in TMDSC for the nascent powders and not for the other polyethylene counterparts suggests that it has to be related to a certain dynamic process which becomes feasible due to the inherent features related to the nascent morphology. The thickening of the crystals can not lead to such thermal effects since it does not necessarily involves any enthalpy change which is necessary to observe the signal in conventional as well as temperature modulated DSC. However perfectioning, which would involve disappearance of the lattice distortions from the crystal, must involve enthalpy change and therefore can be related to the process visible in TMDSC. It has been shown that the α_2 process can be

considered as a mechanism through which disappearance of distortions from the crystal takes place. Such successive reduction of distortions is possible in the case of nascent powders due to the unique morphology and highly disentangled state. The interesting feature that could also be obtained from TMDSC measurements is the insight into kinetics of the perfecting process which highly depends on the initial morphology, notably initial entanglements density. It will be shown in Chapter 5 that the initial morphology, notably crystal topology, plays an important role in choosing an adequate processing route for the nascent powders.

The results presented in this chapter strongly suggest that the anomaly of the high melting temperature of nascent crystals ($\sim 141^\circ\text{C}$) can not only be explained by the reorganisation process during heating. A new concept, which invokes kinetics as a possible cause for the high measured melting point of nascent crystals will be addressed in Chapter 7.

3.5 References

1. Moore, E.P. *The Rebirth of Polypropylene: Supported Catalyst: how the people from Mentedison laboratories revolutionized the PP industry*, Hanser Publishers; Munich, **1998**
2. Hutchinson, R.A.; Chen, C.M.; Ray, W.H. *J. Appl. Polym. Sci.* **1992**, *44*, 1389
3. Laurence, A.J.; Chiovetta, M.G. in: Reichert K.H., *Polymer Reaction Engineering*, Hanser Publishers: Munich, **1983**
4. Scheirs, J.; Kaminsky, W. *Metallocene-based polyolefins: preparation, properties and technology*, Wiley: Chichester, **2000**
5. Mackie, P.; Berger, M.N.; Grieverson, B.M.; Lawson, D. *Polym. Lett.* **1967**, *251*, 563
6. Chanzy, H.D.; Revol, J.F.; Marchessault, R.H.; Lamande, A. *Kolloid Z.Z. Polymere* **1973**, *251*, 563
7. Keller, A.; Willmouth, F.M. *Macromol. Chem.* **1969**, *121*, 42
8. Chanzy, H.; Day, A.; Marchessault, R.H. *Polymer* **1967**, *8*, 567
9. Chanzy, H.; Marchessault, R.H. *Macromolecules* **1969**, *2*, 108
10. Chanzy, H.; Bonjour, E.; Marchessault, R.H. *Colloid Polym. Sci.* **1974**, *252*, 8
11. Munoz-Escalona, A.; Parada, A. *J. Crystal. Growth.* **1980**, *48*, 250
12. Munoz-Escalona, A.; Hernandez, J. G.; Gallardo, J.A.; Sustic, A. *Advances in Polyolefins*, Plenum Press: New York, **1987**
13. Phillips, R.A. *J. Polym. Sci: Part B: Polym. Phys.* **1998**, *36*, 495
14. Lehmus, P.; Rieger, B. *Science* **1999**, *285*, 2081
15. Kageyama, K.; Tamazawa, J.; Aida, T. *Science* **1999**, *285*, 2113
16. Zacharaiades, A.E.; Watts, M.P.C.; Kanamoto, T.; Porter R.S. *J. Polym. Sci.: Polym. Lett. Ed.* **1984**, *22*, 133
17. Kanamoto, T.; Ohama, T.; Tanaka, K.; Takeda, M.; Porter, R.S. *Polymer* **1987**, *28*, 1517
18. Smith, P.; Chanzy, H.D.; Rotzinger, B.P. *Polym. Com.* **1985**, *26*, 258
19. Smith, P.; Chanzy, H.D.; Rotzinger, B.P. *J. Mater. Sci.* **1987**, *22*, 523
20. Rotzinger, B.P.; Chanzy, H.D.; Smith, P. *Polymer* **1989**, *30*, 1814
21. Bastiaansen, C.W.M.; Meyer, H.E.H.; Lemstra, P.J. *Polymer* **1990**, *31*, 1435

22. Wunderlich, B. et al. *ATHAS databank*. <http://web.utk.edu/~athas>
23. Tervoort-Engelen, Y.M.T.; Lemstra, P.J. *Polym Com.* **1991**, 32, 345
24. Egorov, V.M.; Ivankova, E.M.; Marikhin, V.A.; Myasnikova, L.P.; Baulin, A.A. *Polymer Science, Ser. A* **1999**, 41, 1779
25. Cook, J.T.E.; Klein, P.G.; Ward, I.M.; Brain, A.A.; Farrar, D.F.; Rose, J. *Polymer* **2000**, 41, 8615
26. Joo, Y.L.; Han, O.H.; Lee, H.-K.; Song, J.K. *Polymer* **2000**, 41, 1355
27. Keller, A. *Developments in Crystalline Polymers-1*, Applied Science Publisher Ltd.; London, **1982**
28. Wilke, W.; Martis, K.W. *Colloid Polym. Sci.* **1974**, 252, 718
29. Höhne, G.W.H. *Thermochim. Acta* **1997**, 304/305, 209
30. Höhne, G.W.H. *Thermochim. Acta* **1999**, 330, 93
31. Montezinos, D., Wells, B.G. and Burns, J.L. *J. Polym. Sci., Polym. Lett. Ed.* **1985**, 23, 421
32. Wunderlich, B. *Macromolecular Physics: Crystal Melting*, Academic Press: London, **1980**.
33. Hoffman, J.D.; Weeks, I.J. *J. Chem. Phys.* **1965**, 42, 4301
34. Toda, A.; Tomita, C.; Hikosaka, M.; Saruyama, Y. *Polymer* **1998**, 39, 5093
35. Saruyama, Y., *J. Therm. Anal.* **2000**, 59, 271
36. Schick, C.; Wurm, A.; Mohamed, A. accepted for NATAS
37. Höhne, G.W.H.; Kurelec, L. *Thermochim. Acta*, in press
38. Mayr, P.U. *Ph.D. thesis*, University Ulm, **1999**
39. Okazaki, I.; Wunderlich, B. *Macromolecules* **1997**, 30, 1758
40. Androsch, R.; Wunderlich, B. *Macromolecules* **2000**, 33, 9076
41. Meier, D.J. *Molecular Basis of Transitions and Relaxations*, Gordon and Breach Science Publishers: New York, **1978**
42. Wunderlich, B. *Macromolecular Physics: Crystal Nucleation, Growth, Annealing*, Academic Press: London, **1976**
43. Vogel, W. *Kolloid-Z. u. Z. Polymere* **1972**, 250, 499

Chapter 4

Phase transformations in nascent UHMW-PE powder at elevated pressure as revealed by in-situ Raman spectroscopy

4.1 Introduction

The role of the hexagonal phase in crystallisation of polyethylene has been discussed in detail in Chapter 2. It has been shown that the stability of the hexagonal phase highly depends on the initial crystal size. For small lamellar crystals of 12 nm, the appearance of the hexagonal phase has been observed even at pressures of 1600 bar, which is much below the equilibrium triple point ($P_Q \sim 4000$ bar; $T_Q = 250^\circ\text{C}$)². As discussed before, a prominent feature of the hexagonal phase is the enhanced molecular mobility in the chain direction, which ultimately leads to the formation of extended chain crystals. The structural characteristics of the hexagonal phase in polyethylene have been extensively studied using different experimental techniques (high pressure DTA^{3,4,5}, dilatometry^{6,7}, wide angle X-ray scattering^{8,9}, NMR^{10,11}). Detailed studies on the crystallographic parameters of the hexagonal phase revealed the absence of the positional long range order in the chain direction, and accordingly the lack of crystallographic register along this direction¹². The molecular packing of the phase has therefore been defined as “a liquid-crystalline” one, though other terms like conformational disordered (condis) phase or columnar mesophase are often used in literature¹³.

The high degree of the conformational disorder in the hexagonal phase has been studied by NMR^{10,11} and vibrational spectroscopy^{14,15}. Raman spectroscopy has been widely used to follow changes in the chain conformation of polyethylene in the hexagonal phase. Since no distinction between the Raman spectra of the hexagonal phase and the melt could be observed by Takamura^{10,14} et al. and Wunder¹⁵, it has been concluded that a conformational disorder, similar to the melt, exists in the intermediate hexagonal phase. These results were rather different from the results obtained on the intermediate rotator phase observed on heating of n-alkanes at atmospheric pressure. It has been shown by Raman spectroscopy that the chains within the rotator phase retain their all-trans conformation which makes this phase conformationally more similar to the orthorhombic structure than to the melt^{16,17}. These findings resulted in a completely separate treatment of these two phases. However,

Reproduced from:

Kurelec, L.; Rastogi, S.; Meier, R.J.; Lemstra, P.J. *Macromolecules* **2000**, *33*, 5593-5601

Ungar^{13,18,19} showed that the rotator phase in n-alkanes and the high pressure hexagonal phase in polyethylene can not be treated separately since there is a continuity in the phase behavior between the two phases.

Recently, Tashiro²⁰ et al. tried to show the usefulness of Raman spectroscopy in the identification of the orthorhombic to hexagonal and the hexagonal to melt transitions. In order to avoid complicated set-ups, needed to enter the high pressure region of the hexagonal phase, the experiments were performed on constrained ultra high modulus fibres which, before melting, pass through the hexagonal phase^{21,22}. The results were discussed in combination with IR and X-ray data. A clear distinction between the orthorhombic to hexagonal and the hexagonal to melt transition was shown by in-situ X-ray scattering and IR spectroscopy, whereas no distinction between the hexagonal phase and the melt could be made by Raman spectroscopy. The insensitivity of Raman spectroscopy, to distinguish between the hexagonal phase and the melt, was related to trans sequence length being shorter than five CH₂ units in the hexagonal phase²³.

So far, no experimental observations have been reported which follow in real time the appearance of the hexagonal phase under pressure making use of X-ray and Raman spectroscopy under the same conditions. In this chapter, the first in-situ experimental observations by X-ray and Raman spectroscopy on nascent UHMW-PE powder under pressure will be discussed. Unlike the previously reported observations, it will be shown that the distinction between the orthorhombic and the hexagonal phase, as well as the melt, can be obtained using Raman spectroscopy. Next to the three phases mentioned so far (orthorhombic, hexagonal, melt) the onset of a monoclinic phase in polyethylene under increased pressure at room temperature will also be discussed. The origin of this transition is explained as a result of shear²⁴⁻²⁷.

4.2 Raman spectroscopy of polyethylene - a review

Before proceeding with the experimental observations, a brief summary of the salient findings on the conformational Raman bands of polyethylene, reported in literature, will be given in this paragraph.

The phase transformations of polyethylene at elevated pressure and temperature will be discussed in the spectral region between 700 and 1700 cm⁻¹, which can be divided into three different regions²⁸.

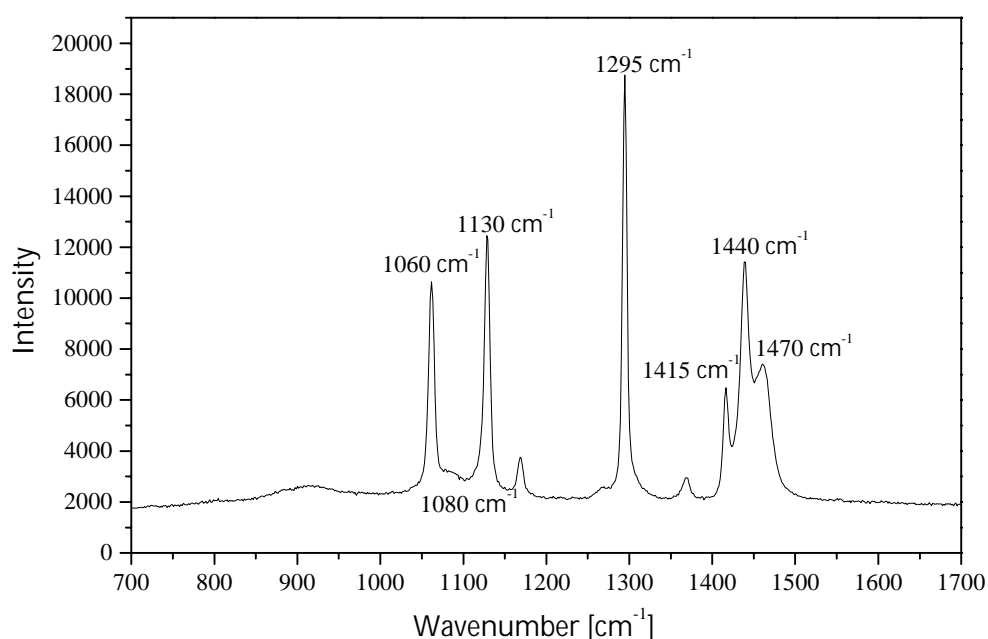


Figure 4.1: Raman spectrum of nascent UHMW-PE powder at the ambient conditions. The Raman bands denoted are assigned to the following vibrational bands: 1060 cm^{-1} asymmetric C-C stretching vibration in crystalline domain; 1080 cm^{-1} C-C stretching in amorphous polyethylene; 1130 cm^{-1} symmetric C-C stretching, crystalline; 1295 cm^{-1} CH_2 twisting, crystalline; $1415\text{ cm}^{-1}/1440\text{ cm}^{-1}$ crystal field splitting of the bending vibrational mode³¹.

The first region, see Figure 4.1, is the skeletal C-C vibration mode between 1000 and 1200 cm^{-1} . It consists of two narrow bands representing in-phase and out-of-phase vibrations appearing at 1060 cm^{-1} and 1130 cm^{-1} respectively. In the melt, a broad band centred around 1080 cm^{-1} becomes dominant while the bands at 1060 and 1130 cm^{-1} disappear completely. A relative measure of the trans-bond content has been given by the intensity ratio of either the 1060 cm^{-1} or the 1130 cm^{-1} to the intensity of the 1080 cm^{-1} ¹⁵.

The second region comprises the CH_2 twisting vibration mode, which can be distinguished at 1295 cm^{-1} . This region has been shown to be independent of conformational changes and is used as an internal intensity standard^{29,30}. However, in the experimental set-up used in this work, the two diamond windows of the pressure cell give a strong phonon vibration around 1350 cm^{-1} . Upon heating, the phonon band from the diamond windows broadens and interferes with CH_2 twisting mode of polyethylene. Due to this reason the mode is not used as an internal calibrant for the spectra recorded at the elevated temperatures (above 200°C).

The third region of interest is the complex bending vibration mode between 1400 and 1500 cm^{-1} . It consists of the well-resolved triplet at 1415 , 1440 and 1470 cm^{-1} . It has been well established that the bands at 1415 and 1440 cm^{-1} are the correlation split doublet corresponding to the $\delta(\text{CH}_2)$ mode of symmetry A_g for the single chain³¹. The experiments

showed that the band at 1415 cm^{-1} originates from the CH_2 in phase bending mode (A_g) while the band at 1440 cm^{-1} originates from the CH_2 out of phase bending mode (B_{1g})^{32,33}. The intensity ratio $I(A_g)/I(B_{1g})$, is determined mostly by the setting angle between the two chains in the orthorhombic unit cell³⁴. The crystal field splitting is characteristic of the orthorhombic unit cell, occupied by two structural units (molecular chains)³⁵. The spectrum in the methylene bending range is, however, severely complicated due to the presence of combination bands and overtones, in particular the presence of Fermi resonance arising from the $720\text{--}731\text{ cm}^{-1}$ methylene rocking bands which are IR active. From Raman spectra of stretched-oriented polyethylene, it has been shown experimentally³² that the Raman line observed at 1470 cm^{-1} originates from B_{1g} overtones and binary combinations in Fermi resonance with the fundamental at 1440 cm^{-1} . The large set of overtones and combinations, in principle very weak, becomes noticeable only because they share intensity with the 1440 cm^{-1} fundamental. All these contributions will strongly affect the quantitative analysis of this region of the spectra. Due to this reason the intensity ratio of the A_g/B_{1g} components of the factor-group split of CH_2 bending fundamentals has to be evaluated by considering the ratio between the 1415 cm^{-1} band and two other bands whose origin is taken to be B_{1g} ($I_{1415}/I_{1440}+I_{1470}$)³⁴.

In order to define the phase transition in polyethylene under elevated pressure discussion will be focused on the relative changes in the skeletal ($1000\text{--}1200\text{ cm}^{-1}$) and the bending ($1400\text{--}1500\text{ cm}^{-1}$) region. This method was also used in the interpretation of the Raman spectra of n-alkanes during heating at atmospheric pressure^{16,17}, when n-alkanes undergo the first-order transition into the rotator phase, as already mentioned in the introduction. In the rotator phase, the typical C-C skeletal bands of Raman spectrum, characteristic of the trans-zigzag conformation, do not lose intensity, while the triplet in C-H bending region, characteristic of orthorhombic phase, merges into a broad singlet centered around 1440 cm^{-1} . These results lead to the conclusion that the chains in n-alkanes retain a relatively larger proportion of the all-trans conformation within the rotator phase compared to the hexagonal phase of polyethylene in constrained fibers²⁰.

4.3 Experimental

4.3.1 Materials

Laboratory scale nascent UHMW-PE powder synthesized with help of Ziegler-Natta catalyst (ES grade in Table 3.1, Chapter 3) has been used in this study. Structural and morphological characteristics of this powder are given in detail in Chapter 3.

4.3.2 Pressure cell

The same pressure cell³⁶ as described in the experimental section of the Chapter 2 has been used.

4.3.3 In-situ Wide Angle X-ray Scattering (WAXS)

In situ X-ray experiments were performed, using monochromatic X-rays of wavelength 0.798Å and a high flux available on beamline ID11-BL2 at European Synchrotron Facilities (ESRF) in Grenoble. The low wavelength was required to avoid X-ray absorption from the diamond windows. Each diffraction pattern was recorded for 15s on a two dimensional CCD detector. Using the FIT2D program developed within ESRF, 2D X-ray patterns were transformed into one dimensional patterns by performing an integration along the azimuthal angle.

4.3.4 In-situ Raman spectroscopy

Raman spectroscopy was recorded with a Labram spectrometer from Dilor S.A. (France). A Spectra Physics Millenium II Nd:YVO₄ laser at 532 nm was used as an excitation source. The initial laser power was 0.20 W. Laser light was focused on the sample using a slit width of 100µm and a 20x microscope objective. The back-scattered light from the sample was dispersed with an 1800 mm⁻¹ grating on the CCD detector. The analysis of the Raman spectra involved baseline correction and curve-fitting procedures. The curve fitting has been performed in two ways: (i) using the GRAMS package including Voigt line profiles³⁷ and (ii) LabSpec software using Gauss line shape. All Raman spectra are displayed along the y-axis for reasons of clarity, but no rescaling has been applied to any spectrum.

4.4 Results and discussion

The discussion of the experimental results will be divided into two different sections. In the first part the orthorhombic to monoclinic phase transition (orth→mono) occurring on raising the pressure at room temperature will be presented. In the second section, the changes occurring on heating the sample at a constant pressure of 4000 bar will be discussed in the terms of the monoclinic to orthorhombic (mon→orth), orthorhombic to hexagonal (orth→hex) and hexagonal to melt (hex→melt) transitions. A schematic diagram of the routes used in this study is given in Figure 4.2. The phase transformations encountered on raising the pressure and subsequent isobaric heating are followed by in-situ X-ray and Raman spectroscopy.

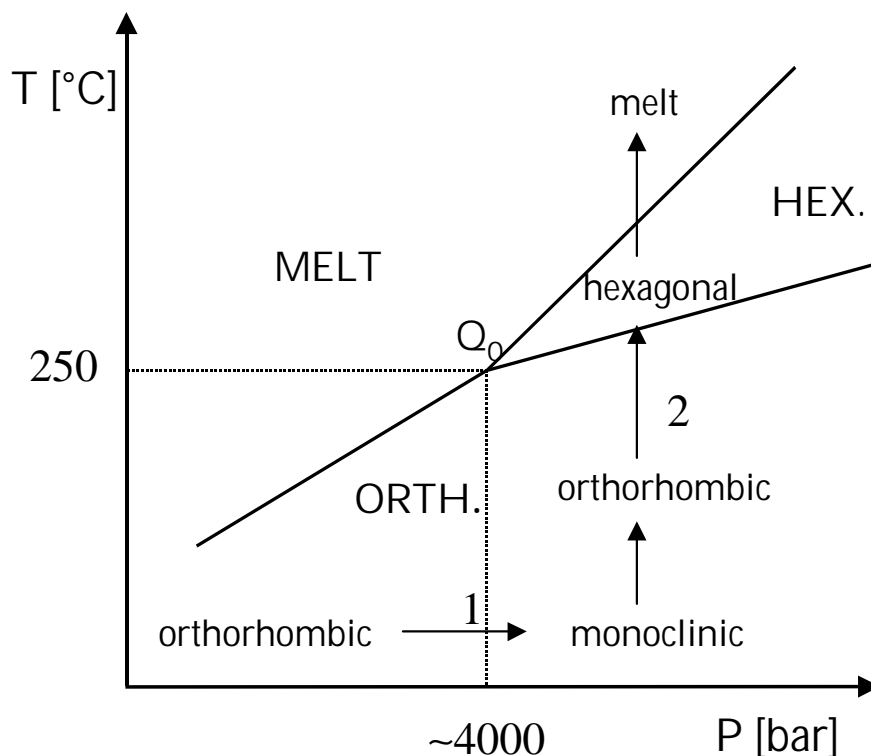


Figure 4.2: Schematic drawing of the experimental routes performed in this study with respect to the equilibrium phase diagram of polyethylene. The route denoted with **1** is related to the phase transformations occurring while raising the pressure up to 4000 bar at room temperature. The route denoted with **2** is related to the phase transformations occurring while heating the sample from 25 °C to 250 °C isobarically at 4100 bar.

4.4.1 Raising the pressure at room temperature

Figure 4.3 shows the X-ray patterns of the nascent UHMW-PE powder recorded in-situ when raising the pressure at room temperature. The starting diffraction pattern (Figure 4.3a), at 160 bar, is taken at the minimum attainable pressure within the pressure cell used in this study. Here, next to the usual (110) and (200) orthorhombic reflections, a relatively strong (100) monoclinic reflection is also present, indicating that part of the orthorhombic crystals transformed into the monoclinic ones. As shown in Chapter 3, the nascent powder consists of very small, irregularly stacked, folded chain crystals. Such small crystals are prone to shear, leading to the transformation from the orthorhombic to the monoclinic crystal structure at relatively low pressures³⁸. In order to confirm the transformation, Figure 4.3g shows the X-ray diffraction pattern of the same UHMW-PE grade in its powder form at ambient conditions (out of the pressure cell). Here, strong (110) and (200) orthorhombic reflections can be observed together with a relatively weak (100) reflection of the monoclinic phase. However, on raising the pressure the monoclinic (100) reflection intensifies while the (110) and (200) orthorhombic reflections loose intensity, Figures 4.3a to 4.3f.

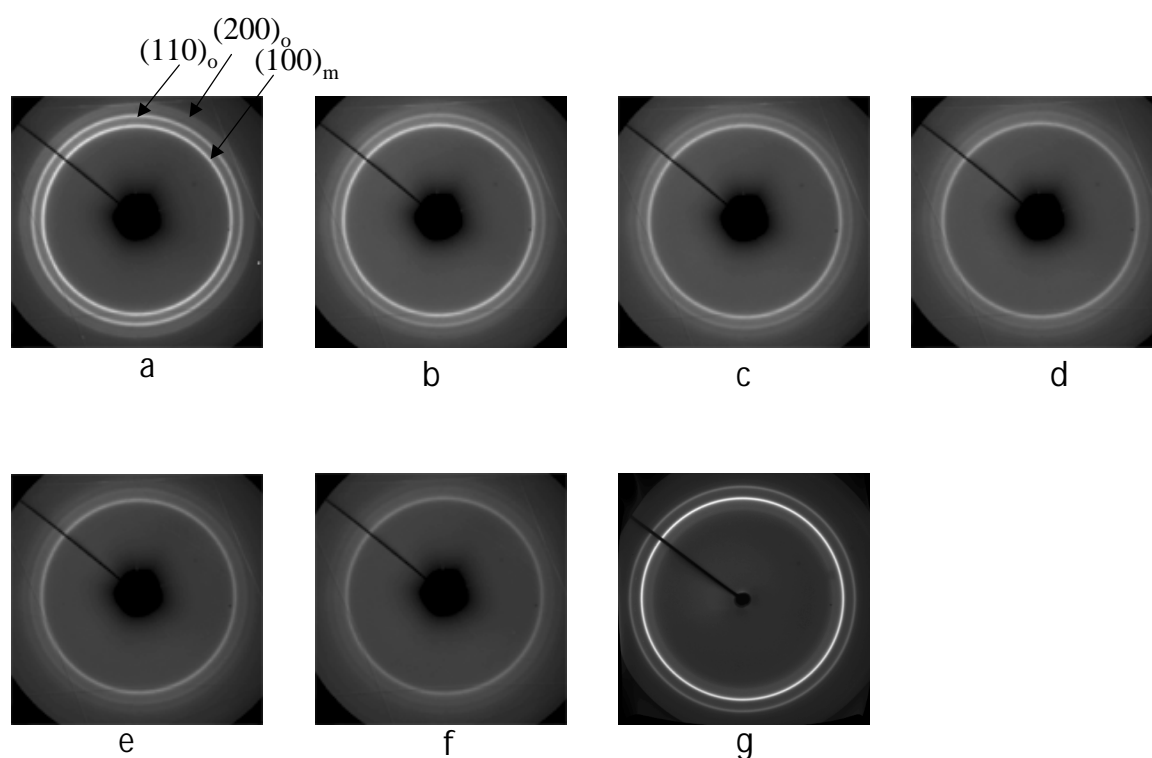


Figure 4.3: X-ray patterns of nascent UHMW-PE recorded in-situ when raising pressure at 25°C. (a) 160 bar (b) 960 bar (c) 1760 bar (d) 2400 bar (e) 3400 bar (f) 4000 bar (g) ambient pressure (out of the pressure cell).

The same set of time resolved experiments was performed using Raman spectroscopy. The spectra in Figure 4.4 were recorded while raising the pressure at room temperature under the same conditions as those of the WAXS experiments discussed above. In the starting spectra (at 160 bar) the anticipated triplet for the orthorhombic phase in the bending region ($1400\text{--}1500\text{ cm}^{-1}$) as well as the two narrow peaks corresponding to the in-phase and out-of-phase skeletal C-C vibrations ($1000\text{--}1200\text{ cm}^{-1}$ spectral range) can be observed. From this spectrum alone, the presence of the monoclinic phase can not be clearly distinguished. Nevertheless, as the amount of monoclinic phase increases with increasing pressure, changes in the vibrational bands in the region $1400\text{--}1500\text{ cm}^{-1}$ are observed. As stated earlier, the bending mode with its typical crystal field splitting is a measure of the orthorhombic crystal structure and the changes within this mode should be related to the changes concerning the phase transformation.

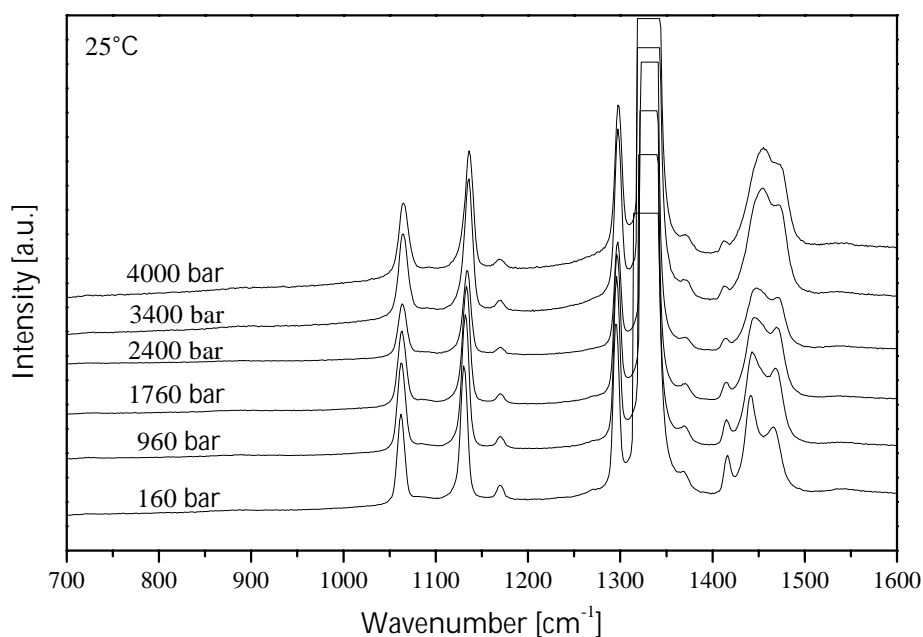


Figure 4.4: Raman spectra of UHMW-PE recorded in-situ on raising the pressure at room temperature, revealing the transformation from the orthorhombic to the monoclinic phase.

When raising the pressure, up to 4000 bar, as the monoclinic phase gets dominant, the band at 1415 cm^{-1} loses intensity relative to the band at 1440 cm^{-1} , indicating the disappearance of the initially pronounced crystal field splitting in the spectral range of the bending mode. Because of the complications in the $1415\text{--}1460\text{ cm}^{-1}$ spectral range due to Fermi resonance, which are discussed in details in section 4.2, quantification of the changes within CH_2 bending region becomes difficult and is not free of ambiguity. Using the intensity ratio $(I_{1415}/(I_{1440}+I_{1470}))^{34}$ as a measure of the phase transformations in polyethylene, from the orthorhombic into the monoclinic phase, as suggested in section 4.2, is not completely appropriate. Namely, the changes in the ratio $(I_{1415}/I_{1440}+I_{1470})$ could be also assigned to changes of the setting angle, which may occur within the orthorhombic lattice as an influence of pressure. In order to follow changes in the concentration of the orthorhombic modification within the sample, the intensity ratio of the 1415 cm^{-1} and 1295 cm^{-1} band have been used alternatively, because the latter is very much independent of chain conformation^{28,29}. The results are shown in Figure 4.5.

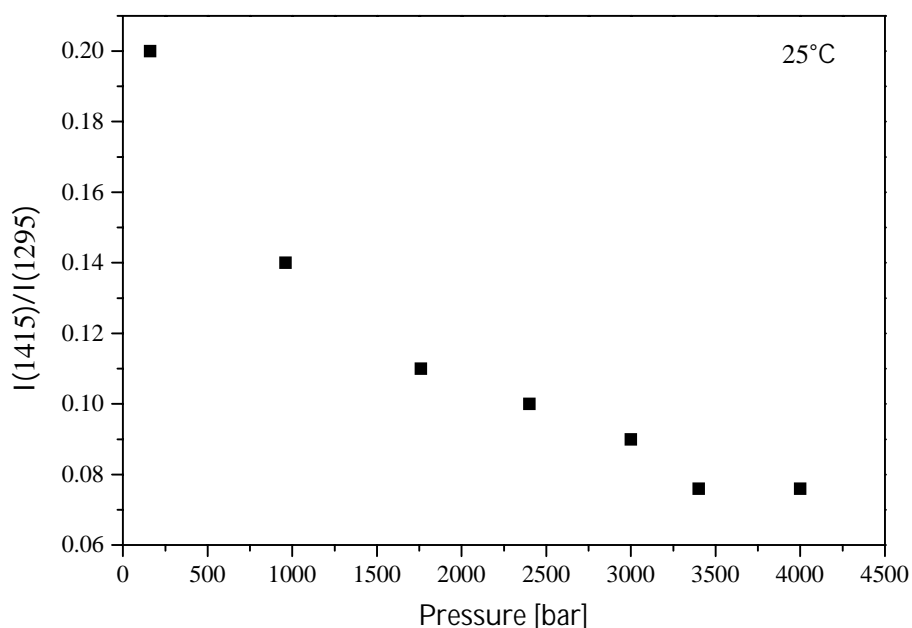


Figure 4.5: Ratio $I(1415)/I(1295)$ vs. pressure for UHMW-PE at 25°C. The decrease in the ratio is related to the disappearance of the orthorhombic phase.

When raising the pressure, up to 4000 bar, the intensity ratio between 1415 cm^{-1} and 1295 cm^{-1} decreases gradually from about 0.2 to 0.07. Disappearance of the band at 1415 cm^{-1} indicates that the concentration of the orthorhombic phase, characterised by two chains per unit cell, decreases while raising the pressure. The X-ray results (Figure 4.3) suggest that upon raising the pressure at room temperature, a phase transformation from the orthorhombic to the monoclinic phase takes place. As the monoclinic phase gets dominant, the band at 1415 cm^{-1} loses intensity indicating the disappearance of the orthorhombic crystal structure within the sample. The disappearance of the crystal field splitting is related to the fact that the monoclinic unit cell possesses one molecular chain per unit cell. From lattice dynamics it is well established that for the monoclinic (and hexagonal) modification(s), the dynamics of the single and isolated unit cell is a very acceptable approximation^{39,40}.

Additionally, a pronounced shift in the frequency of the single line at 1440 cm^{-1} takes place with increasing pressure (Figure 4.6) as the crystal transforms from the orthorhombic to the monoclinic phase. The 1440 cm^{-1} envelope shifts to a maximum value of 1455 cm^{-1} at a pressure of 3400 bar. Simultaneously, a small shift in the 1470 cm^{-1} band to higher frequencies is also observed whereas band at 1415 cm^{-1} does not change in frequency. In the region of the orth→mon transformation the band at 1060 cm^{-1} (asymmetric C-C stretching) stays unchanged while the band at 1130 cm^{-1} (symmetric C-C stretching) exhibits a pronounced shift to the higher frequencies (as observed in Figure 4.6).

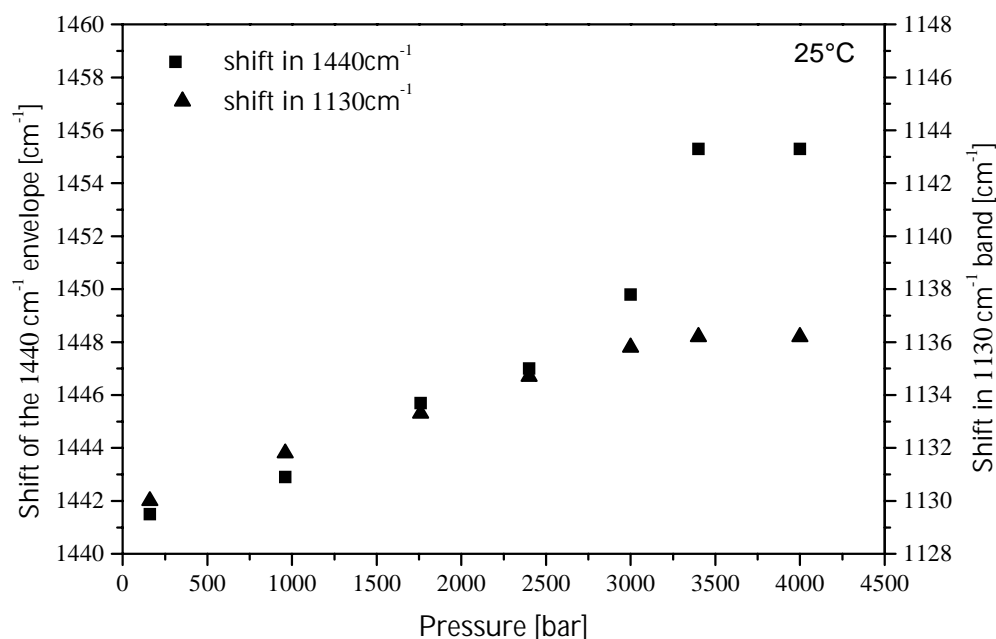


Figure 4.6: Frequency shift of the 1440 cm^{-1} envelope and 1130 cm^{-1} band as function of applied pressure at room temperature.

These observations may appear to be in disagreement with the results obtained for long n-alkanes where the frequencies of the orthorhombic, monoclinic or triclinic lattices (at room temperature and atmospheric pressure) do not shift as much as in polyethylene (at high pressure)^{16,17}. This discrepancy can be a consequence of shrinkage in the intermolecular distances with increasing pressure (as observed by X-ray in Figure 4.3). As a result of shrinkage, intermolecular forces stiffen and frequencies of the modes, which mostly probe the environment around the chain, raise. At the same time, the intensities of both skeletal vibrations (at 1060 and 1130 cm^{-1}) relative to the intensity of the internal standard (1295 cm^{-1}) stay unchanged (crystal field splitting can only be observed at low temperatures for these bands, and is only a few wavenumbers in magnitude). These results confirm that, though large parts of crystals no longer exist in the orthorhombic phase, the chain conformation remains unaltered, in line with the X-ray observations. The weak band at 1415 cm^{-1} stays even at 4000 bars due to the fact that not all the crystals have transformed into the monoclinic phase, as shown by WAXS data in Figure 4.3f.

4.4.2 Heating the sample at 4000 bar

Figure 4.7 shows a 3-D plot of WAXS integrated patterns recorded in-situ during heating at 4000 bar.

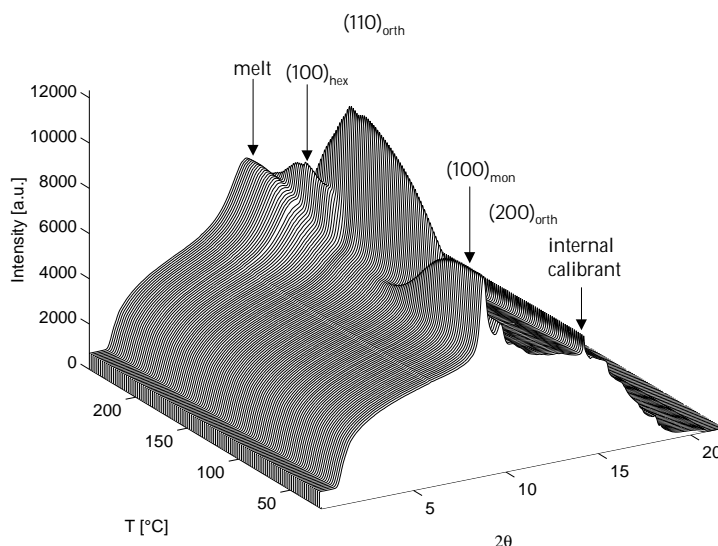


Figure 4.7: 3-D plot of integrated WAXS patterns recorded in-situ on heating UHMW-PE at a fixed pressure of 4000 bar. Initially strong (100) monoclinic and, relatively weak, (110) and (200) orthorhombic reflections can be observed. In the course of heating the (100) monoclinic reflection disappears, while the (110) and (200) orthorhombic ones gain in intensity. At about 215°C, the (100) hexagonal reflection appears and it strengthens on further heating. In the temperature range of 225-230°C, the hexagonal phase becomes dominant. In this region an amorphous halo appears and sample finally melts via the hexagonal phase. The internal calibrant shown in the figure results from the edges of the CCD detector dimensions.

In the course of heating, the (100) monoclinic reflection diminishes while the orthorhombic (110) and (200) reflections intensify, indicating the transformation from a monoclinic to an orthorhombic crystal structure. This may be explained as a release in shear constraints on heating²⁴. Upon further heating at 4000 bar, the (100) hexagonal reflection appears and gains in the intensity, while the orthorhombic (110) and (200) reflections diminish. In the temperature interval between 225 and 230°C the hexagonal (100) reflection stays while the orthorhombic (110) and (200) reflections nearly vanish. This confirms the equilibrium stability region for the hexagonal phase at 4000 bar^{1,3}. As the sample is heated further isobarically, an amorphous halo starts appearing, which intensifies, while the hexagonal (100) reflection decreases in intensity, indicating melting of the hexagonal crystals.

All three phase transformations, mon→orth, orth→hex and hex→melt, have been followed in-situ by Raman spectroscopy as shown in the Figures 4.8 and 4.11.

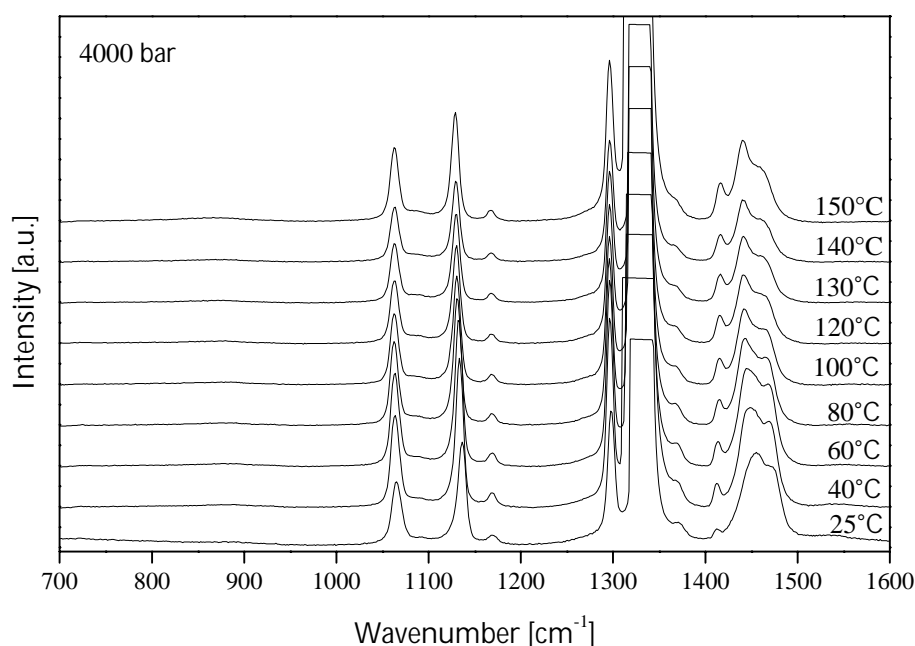


Figure 4.8: Raman spectra of UHMW-PE recorded in-situ on raising the temperature from 25°C to 150 °C at a fixed pressure of 4000 bar. The figure comprises the temperature range of the monoclinic to orthorhombic transition.

Figure 4.8 shows the Raman spectra, recorded in situ, when heating the sample from 25°C to 150°C at 4000 bars. In this temperature region the mon→orth transformation takes place as observed by X-ray diffraction (Figure 4.7). The discussion will be again restricted to the relative changes occurring in the CH₂ bending (1400-1500 cm⁻¹) and C-C skeletal regions (1000-1200 cm⁻¹) of the spectrum. Once more, the changes in the concentration of the orthorhombic crystal lattice within the sample will be followed by showing the intensity ratio between 1415 cm⁻¹ and 1295 cm⁻¹ band, as discussed in the previous section. If compared with WAXS data (Figure 4.7) it can be observed that the ratio $I(1415)/I(1295)$ increases precisely in the temperature region corresponding the change in the unit cell from the monoclinic to the orthorhombic phase (Figure 4.9). Once all crystals have transformed back to the orthorhombic crystal structure, i.e. above 120°C, the ratio $I(1415)/I(1295)$ stays constant.

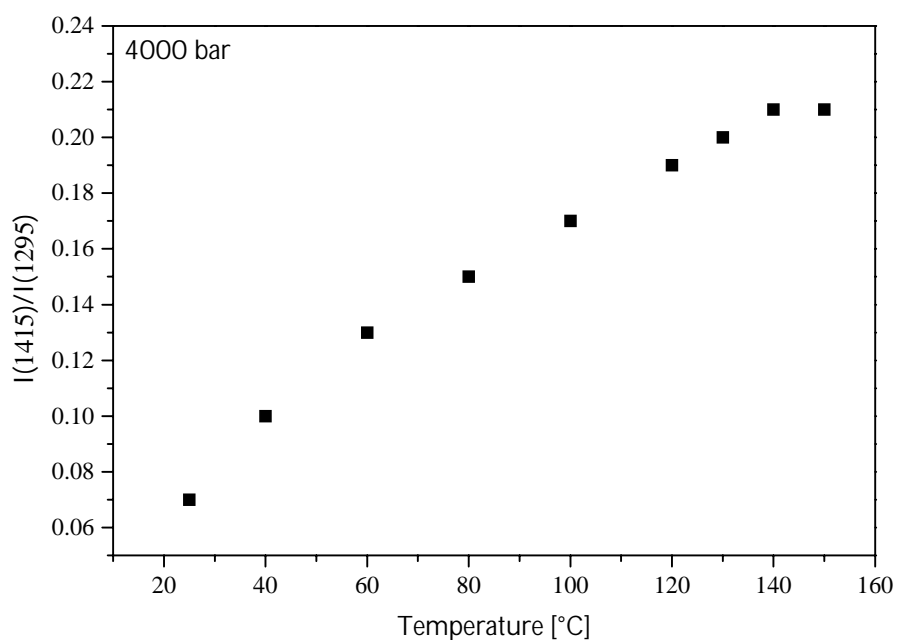


Figure 4.9: The $I(1415)/I(1295)$ vs. temperature plot for UHMW-PE at fixed pressure of 4000 bar. The increase in the ratio is related to the reappearance of the orthorhombic phase.

While raising the temperature at 4000 bar, during the mon→orth transformation, the 1440 cm^{-1} envelope shifts back to the lower values of wavenumbers. Figure 4.10 shows that the single line shifts from 1455 cm^{-1} back to the value of 1440 cm^{-1} , which has been the starting point before raising the pressure at room temperature. The same trend has been observed in the skeletal mode of the spectrum. Once the transformation from the monoclinic to the orthorhombic phase takes place, the symmetric C-C stretching band now positioned at around 1136 cm^{-1} shifts back to its initial position at 1130 cm^{-1} (Figure 4.10). Again no changes in the intensity ratio of the two skeletal vibrations at 1060 cm^{-1} and 1130 cm^{-1} with respect to 1295 cm^{-1} band (internal standard) has been observed during the mon→orth transformation which confirms that no change in the chain conformation takes place.

Figure 4.11 shows the Raman spectra of UHMW-PE on heating the sample, in the temperature region between 180 and 250°C, i.e. the region comprising the orth→hex and the hex.→melt transitions as shown by the WAXS integrated pattern in Figure 4.7.

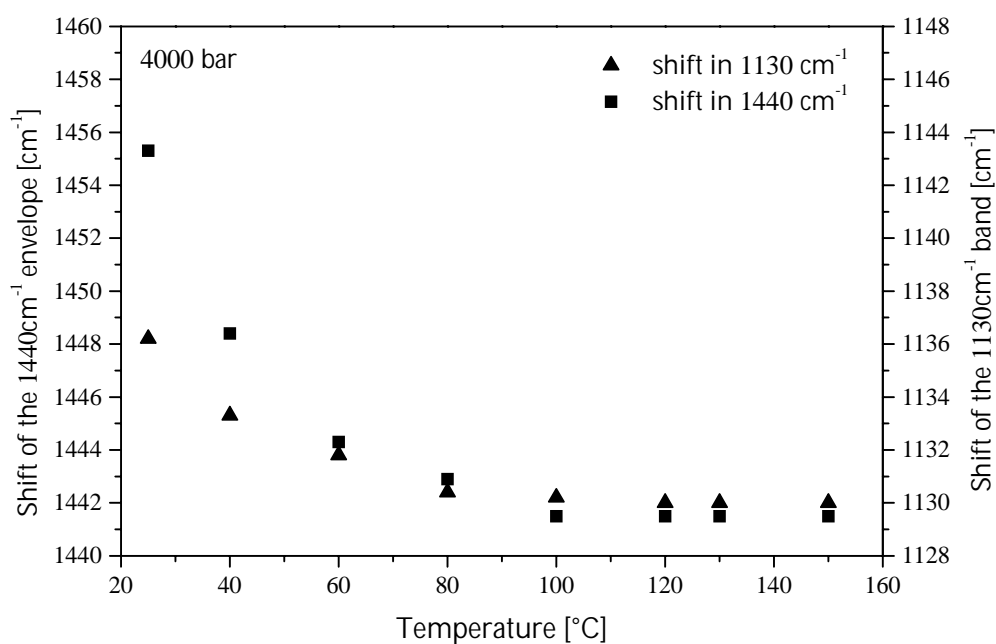


Figure 4.10: Frequency shift of the 1440 cm^{-1} envelope and 1130 cm^{-1} band as function of temperature raised at a pressure of 4000 bar.

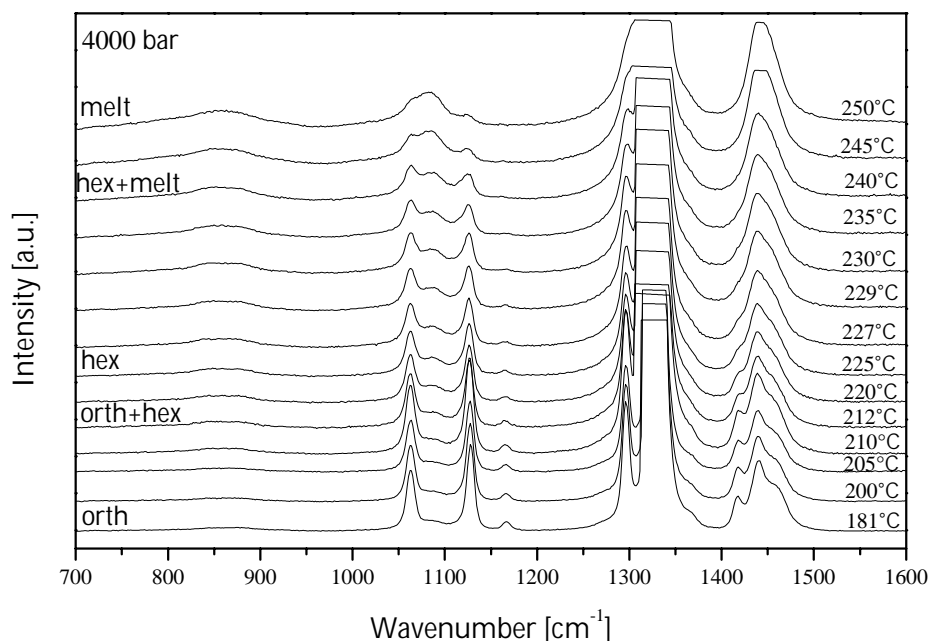


Figure 4.11: Raman spectra of UHMW-PE recorded in-situ on raising temperature from $181\text{ }^{\circ}\text{C}$ to $250\text{ }^{\circ}\text{C}$ at a fixed pressure of 4000 bar. The figure comprises the temperature range of the orthorhombic to hexagonal and the hexagonal to melt transition.

The starting spectrum in Figure 4.11 is typical for semi-crystalline polyethylene with an orthorhombic unit cell as discussed previously. Upon heating, the 1415 cm^{-1} and 1440 cm^{-1} band merge slowly towards each other. Since the $1000\text{--}1200\text{ cm}^{-1}$ spectral region is

essentially unaffected within the region of the orthorhombic phase, the overall crystallinity level is constant and the features observed in the 1400-1500 cm^{-1} spectral region can be attributed to a change in crystalline structure. In the region of mixed orthorhombic and hexagonal crystals (212 to 225°C), the 1415 cm^{-1} band stays in the form of a shoulder attached to the band centered at 1440 cm^{-1} . When entering the region of the equilibrium stability of the hexagonal phase (between 225-230°C), the triplet loses its form and only a broad single band centered at 1440 cm^{-1} can be observed within the bending region. In the spectrum of the hexagonal phase, the frequency shifts of the 1440 cm^{-1} and 1130 cm^{-1} bands, with respect to their position in the orthorhombic phase are not observed. This is in contrast with the results obtained for the monoclinic phase, where the frequency shift of the 1440 cm^{-1} as well 1130 cm^{-1} band to higher values of the wavenumbers has been shown. In the region of the orth \rightarrow hex transformation the band at 1080 cm^{-1} starts appearing, suggesting the initiation of gauche defects in the regular trans zigzag conformation. An additional broad band around 870 cm^{-1} can be observed in the spectrum of the pure hexagonal phase (temperature region between 235 and 240°C). The existence of this band in the spectrum of polyethylene melt has been reported before and is considered to be an additional feature of the gauche content within the chain^{17,30,41}. Though present, the intensity of the amorphous band at 1080 cm^{-1} stays relatively weak throughout the narrow region of the hexagonal phase, leaving the bands at 1060 and 1130 cm^{-1} dominant in the skeletal region of the spectrum. As the amorphous content starts increasing (appearance of the amorphous halo in Figure 4.7), indicating melting of hexagonal crystals, the band at 1080 cm^{-1} intensifies while the bands at 1060 and 1130 cm^{-1} start disappearing. The changes in the chain conformation (i.e. trans content) during the orth \rightarrow hex and hex \rightarrow melt transition are given in the Figure 4.12 and are expressed as the intensity ratio of the skeletal 1130 cm^{-1} and the gauche 1080 cm^{-1} band vs. temperature. The figure is divided into three separate regions, the vertical lines being drawn from the experimental observations made by in-situ X-ray studies. Region I (from 120 to 212°C) is a temperature region of the orthorhombic phase. Here, the intensity ratio between 1130 cm^{-1} and 1080 cm^{-1} is high and does not change while increasing pressure or temperature. The temperature region comprising the hexagonal phase is divided into three subregions IIa, IIb, IIc. In subregion IIa, the orth \rightarrow hex transition starts at about 212°C and can be distinguished in Figure 4.12 by the subsequent decrease of the characteristic intensity ratio. In subregion IIb, the stability region of the hexagonal phase at a pressure of 4000 bar (between 225 and 230°C), a clear decrease in the slope I(1130)/I(1080) vs. T can be observed. Upon raising the temperature further the amorphous halo intervenes (as discussed in Figure 4.7) and the gauche content slowly increases (i.e. I(1130)/I(1080) decreases) due to the partial melting of hexagonal crystals (region IIc). Once the sample is melted, the characteristic intensity ratio stays constant giving a value typical for the melt (region III). The decrease in the trans

content, within region II, is not continuous (intervention of region IIb, Figure 4.12) and that implies that a clear distinction between the hexagonal phase and the melt can be obtained for polyethylene by Raman spectroscopy.

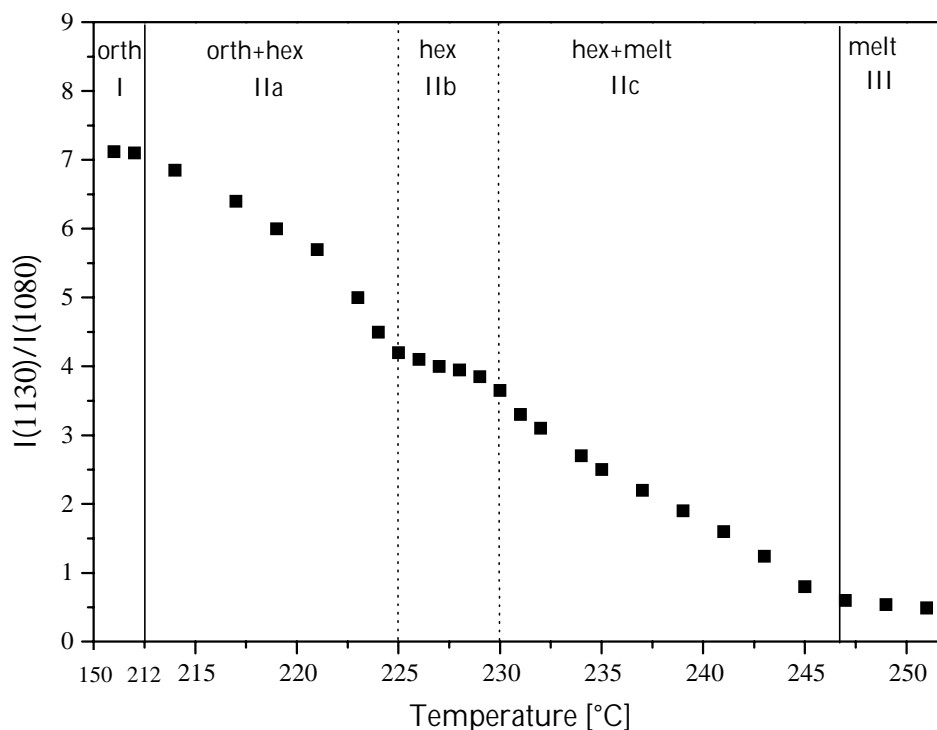


Figure 4.12: The $I(1130)/I(1080)$ vs. temperature plot for UHMW-PE at fixed pressure of 4000bar. The temperature range is divided into three temperature regions according to the X-ray results. Region I is the region of the pure orthorhombic phase. In the region II the intervention of the hexagonal phase becomes prominent. The region is subdivided into three separate sub-regions: the orthorhombic to hexagonal transition region (IIa), the pure hexagonal phase (IIb) and the melting region of the hexagonal phase (IIc). Region III is the region of the pure melt.

Figure 4.13 is a composite picture of the Raman spectra of the orthorhombic phase, the monoclinic phase, the hexagonal phase and the melt. From here it is evident that the Raman spectrum of the hexagonal phase is similar to the one of the rotor phase in alkanes⁴¹.

Though these results differ from earlier observations made by Tashiro et al.²⁰, the difference may be due to different experimental conditions. The drop in the intensity ratio $I(1130)/I(1080)$ from 7.8 (Region I; Figure 4.12) to 4 (Region IIb, Figure 4.12) suggests a relative increase in the gauche content in the hexagonal phase at 4000 bar. A sufficiently high trans content within the hexagonal phase compared to that of the melt results in feasible distinction between the hexagonal phase and the melt.

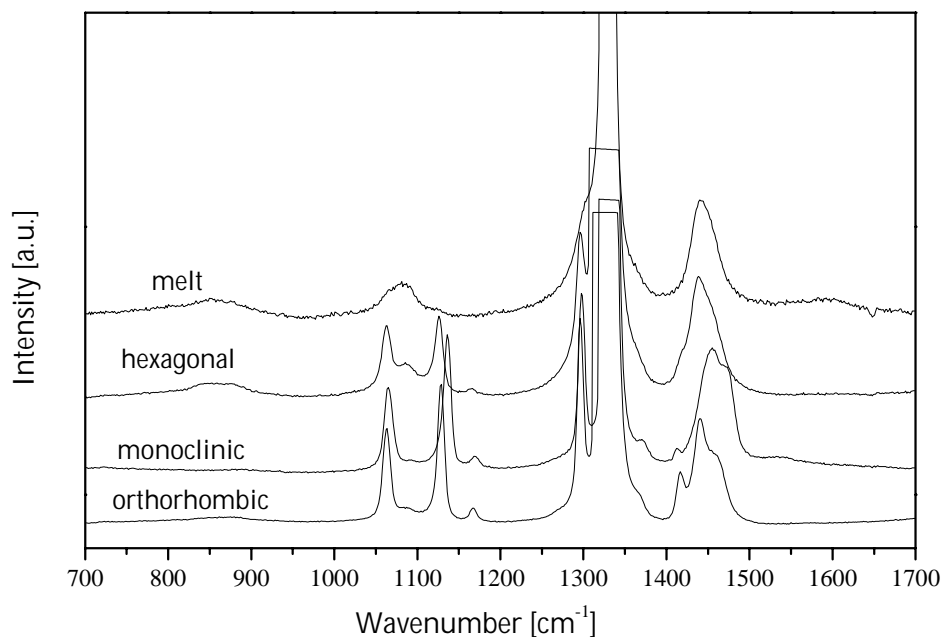


Figure 4.13: Composite figure showing Raman spectra of the orthorhombic phase, the monoclinic phase, the hexagonal phase and the melt.

In order to strengthen our observations, in-situ Raman results on melting the same UHMW-PE at atmospheric pressure, i.e. without the intervention of the hexagonal phase, are shown in Figure 4.14.

Here a continuous increase in the intensity of the gauche band at 1080 cm^{-1} can be seen above 115°C , on raising the temperature. As the gauche band increases in intensity, the crystal field splitting ($1415\text{ cm}^{-1}/1440\text{ cm}^{-1}$) in the bending mode disappears continuously and around 143°C only a broad band centered around 1440 cm^{-1} can be observed within the bending region. Within the skeletal region of the Raman spectrum at 141°C only the gauche band at 1080 cm^{-1} can be seen. The continuous change of gauche content when melting the UHMW-PE powder via orthorhombic phase is shown in Figure 4.14b where the ratio $I(1130)/(1080)$ vs. T is plotted the same way as in the Figure 4.12. Upon melting of UHMW-PE powder at atmospheric pressure, the characteristic ratio $I(1130)/(1080)$ (measure of the trans content) decreases continuously within the temperature range of about 20°C , not revealing any disturbance like the plateau in the Figure 4.12 (region IIb). This was confirmed by DSC measurements performed on the same UHMW-PE powder under the same conditions as the Raman experiments at atmospheric conditions (using the same heating rate), where a melting point at 143°C and the width of the melting peak of about 20 K could be observed. In the case of melting UHMW-PE at 4000 bar the temperature range of the melting becomes wider ($\sim 32\text{ K}$) showing clearly two different conformational regions due to the intervention of the intermediate hexagonal phase. Observations similar to that at atmospheric pressure were also observed by Raman spectroscopy when a sample of UHMW-PE having thick crystals ($>50\text{ nm}$) was melted at the pressures below 4000 bar . It is to be noted that WAXS studies suggest

that the sample having thick crystals, directly melts via the orthorhombic phase on heating below 4000 bar².

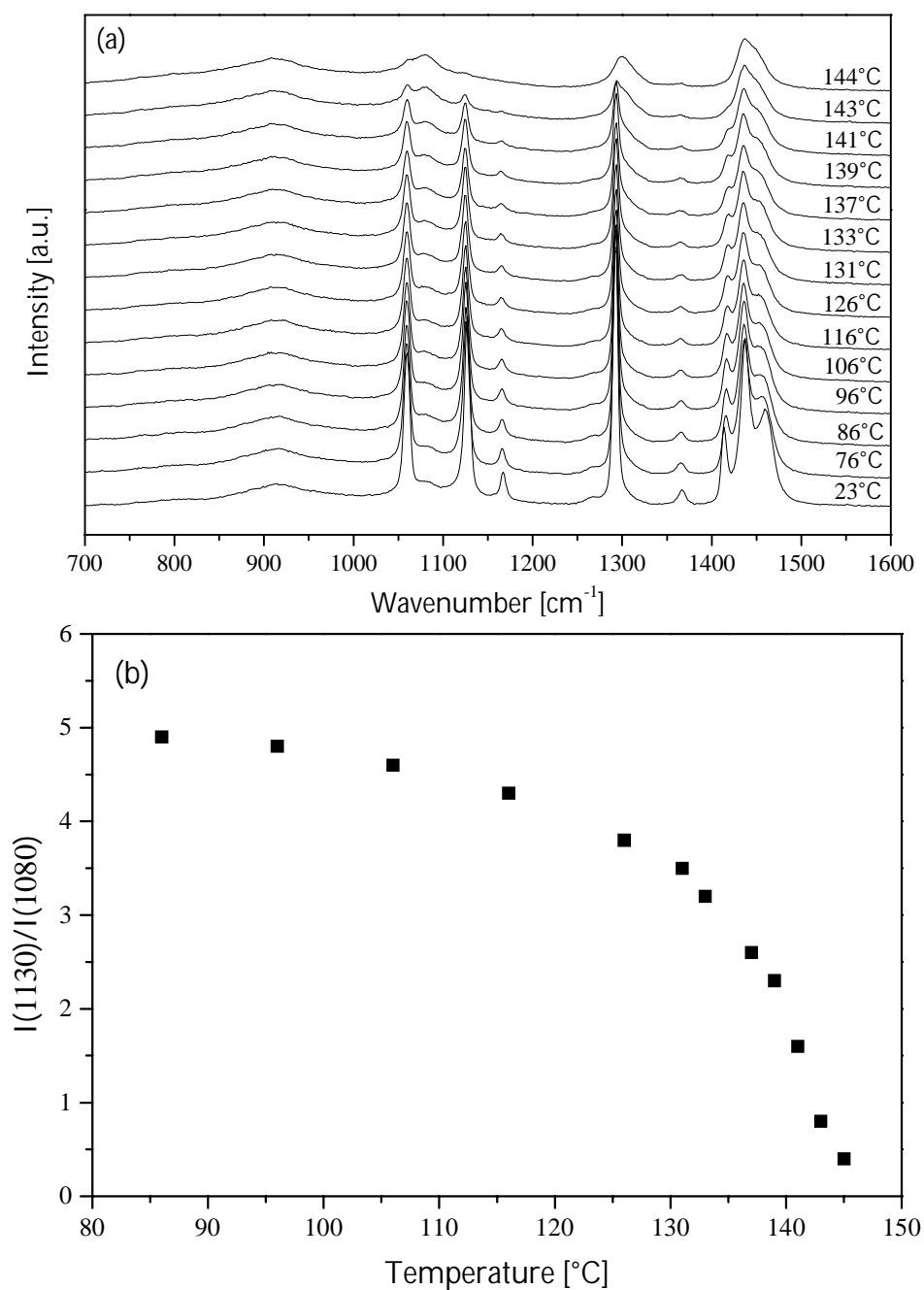


Figure 4.14: Results of in-situ Raman spectroscopy of UHMW-PE powder at ambient conditions using a Linkam hotstage. (a) Raman spectra recorded in-situ when heating UHMW-PE powder to 150°C with the rate of 2°C/min. (b) The $I(1130)/I(1080)$ vs. temperature plot.

4.5 Conclusions

The first observations of the phase transformations in polyethylene under elevated pressure, using in-situ X-ray and Raman spectroscopy under the same experimental conditions, have been presented in this chapter. X-ray analysis has been used to explore the phase diagram of polyethylene. From the work presented in this chapter it is shown conclusively that the combination of X-ray with Raman spectroscopy can provide information on structural and conformational changes during phase transformations.

In order to distinguish between different phases in polyethylene, the bending mode of the Raman spectrum was discussed in combination with the skeletal one ($1000\text{-}1200\text{ cm}^{-1}$), providing a measure for the conformational changes.

Our experimental observations suggest that a clear distinction can be made between the orthorhombic, hexagonal/monoclinic phase within the bending region of the spectrum, most clearly shown by the spectra displayed in Figure 4.13. The orthorhombic phase is characterized by a well resolved triplet within the bending region of the spectrum. The characteristic form of the bending mode results from the crystal field splitting, which is a consequence of the presence of two chains within the orthorhombic unit cell. On the other hand, the monoclinic and the hexagonal phase, having one chain per unit cell, do not exhibit the 1415 cm^{-1} band (or it is greatly reduced attributed to coexistence of phases) but a single line at about 1440 cm^{-1} . The 1440 cm^{-1} band shifts to higher frequencies with increase in pressure. The pronounced shift in the 1130 cm^{-1} band within the skeletal region of the spectrum has also been observed for the monoclinic phase, whereas its position stays the same for the orthorhombic and the hexagonal phase. The intensity of the skeletal bands within the $1000\text{-}1200\text{ cm}^{-1}$ spectral range does not change for the orthorhombic and monoclinic phase (low temperature experiments would have revealed crystal field splitting also here), whereas for the hexagonal phase a significant increase in the intensity of the gauche band at 1080 cm^{-1} can be observed.

From the results presented in this chapter it becomes obvious that the phase transformations in polyethylene can be followed quantitatively in the skeletal range of the spectrum. Due to the complications within the bending mode, which are discussed in detail within this chapter, it has been shown that the phase changes in polyethylene can be followed qualitatively (due to the presence of the crystal field splitting) but the quantification of the changes becomes ambiguous.

4.6 References

1. Hikosaka, M; Tsukijama, K.; Rastogi, S.; Keller, A. *Polymer* **1992**, 33, 12, 2502
2. Rastogi, S.; Kurelec, L.; Lemstra, P.J. *Macromolecules* **1998**, 31, 5022
3. Basset, D.C.; Khaifa, A.; Turner, B. *Nature (London)* **1972**, 106, 239; *ibid.* **1972**, 240, 146
4. Yasuniwa, M.; Takemura, T. *Polymer* **1974**, 15, 661
5. Basset D.C.; Turner, B. *Philos. Mag.* **1974**, 29, 925
6. Maeda, Y.; Kanetsuna, H. *J. Polym. Sci. Polym. Phys. Ed.* **1974**, 12, 2551
7. Maeda, Y.; Kanetsuna, H. *J. Polym. Sci. Polym. Phys. Ed.* **1975**, 13, 637; **1976**, 14, 2057
8. Yasuniwa, M.; Enoshita, R.; Takemura T. *Jap. J. Appl. Phys.* **1976**, 15, 1421
9. Yamamoto T.; Miyaji H.; Asai K. *Jap. J. Appl. Phys.* **1977**, 16, 1891
10. Takemura, T. *Polymer Preprints* **1979**, 20, 270
11. Langen de, M. *Phd. Thesis*, University Amsterdam, **1998**
12. Basset, D.C.; Block, S.; Piermarini, G. J. *J. Appl. Phys.* **1974**, 45, 4146
13. Ungar, G. *Polymer* **1993**, 34, 2050
14. Tanaka, T.; Takemura, T. *Polym. J.* **1980**, 12, 355
15. Wunder, S. L. *Macromolecules* **1981**, 14, 1024
16. Barnes, J.D.; Fanconi, B.M. *J. Chem. Phys.* **1972**, 56, 5190
17. Kim, Y.; Strauss, H.L.; Snyder, R.G. *J. Phys. Chem.* **1989**, 93, 7520
18. Vaughan, A.S.; Ungar, G.; Bassett, D.C.; Keller, A. *Polymer* **1985**, 26, 726
19. Ungar, G. *Macromolecules* **1986**, 19, 1317
20. Tashiro, K.; Sasaki, S.; Kobayashi, M. *Macromolecules* **1996**, 29, 7460
21. Pennings, A.J.; Zwijnenburg, A. *J. Polym. Sci. Polym. Phys. Ed.* **1979**, 17, 1011
22. Lemstra, P.J.; van Aerle, N.A.J.M.; Bastiaansen, C.W.M. *Polym. J.* **1987**, 19, 85
23. Cho, Y.; Kobayashi, M.; Tadokoro, H. *Polym. Prepr. Jpn.* **1986**, 30, 1842
24. Seto, T.; Hara, T.; Tanaka, K. *Jap. J. Appl. Phys.* **1968**, 1, 31
25. Allan, P.; Bevis, M. *Phil. Mag.* **1975**, 31, 1001, **1977**, 35, 405
26. Young, R.J.; Bowden, P.B. *Phil. Mag.* **1974**, 29, 1061
27. Bevis, M.; Crellin, E.B. *Polymer* **1971**, 12, 666
28. Gall, M.J.; Hendra, P.J.; Peacock C.J.; Cudby, M.E.; Willis, H.A. *Spectrochim. Acta* **1972**, 28A, 1485
29. Strobl, G.R.; Hagedorn, W. *J. Polym. Sci., Polym. Phys. Ed.* **1978**, 16, 1181
30. Koglin, E.; Meier R.J. *Comp. and Theor. Polym. Sci.* **1999**, 9, 327
31. Bower, D.I.; Maddams, W.F. *The vibrational spectroscopy of polymers*, Cambridge University press: Cambridge, **1989**
32. Masetti, G.; Abbate, S.; Gussoni, M.; Zerbi, G. *J. Chem. Phys.* **1980**, 73, 4671
33. Abbate, S.; Gussoni, M.; Zerbi, G. *J. Chem. Phys.* **1980**, 73, 4680
34. Abbate, S.; Zerbi, G.; Wunder, S.L. *J. Chem. Phys.* **1982**, 86, 3140
35. Boerio, F.J.; Koenig, J.L. *J. Chem. Phys.* **1970**, 52, 3425
36. Hikosaka, M.; Seto, T. *Jpn. J. Appl. Phys.* **1982**, 21, L332
37. Armstrong, B.H. *J. Quantum Spectrosc. Radioat. Transfer* **1967**, 7, 61
38. Ottani, S.; Porter, R.S. *Polymer* **1990**, 31, 369
39. Tasumi, M; Krimm, S. *J. Chem. Phys.* **1967**, 46, 755
40. Tasumi, M; Shimanouchi, T. *J. Chem. Phys.* **1965**, 43, 1245
41. Mutter, R.; Stille, W.; Strobl, G. *J. Polym. Phys* **1993**, 31, 99

Chapter 5

A novel route to sinter UHMW-PE nascent powders into homogeneous, grain boundary free, products

5.1 Introduction

As already mentioned in the general introduction (Chapter 1), the strong dependence of the melt viscosity and reptation time on molecular weight implies that polymers possessing a high molecular weight are rather intractable. On the other hand, mechanical properties such as toughness, strength, wear and fatigue increase with increasing molecular weight. The problem of compromising between good mechanical properties and ease of processing becomes evident for UHMW-PE. Due to its superior intrinsic mechanical properties, UHMW-PE has been selected as material of choice in bearing surfaces of artificial knee and hip joints. However, such artificial joints, where UHMW-PE is used as an interface between human bone and metal pin (Figure 1.2), do not meet the requirements of a long lifetime and, in the most of the cases, it is the UHMW-PE part that fails during its service life in the human body^{1,2}. The failure of UHMW-PE in artificial joints has been extensively studied, and though the problem is rather complex, it is very often related to improper fusion of the original powder particles which is a consequence of the intractability of this material^{2,3}. Since it can not be processed via conventional processing routes such as injection moulding or extrusion, UHMW-PE is usually compression moulded or ram-extruded followed by sintering into semi-finished parts, which are subsequently machined into the desired shape. Due to high melt viscosity (and long reptation times at 180°C the relaxation time has been shown to be above 10^4 s)^{4,5} molecular chains are not able to diffuse from one powder particle to another, which results in products possessing residues of the original powder particles, usually referred to as grain boundaries or fusion defects⁶.

Intractability of UHMW-PE is a consequence of the fundamental restrictions ($\eta_0 \sim M_w^{3.4}$) related to the ability of the long chains to entangle^{7,8}. It was believed that, in order to overcome this fundamental barrier, the chains should be disentangled prior to processing, which seemed rather reasonable regarding the long reptation times needed for long molecular chains to re-entangle⁹. A disentanglement of long molecules can be achieved by dissolution

(precursor for solution spinning process¹⁰⁻¹³ discussed in Chapter 1) or directly during synthesis at low temperatures (below the crystallisation temperature of a polymer chain in the reaction medium) using low activity catalyst systems. Such synthesis conditions lead to the creation of so-called nascent powders, possessing unique morphological characteristics as discussed in Chapter 3. However, experiments proved that this idea of profiting from the initially disentangled state in melt processing could not be realised since immediate re-entangling takes place upon melting^{4,5}. This process of fast re-entanglement has been experimentally accessed with the help of neutron scattering by Barham and Sadler¹⁴. Their results showed that, upon melting single crystal mats of high density polyethylene, chains are rejected from the crystal, which is accompanied by sudden increase in radius of gyration, process usually referred to as “chain explosion”. In this chapter it will be shown that the instantaneous increase in radius of gyration during “chain explosion” can be utilised to sinter UHMW-PE into homogeneous (grain boundary free) products. The only prerequisite for such an instantaneous re-entanglement is that the material must be fully disentangled prior to melting.

As shown in Chapter 3, commercial grades of nascent powders are synthesised via Ziegler Natta catalysts, which always leads to powders possessing certain initial number of entanglements. Such systems have to be disentangled prior to melting in order to surpass the phenomenon of “chain explosion” upon melting. It has been shown recently that, after annealing solid state compacted nascent UHMW-PE at 7000 bar and 265°C, the drawing characteristics of nascent powders substantially increase^{15,16}. This has been associated with the intervention of the hexagonal phase, characterised by enhanced chain mobility, which ultimately leads to the formation of extended chain crystals. The thickening of the crystals within the hexagonal phase can be regarded as a disentanglement process, as the chains are successively being pulled into a crystal¹⁷.

The potential influence of the enhanced chain mobility within the hexagonal phase in processing of UHMW-PE has intrigued scientists for quite a long time. The problem that had to be encountered is the high pressure and temperature needed to reach the thermodynamic stable state of the hexagonal phase ($P_Q \geq 4000$ bar and $T_Q \geq 250^\circ\text{C}$)¹⁸. Due to this reason, processing of polyethylene via the hexagonal phase has remained a rather academic topic. However, an interesting phenomenon has been observed while extruding UHMW-PE in the melt. It has been shown that there is a narrow temperature window in which the material could be extruded into rather homogeneous strands¹⁹⁻²². At temperatures above as well as below this narrow temperature window, the extrusion failed resulting in rather inhomogeneous extrudates. This temperature window has been associated with intervention of the hexagonal phase, which in that case lubricates the extrusion of UHMW-PE¹⁹. The

appearance of the hexagonal phase was related to full extension of the molecular chains in the course of flow, changing the free energy of the system in such a way that the originally metastable hexagonal phase becomes stable. The same melting behavior has been well recognised for constrained UHMW-PE fibres²³. However, the experimental evidence of the intervention of the hexagonal phase during extrusion of UHMW-PE has never been fully proven and it remained rather speculative.

In this chapter a novel approach to sinter UHMW-PE powders into homogeneous 3D products will be introduced. In order to fuse powder particles, the substantial increase in radius of gyration during “chain explosion” upon melting will be used in order to overcome the restrictions of the long reptation times characteristic for the long molecular chains within the melt. The disentanglement of the chains prior to melting will be achieved in the hexagonal phase, which for the small folded chain crystals of the nascent powders will be shown to be stable at pressures much below the thermodynamic triple point, i.e. at pressures feasible in polymer processing.

5.2 Experimental section

5.2.1 Materials

The experiments discussed in this chapter have been performed on the same three types of the nascent powders as described in the experimental section of the Chapter 3.

5.2.2 Pressure cell with diamond windows (PCDW)

For high pressure experiments the same type of the pressure cell has been used as described in Chapters 2 and 4. The pressure cell was used for wide angle X-ray scattering experiments as well as for the compaction of the nascent powders at different pressures. Phase transformations during compaction of the powders were followed in-situ by Raman spectroscopy as well as Wide angle X-ray scattering.

5.2.3 In-situ Wide Angle X-ray Scattering (WAXS)

In situ X-ray experiments were performed using monochromatic X-rays of wavelength 0.798Å and a high flux available on beamline ID11-BL2 at European Synchrotron Radiation Facilities (ESRF) in Grenoble. The low wavelength was required to avoid X-ray absorption from the diamond windows. Each diffraction pattern was recorded for 15 seconds on a two dimensional CCD detector. Using the FIT2D program developed within ESRF, 2D X-ray patterns were transformed into one dimensional patterns by performing an integration along the azimuthal angle.

5.2.4 Light microscopy (LM)

All the compacted samples were sectioned under liquid nitrogen using a glass knife into thin slides having a thickness of 10-15 μm . The presence of the grain boundaries was investigated by light microscopy using a phase contrast technique.

5.3 Results and Discussion

5.3.1 Melting of nascent powders via the hexagonal phase at pressures below the equilibrium triple point

It has been shown in Chapter 3 that all three types of nascent powders, used in this study, consist of folded chain crystals possessing small dimensions in thickness as well as lateral direction. Consequently, from Chapter 2 it follows that such small crystals should melt via the hexagonal phase at pressures below the pressure of the equilibrium triple point ($P_Q \geq 4000$ bar and $T_Q \geq 250^\circ\text{C}$)¹⁸. In-situ WAXS experiments at elevated pressures have been performed on all three powder grades in order to access the phase behavior below the equilibrium triple point. It has been observed that all grades melt via the hexagonal phase at pressures around 1000 bar. At pressures below this value intervention of the hexagonal phase could be observed for none of the three powder grades. The result of in-situ WAXS experiments on laboratory scale nascent powder is shown in Figure 5.1.

Prior to heating, at a pressure of 1200 bar, the monoclinic (100) reflection is dominant and it coexists with rather weak orthorhombic (110) and (200) reflections. The existence of the monoclinic phase at elevated pressure has already been discussed in Chapter 4 and it is attributed to shearing of the small folded chain crystals within the pressure cell. Upon heating, the monoclinic (100) reflection disappears (about 100°C) and the orthorhombic (110) and (200) reflections become dominant. Upon further heating, at around 165°C , the orthorhombic crystals transform into the hexagonal phase, which becomes dominant in temperature region between 175 and 190°C . At about 195°C the hexagonal crystals melt.

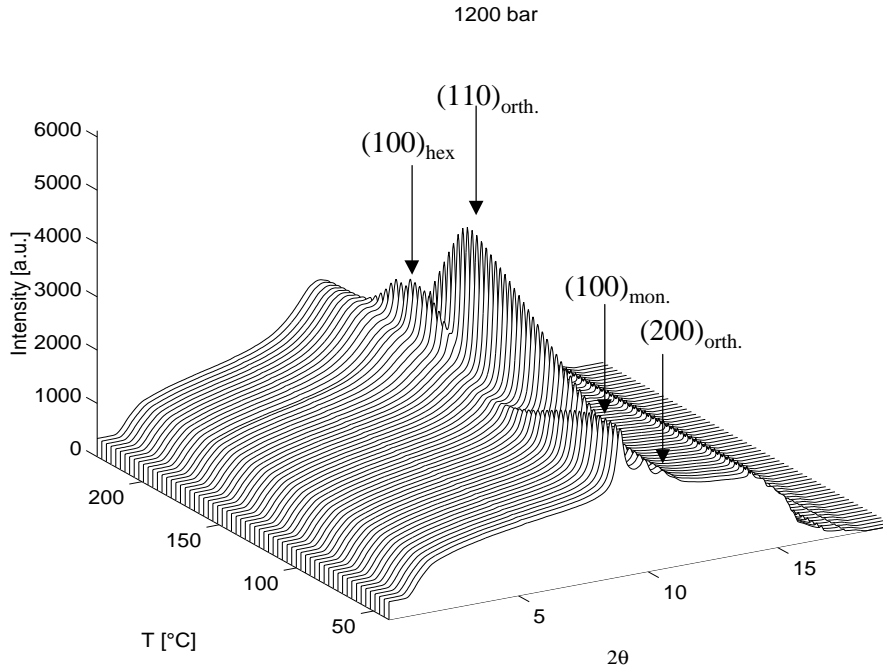


Figure 5.1: *Three-dimensional integrated wide angle X-ray patterns recorded in-situ while heating a laboratory scale UHMW-PE powder at 2°C/min from 30 to 250°C at 1200 bar.*

These results are similar to those of solution-crystallised films presented in Chapter 2, which also melt via the hexagonal phase at pressures much below the equilibrium triple point. The lowest pressure at which the hexagonal phase has been found for solution-crystallised film, is 1500 bar. This is slightly higher than the pressure observed for the nascent material, where for each grade the intervention of the hexagonal phase has been observed at about 1000 bar. This difference can be related to the smaller lateral dimensions of the nascent powders. As already discussed in Chapter 3, due to the small dimensions of the nascent crystals in thickness direction as well as laterally, size dependence of the phase stability has to be considered using an extended form of Gibbs-Thompson equation (Eq. 2.1) which also takes into account the lateral dimensions of the crystal. Consequently, $(T_m^0 - T_m)_{\text{nascent,orth.}}$ becomes larger than $(T_m^0 - T_m)_{\text{solcryst.,orth.}}$ because the lateral dimensions of the solution-crystallised film are several orders of magnitude larger than the dimensions of the nascent powders and, therefore, can be neglected in Eq. 2.1. From this it follows that the orthorhombic to the hexagonal phase transition will occur at lower temperatures and pressures for the nascent material than for the solution-crystallised film, which explains the experimental observations reported in this section.

5.3.2 Sintering of different nascent powders

In the previous section, it has been shown that for the nascent powders, due to the small crystal dimensions, the hexagonal phase can be stable at much lower pressures than the thermodynamic stability region, which makes it attractive for use in polymer processing. The question that arises is whether the intervention of the hexagonal phase can be beneficial in sintering of the nascent powders into homogeneous products, free of fusion defects. The experimental observations on sintering behaviour of different grades of nascent UHMW-PE powders will be presented in this section. The results showing different sintering behaviour for different nascent grades will lead to a new model for sintering UHMW-PE which utilises the phenomenon of the “chain explosion” and the involvement of the hexagonal phase in disentanglement process prior to melting. The experimental evidence of the role of the hexagonal phase as well as “chain explosion” will be treated separately.

5.3.2.1 Experimental observations on sintering behaviour of different nascent powders

In order to assess the influence of the hexagonal phase in the sintering behaviour of UHMW-PE powders, experiments at three different pressures have been performed. The schematic drawing of these experiments with respect to the phase diagram of polyethylene is given in Figure 5.2.

In experiment (a) the powders are compacted at 200 bar and, subsequently, heated to 180°C at a rate of 2°C/min. After leaving the sample in the melt for 10 min, the material is quenched. These processing conditions are very similar to the industrial compression molding used nowadays for the sintering of UHMW-PE powders. In experiment (b), the powders are compacted at 1500 bar and, subsequently, heated to temperatures of 240°C. Upon heating at this pressure all nascent grades undergo the orthorhombic to hexagonal transition prior to melting. After leaving the sample in the melt for 10 min, the pressure is released to 200 bar and the material is, subsequently, quenched to room temperature. It has been shown in Chapter 2 that upon annealing of small folded chain crystals in the hexagonal phase at 1500 bar (below the equilibrium triple point) the isothermal phase reversal takes place due to the thickening of the crystals. This implies that long annealing in the hexagonal phase below triple point pressure is not feasible and, therefore, the long annealing experiments in the hexagonal phase prior to melting need to be performed at a pressure above the equilibrium triple point. This experiment is denoted as experiment (c). Here, the powder is compacted just above 4000 bar and, subsequently, heated up to 265°C at 2°C min⁻¹. From in-situ WAXS and Raman spectroscopy (Chapter 4) it is known that the crystals are fully transformed into the hexagonal phase. At these conditions, the powder is annealed during different times and, subsequently, melted. After releasing the pressure the material is cooled to room temperature.

The fusion of original powder particles is examined by light microscopy using a phase contrast technique.

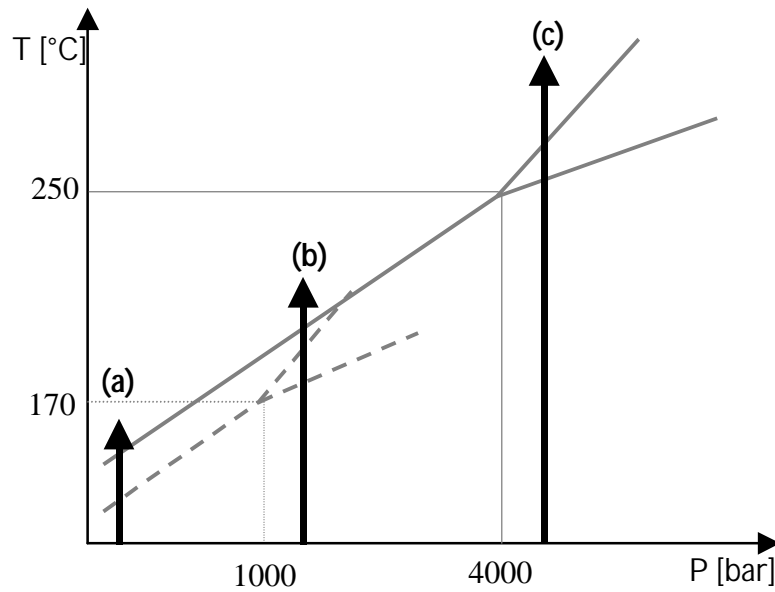


Figure 5.2: Schematic drawing of the sintering experiments with respect to the phase diagram of polyethylene. Full lines represent the equilibrium stability position of the phase diagram while the dotted lines refer to the shifted phase diagram due to the small initial crystal size of the nascent powder (metastable region of the hexagonal phase). Arrows represent the sintering experiments at different pressures performed in this study: (a) 200 bar, (b) 1500 bar, (c) 4100 bar. In all the three experiments the heating rate was $2^{\circ}\text{C min}^{-1}$. After reaching the melt, the pressure was released to 200 bar and the sample was, subsequently, cooled at $10^{\circ}\text{C min}^{-1}$.

(a) Sintering of the different nascent powders at 200 bar (no intervention of the hexagonal phase)

Figure 5.3 shows the results on sintering of the three different powder grades after compaction at 200 bar and subsequent melting.

It can be seen that in the case of the metallocene grade full fusion of the powder particles occurred. On the contrary, the Ziegler-Natta grades, both laboratory and commercial one, still exhibit residues of the original powder particles, as usually observed in the UHMW-PE products available in the market.

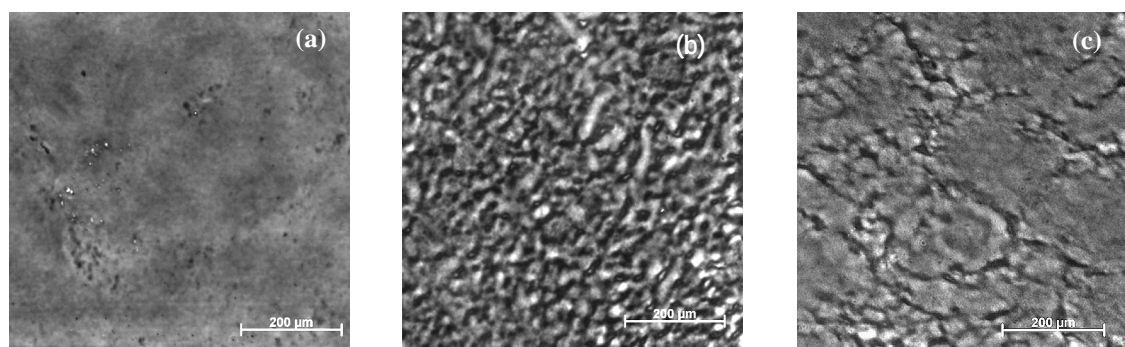


Figure 5.3: Results of sintering three different grades of UHMW-PE at 200 bar. At this pressure no intervention of the hexagonal phase could be observed. (a) Metallocene grade, (b) Laboratory scale Ziegler-Natta grade, (c) Commercial Ziegler-Natta grade.

(b) Sintering of different powders at 1500 bar (intervention of the hexagonal phase)

Figure 5.4 shows the results of sintering of the three different powder grades after compaction at 1500 bar and, subsequent, heating up to the melt at 2°C/min. All sintering experiments are performed in the pressure cell with diamond windows. During the experiments, in-situ Raman spectra were recorded in order to follow phase transformations taking place during sintering, as discussed in detail in Chapter 4. The intervention of the hexagonal phase during heating has been observed for all three powder grades. Figure 5.4 shows that the metallocene grade, as well as laboratory scale Ziegler Natta grade, exhibit full fusion of the powder particles after sintering at 1500 bar. The commercial grade is not properly fused at these sintering conditions, showing clearly the presence of grain boundaries.

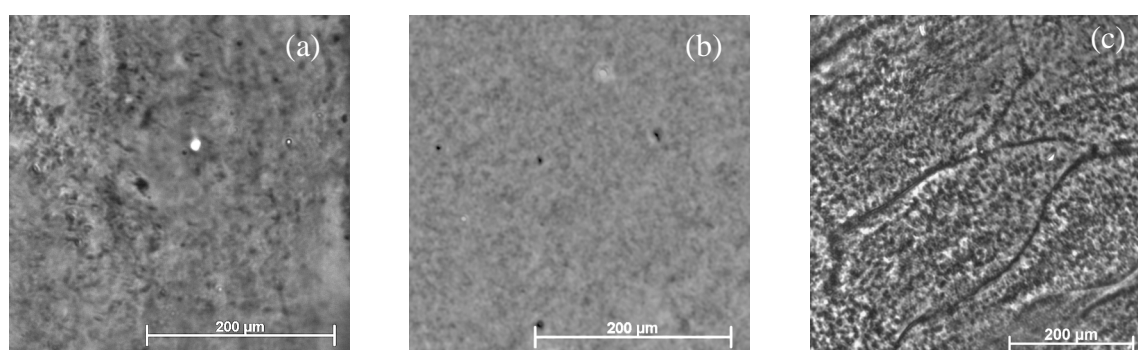


Figure 5.4: Results of sintering three different grades of UHMW-PE at 1500 bar. At this pressures intervention of the hexagonal phase has been observed for all three grades. (a) Metallocene grade, (b) Laboratory scale Ziegler-Natta grade, (c) Commercial Ziegler-Natta grade.

(c) Sintering of different powders after annealing in the thermodynamic stable region of the hexagonal phase (4000 bar)

Since the commercial grade could not be fused by intervention of the hexagonal phase at pressure of 1500 bar (metastable region of the hexagonal phase) experiments were performed at a higher pressure (4000 bar), i.e. in the thermodynamic stable region of the hexagonal phase. At such a high pressure, the temperature window of the hexagonal phase is much broader and, therefore, the residence time of the crystals within the hexagonal phase is much longer. After heating the different powder grades at 4000 bar up to the melt at $2^{\circ}\text{C min}^{-1}$, the metallocene as well as laboratory scale Ziegler-Natta grade exhibited full fusion just like shown in Figure 5.4. On the other hand, the commercial grade stayed improperly fused, exhibiting clearly the presence of the original powder particles, as shown in Figure 5.5a. Therefore further experiments at 4000 bar focused only on the fusion characteristics of the commercial grade of the nascent powder. The samples were annealed in the hexagonal phase during different times prior to melting. Here only the results of annealing for 5 and 12 hours are displayed. It can be seen that after annealing in the hexagonal phase for 5 hours (Figure 5.5b) prior to subsequent melting residues of the original powder particles are still visible, indicating that no fusion has occurred. However after annealing for 12 hours (Figure 5.5c) in the hexagonal phase and subsequent melting the material looks rather homogeneous suggesting full fusion of the original particles.

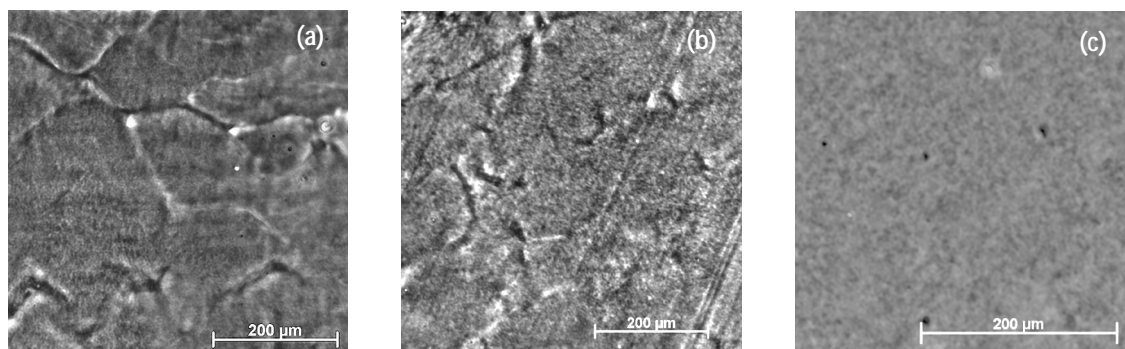


Figure 5.5: Results of sintering of commercial grade of UHMW-PE at 4000 bar, i.e. in the equilibrium stability region of the hexagonal phase. (a) After heating the powder at 4000 bar up to the melt at 2°C/min , (b) After annealing in the hexagonal phase (4000 bar and 270°C) for 5 hours prior to melting, (c) After annealing in the hexagonal phase (4000 bar and 270°C) for 12 hours prior to melting.

These results imply that the hexagonal phase plays an important role in successful sintering of the nascent powders. The influence of the hexagonal phase in the sintering process clearly differs for different powder grades. One of the most prominent differences between the three grades, used in this study, is believed to be the initial entanglement density of the original powder, as suggested in Chapter 3. It has been shown that the metallocene grade can be

compacted at low temperatures (below the α -transition temperature) in fully coherent and transparent films (Figure 3.1), which has been associated to the low initial entanglement density. Such morphological characteristics are believed to be a consequence of the synthesis characteristics, notably the use of homogeneous metallocene catalysts. For such, almost fully, disentangled chains “chain explosion” upon melting becomes feasible and the chains, which undergo a huge increase in radius of gyration, are able to cross from one powder particle to another. On the other hand, the ductility for Ziegler-Natta grades at temperatures below the α -relaxation temperature is less (Figure 3.1), suggesting that the chains are entangled to a certain extent. This extent highly depends on the synthesis conditions and it is shown to be less for laboratory scale Ziegler Natta powder, which is synthesised at lower temperatures, using a lower activity catalyst. In order to fuse powder particles through the process of “chain explosion”, it is necessary to disentangle molecular chains prior to melting. The disentanglement of the chains is possible within the hexagonal phase, which is characterised by enhanced chain mobility in the chain direction, ultimately leading to formation of the extended chain crystals. As already mentioned in the introduction, thickening within the hexagonal phase can be regarded as a process of pulling chains into a crystal, which is in fact a process of disentanglement¹⁷. Depending on the initial entanglement density, different residence times within the hexagonal phase are needed for the process of disentanglement. For laboratory scale Ziegler-Natta grade the residence time while heating the sample at 1500 bar at 2°C/min is enough for the chains to disentangle sufficiently prior to melting. On the other hand, highly entangled commercial grades of nascent powder, require rather long times within the hexagonal phase in order to disentangle to the extent needed to undergo the “chain explosion” upon melting. If this is the case, the thickening of the crystals within the hexagonal phase should be different for different nascent grades. In order to confirm this assumption, the following experiment has been performed on laboratory as well as commercial Ziegler-Natta grades. The samples were compacted at 1500 bar and, subsequently, heated at 2°C min⁻¹. The experiments were performed within the pressure cell which enabled in-situ recording of the Raman spectra during the phase transformation from the orthorhombic into the hexagonal phase. Once all the crystals have been transformed into the hexagonal phase, heating was stopped (before melting of the crystals) and the sample was cooled. In order to observe different thickening behavior, transmission electron microscopy was performed on both samples. The results are shown in Figure 5.6. These results confirm that the ability of nascent crystals to thicken within the hexagonal phase, highly depends on the initial entanglement density. For the grade possessing a lower initial entanglement density (laboratory scale Ziegler-Natta grade), even relatively short residence times within the hexagonal phase are sufficient for crystals to thicken up to lamellar thickness of about 100 nm. On the other hand, for the initially highly entangled state (commercial Ziegler-Natta

grade) the same time within the hexagonal phase leads to the crystal thickness not higher than 30 nm. Consequently, the disentanglement process of the initially highly entangled system, within the hexagonal phase, requires much longer times than in the case of the initially disentangled state.

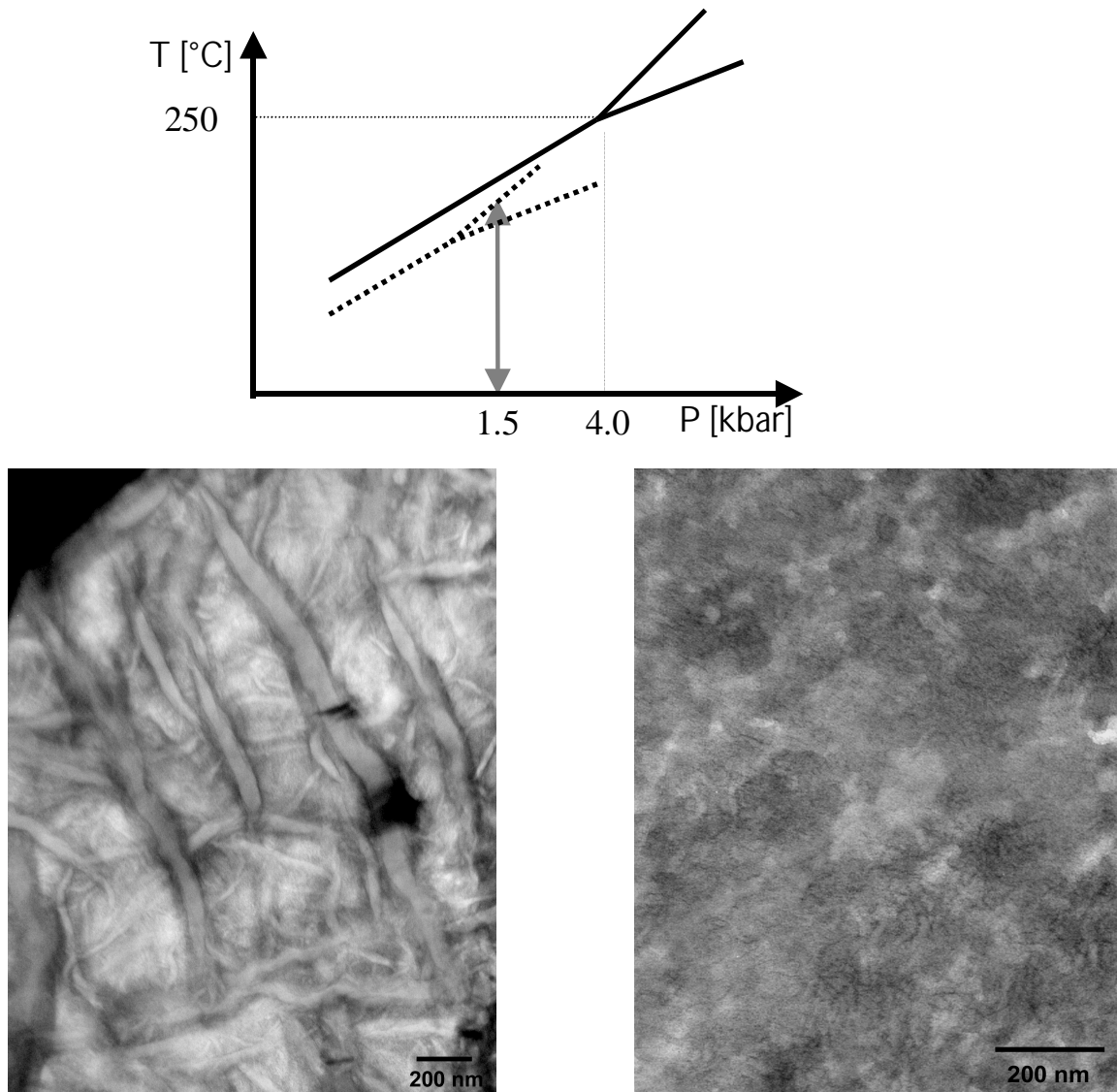


Figure 5.6: Transmission Electron Micrograph of (a) laboratory scale Ziegler Natta grade of UHMW-PE and (b) commercial grade UHMW-PE pressed and heated at $2^\circ\text{C}/\text{min}$ up to the hexagonal phase at 1500 bar as depicted in schematic drawing above the micrographs. Full lines present the thermodynamic equilibrium position of the phase diagram. The dotted line is the stability phase diagram for initially small crystal sizes. The experiments depicted in this figure are performed in this metastable region of the hexagonal phase (dotted stability diagram).

Following this discussion a new mechanism has been proposed to describe the role of the hexagonal phase, as well as “chain explosion”, in the sintering of the nascent powders. The model is drawn schematically in Figure 5.7.

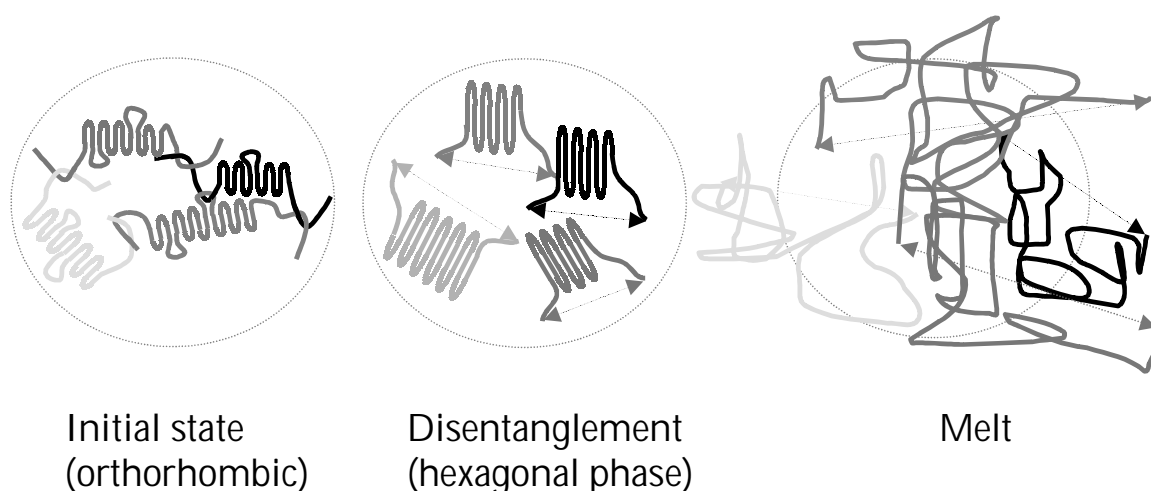


Figure 5.7: A cartoon describing the motion of the chain, anticipated to occur during processing of the nascent powder via the hexagonal phase.

Initially small folded chain crystals, which are entangled to a certain extent (in the case of the Ziegler-Natta grade), will thicken within the mobile hexagonal phase. During this thickening process, chains are pulled into a crystal which ultimately leads to a more disentangled state. Upon melting, such disentangled crystals will undergo the process of “chain explosion”, which will subsequently lead to the fusion of the powder particles. In the case of an initially fully disentangled state (metallocene grade), a disentanglement process within the hexagonal phase is not required and the process of “chain explosion” can occur even without prior intervention of the hexagonal phase.

In order to elaborate on the proposed model, two different features playing role in the fusion of powder particles, notably disentanglement within the hexagonal phase and “chain explosion” upon melting, will be discussed separately in following sections.

5.3.2.2 Experimental evidence of the importance of the residence time in the hexagonal phase during sintering

From the above set of experiments it is evident that the residence time within the hexagonal phase plays an important role in sintering of different UHMW-PE powder grades. A grade with the highest entanglement density requires the maximum residence time for the crystals in the hexagonal phase. This has already been mentioned in the previous section where the results on the sintering behavior of the commercial Ziegler-Natta grade at 4000 bar has been

discussed. It has been shown that, only after sufficiently long time within the hexagonal phase, fusion of powder particles occurs after melting and subsequent re-crystallisation.

To strengthen this idea, an experiment is performed on a laboratory scale Ziegler-Natta grade. The pressure and temperature regime are kept the same as in the previous experiments (Figure 5.4), whereas the residence time in the hexagonal phase is altered by applying different heating rates. The sample is again compacted to 1500 bar at room temperature and subsequently heated up to the melt at $5^{\circ}\text{C min}^{-1}$ (it should be noticed that the heating rate used in the previous experiment, Figure 5.4, was $2^{\circ}\text{C min}^{-1}$). The results of sintering are given in Figure 5.8, which clearly shows that a heating rate of $5^{\circ}\text{C min}^{-1}$ did not provide sufficient residence time of the material in the hexagonal phase and, consequently, no required disentanglement could be achieved.

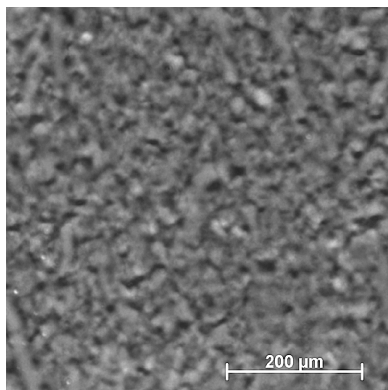


Figure 5.8: *Light micrograph of on laboratory scale Ziegler-Natta grade after heating the powder at 1500 bar to the melt at 5°C/min .*

In the following experiment, the residence time of the crystals within the hexagonal phase, was varied by keeping the heating rate constant and changing the pressure at which the sintering is performed. For this purpose experiments were performed on laboratory scale Ziegler-Natta grade at pressures of 900 bar, 1200 bar and 1500 bar. In all three experiments the powders were compacted at the desirable pressure, heated to the melt at $2^{\circ}\text{C min}^{-1}$ and subsequently cooled at pressure of 200 bar. The results are depicted in Figure 5.9.

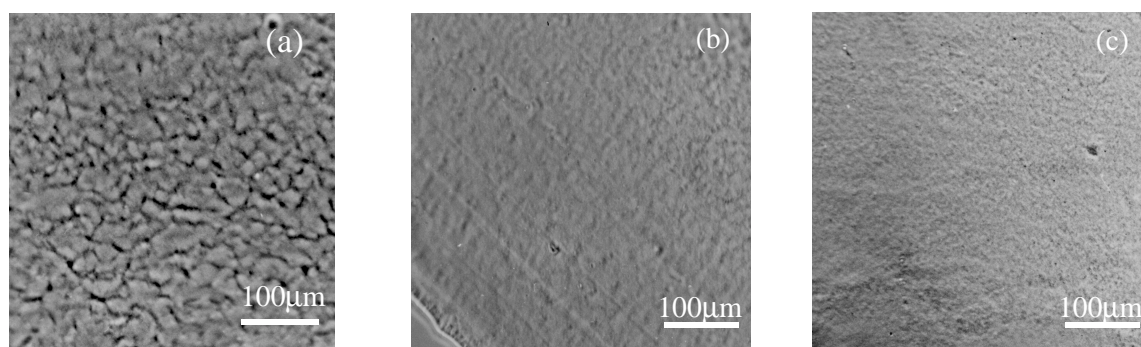


Figure 5.9: Sintering results on a laboratory scale Ziegler-Natta grade after heating the powder up to the melt at different pressures: (a) 900 bar, (b) 1200 bar and (c) 1500 bar.

After sintering the nascent powder at 900 bar, where no intervention of the hexagonal phase could be observed, the powder particles remain unfused, like already shown in Figure 5.3. At 1200 bar, the material melts via the hexagonal phase (as observed by in-situ WAXS experiments) and accordingly sintering results suggest certain improvement in the fusion, however, sample still exhibits residues of the original powder particles (Figure 5.9b). Finally, at 1500 bar the powder particles are fully fused, as already shown in Figure 5.3. These results suggest that the temperature window, in which the hexagonal phase intervenes at a pressure of 1200 bar, is too narrow to allow a full disentanglement of the chains and, consequently, leads to partial fusion of the original powder particles.

These results imply that the hexagonal phase undoubtedly influences the sintering results of the different powders. The following task is to assess the role of the “chain explosion” upon the sintering of nascent powders.

5.3.2.3 Experimental evidence of the role of the “chain explosion” in the sintering of nascent powders

“Chain explosion” is a phenomenon that can not be assessed experimentally using direct methods, specially not for ultra high molecular mass polymers where partial deuteration always leads to phase separation²⁴. Due to this reason, a direct measuring of the molecular trajectories with the help of neutron scattering becomes impossible and therefore an indirect route has been used to assess the phenomenon of “chain explosion” during sintering of the nascent powders. It is believed in the further discussion that the tremendous increase in radius of gyration, which occurs upon “chain explosion”, enables molecular chains to cross from one powder particle to another leading to full sintering of the powder particles. In order to prove that the process of “chain explosion” plays a role in the fusion process, the following set of experiments on the laboratory scale Ziegler-Natta grade has been performed. The schematic drawing of the pathways used in the experiments is given in Figure 5.10.

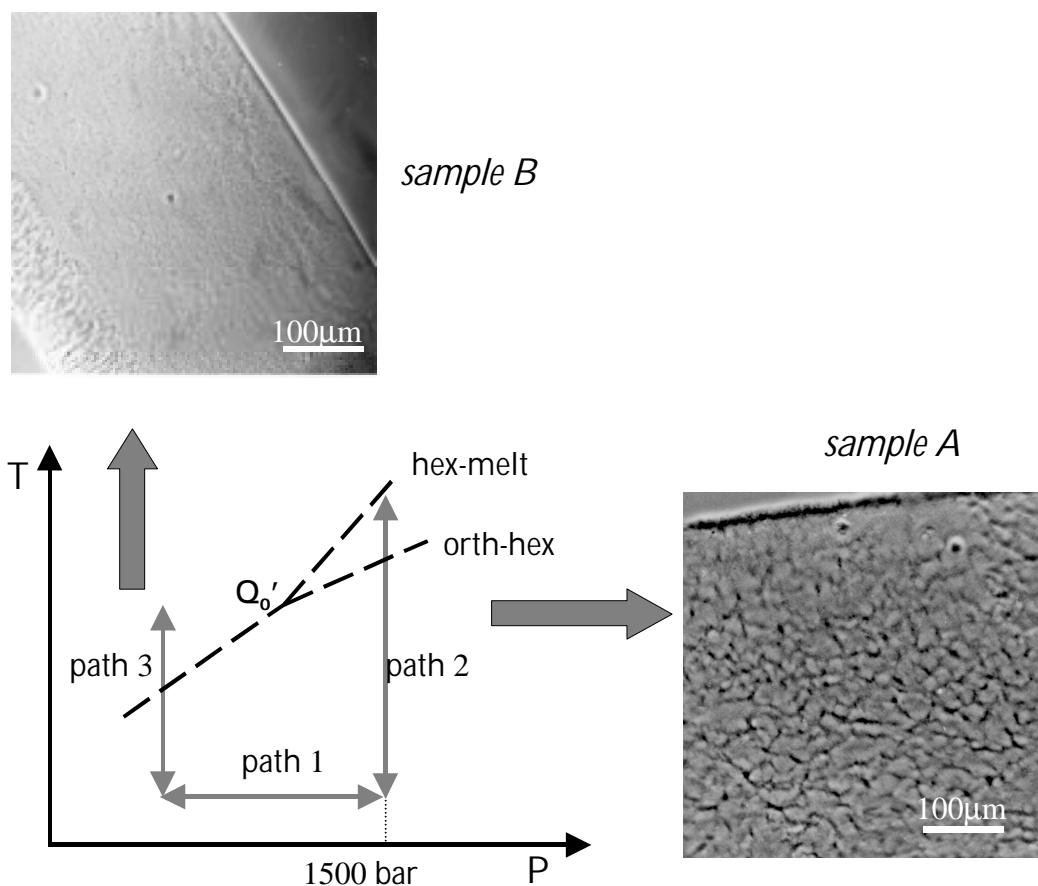


Figure 5.10: Schematic diagram of the pathways used in the experiments. In both experiments pathways 1 and 2 were followed. Sample A represents the sample taken from the pressure cell after cycle 1 and 2. Sample B has been melted and recrystallised (along pathway 3) after an initial step 1 and 2.

The sample was compacted at room temperature to 1500 bar (path 1) and subsequently heated at a rate of $2^{\circ}\text{C min}^{-1}$ up to 230°C (path 2). With help of in-situ Raman spectroscopy it could be seen that at this temperature the polyethylene crystals were fully transformed into the hexagonal phase. After reaching the desired temperature of 230°C , without allowing any melting of the crystals, the sample was cooled immediately to room temperature isobaric along path 2. Subsequently the pressure was released to atmospheric pressure (path 1). The same procedure was done with two different samples of the same Ziegler-Natta grade. The sample named as sample A was immediately taken out of the pressure cell and investigated by optical microscopy. The results are shown in Figure 5.10. It can be concluded that the intervention of the hexagonal phase only, without further melting of the sample, does not lead to fusion of the original powder particles. Therefore another sample (sample B), which was subjected to the same pressure-temperature cycle, was subsequently melted at atmospheric pressure and cooled to room temperature (path 3). Figure 5.10 shows that sample B is fully

free of the residues of the original powder particles. These results strongly suggest that, after sufficiently long time within the hexagonal phase, which allows full disentanglement of molecular chains, the material will undergo the process of “chain explosion” even when melted at atmospheric pressure. The only prerequisite for molecular chains to experience the phenomenon of “chain explosion”, is the presence of a fully disentangled state which can be achieved by sufficiently long annealing in the hexagonal phase, or directly in the reactor using adequate catalyst systems (homogeneous metallocene catalyst).

5.4 Conclusions

In this chapter a new route to sinter UHMW-PE powders has been introduced. It has been shown that the sudden increase in radius of gyration during melting of fully disentangled folded chain crystals, usually referred to as “chain explosion”¹⁴, plays an important role in sintering of the nascent powders. Normally, the mobility of long molecular chains in the melt is restricted due to fundamental laws related to the strong dependence of the zero-shear viscosity and reptation time on molecular weight. Consequently, during melt processing of UHMW-PE powders, chains are not able to reptate from one powder particle to another, which leads to products having residues of the original powder particles, usually referred to as grain boundaries. The experimental results presented in this chapter suggest that the sudden instantaneous increase in the radius of gyration during melting of fully disentangled chains leads to sufficient mobility of the chains which enables them to pass from one powder particle to another. The process of “chain explosion” becomes feasible only if the chains are fully disentangled¹⁴. Most of the commercial grades of UHMW-PE are produced with the help of Ziegler-Natta catalysts. Those catalyst systems are supported, which means that during polymerisation molecular chains are growing relatively close to each other, leading to the system that is hardly ever fully disentangled. Consequently, in order to sinter these powders via “chain explosion” it is necessary to disentangle the initially entangled chains prior to melting. The thickening of the crystals within the hexagonal phase can be seen as a mean of disentanglement as the chains are being pulled during thickening process of crystal. It has been shown that, depending on the initial entanglement density of the original powder particle, different residence times are needed within the hexagonal phase to provide sufficient disentanglement which would subsequently lead to “chain explosion” upon melting. A laboratory Ziegler-Natta grade which is characterised by a lower initial entanglement density, requires much shorter residence times in the hexagonal phase than the initially highly entangled commercial grades of UHMW-PE. The influence of the hexagonal phase in processing of UHMW-PE nascent powders becomes now feasible, since it has been shown that, for a small initial crystal size, the stability region of the hexagonal phase can be obtained at much lower pressures than the equilibrium triple point position. In that sense, by a proper

choice of synthesis conditions it is possible to create Ziegler-Natta based nascent powders which can be processed via the hexagonal phase at pressures below 1500 bar, which is industrially rather feasible.

On the other hand, the results show that it is possible, by the right choice of catalyst type, to synthesise powder which would be sufficiently disentangled to undergo the phenomenon of “chain explosion” upon melting, without prior intervention of the hexagonal phase. Such an alternative type of catalyst is shown to be a homogeneous metallocene catalyst, where the active sites are dispersed within the reaction medium, providing chains growing sufficiently far from each other and, consequently, the resulting powder possesses a rather low number of entanglements, as elaborated in Chapter 3. Such powders can, according to the proposed model, be successfully sintered at minimal pressures, which are in this case only needed to obtain the desired shape of the final product. These findings can be rather beneficial in further processing developments of UHMW-PE powders, since the tedious procedures of the usual two stage processing involving compression moulding (or ram extrusion) into simple shapes and subsequent machining could be replaced by simple process which would allow direct molding into desired shapes. It will be shown in Chapter 6 that grain boundary free materials are characterised by superior mechanical properties, which makes them attractive for the whole spectrum of applications.

5.5 References

1. Li, S.; Burstein, A.H. *J. Bone and Joint Surg.* **1994**, *76A*, 1080
2. Kurtz, S.M.; Muratoglu, O.K.; Evans, M.; Edidin, A.A. *Biomaterials* **1999**, *20*, 1659
3. Schmalzried, T.P.; Callaghan, J.J. *J. Bone and Joint Surg.* **1999**, *81A*, 115
4. Bastiaansen, C.W.M. *Ph.D. thesis*, Eindhoven University of Technology, **1991**
5. Bastiaansen, C.W.M.; Meyer, H.E.H.; Lemstra, P.J. *Polymer* **1990**, *31*, 1435
6. Jenkins, H.; Keller, A. *Macromol. Sci. Phys. Part B* **1975**, *11*, 301
7. Ferry, J.D. *Viscoelastic Properties of Polymers*, John Wiley & Sons: Toronto, **1980**
8. Gedde, U.W. *Polymer Physics*, Chapman&Hall: London, **1995**
9. Salem, D.R. *Structure Formation in Polymeric Fibres*, Hanser Publishers: Munich, **2000**
10. Smith, P.; Lemstra, P.J. UK Patent 2, 051,661, **1979**
11. Smith, P.; Lemstra, P.J. *Makrom. Chem.* **1979**, *180*, 2983
12. Smith, P.; Lemstra, P.J.; Booij, H.C. *J. Polym. Sci., Phys. Ed.* **1982**, *20*, 2229
13. Smith, P.; Lemstra, P.J. *J. Mater. Sci.* **1980**, *15*, 505
14. Barham, P.; Sadler, D.M. *Polymer* **1991**, *32*, 393
15. Shcherbina, M.A.; Chvalun, S.N.; Selikhova, V.I.; Neverov, V.M.; Aulov, V.A.; Ozerin, A.N.; Bakeev, N.F. *Polymer Science, Ser. A* **1999**, *41*, 1121
16. Maxwell, A.S.; Unwin, A.P.; Ward I.M. *Polymer* **1996**, *37*, 3282
17. Psarski, M.; Piorkowska, E.; Galeski, A. *Macromolecules* **2000**, *33*, 916
18. Hikosaka, M.; Tsukijima, K.; Rastogi, S.; Keller, A. *Polymer* **1992**, *33*, 2502

19. Waddon, A.J.; Keller, A. *J. Polym. Sci.: Part B: Polym. Phys.* **1990**, 28, 1063
20. Waddon, A.J.; Keller, A. *J. Polym. Sci.: Part B: Polym. Phys.* **1992**, 30, 923
21. Kolnaar, H.E.H.; Keller, A. *Polymer* **1994**, 35, 3863
22. Kolnaar, H.E.H.; Keller, A. *Polymer* **1995**, 36, 821
23. Bastiaansen, C.W.M.; Lemstra P.J. *Macromol. symp.* **1989**, 28, 73
24. Higgins, J.S.; Benoît, H.C. *Polymers and Neutron Scattering*, Clarendon Press: Oxford, **1994**.

Chapter 6

Wear and fatigue resistance of fully sintered UHMW-PE products for medical applications such as hip and knee joints

6.1 Introduction

It has already been mentioned in Chapters 1 and 5 that UHMW-PE possesses superior mechanical properties in comparison with its thermoplastic counterparts. These excellent properties are a consequence of the high molecular weight ($M_w > 3 \cdot 10^6 \text{ g mol}^{-1}$ according to ASTM D4020). UHMW-PE has been selected as the material of choice in high demanding applications, like bearing surfaces for total knee and hip replacement^{1,2}. However, it has been recognised that the lifetime of such joints, where the UHMW-PE is used as a countersurface paired with metal or ceramics (alumina or zirconia), is not sufficient¹. In most of the cases when revision surgery is required, it is the UHMW-PE part which fails due to excessive wear and wear debris generation in the neighbourhood of the joint^{3,4}. In an artificial hip prosthesis, where a metal (stainless steel or CoCr alloy) or ceramic ball articulates inside of an acetabular cup made of UHMW-PE (Figure 1.2a, Chapter 1), tens of thousand microscopic wear particles are produced during every step of walking^{2,5}. The accumulation of these particles in the neighbourhood of the joint may cause harmful biological tissue reactions which ultimately lead to bone loss (or osteolysis)^{3,6,7,10}. Such debris-induced osteolysis causes pain and discomfort to the patient and, in most of the cases, requires revision surgery. In the knee joint, however, a convex metallic femoral component articulates against a non-conformal UHMW-PE tibial plate (Figure 1.2b, Chapter 1). Because of the incongruent contact in the knee joint, much higher contact stresses are experienced by the UHMW-PE tibial component which consequently leads not only to the generation of microscopic wear particles but also to macroscopic wear induced by delamination and pitting^{8,9}. The failure of the UHMW-PE part in a total joint replacement is still a subject of many extensive studies, which comprise detailed survey into structure, morphology and mechanical properties of the polymer at every stage of its production from original powder into stock material and final product². In general, wear resistance of the UHMW-PE component in artificial joints is considered to be determined by the original powder characteristics, the manufacturing and the method of sterilisation¹⁰.

It has been already discussed in the previous chapters that melt processing of UHMW-PE is difficult because of its high molecular weight which causes a high melt viscosity and long reptation times. Consequently, products made of UHMW-PE contain residues of the original powder particles, which have always been considered as one of the possible reasons for insufficient lifetime of UHMW-PE components in high demanding applications¹¹. This subject remained rather speculative, since no considerable progress has been made so far to obtain products fully free of fusion defects, which could serve as test samples for further investigations. In Chapter 5 a novel route to process UHMW-PE nascent powders into products, free of grain boundaries, has been introduced. The feasibility of making such homogeneous products made it possible to study the influence of enhanced fusion on wear and fracture characteristics of the material. This study will be addressed in this chapter.

In order to be able to understand and discuss the experimental results, some fundamental features of wear mechanisms, related to the complex kinematics of the human joint, will be recapitulated in a short literature survey.

6.1.1 Wear mechanism acting on UHMW-PE components in artificial hip and knee joints: a literature survey

Tribology, which embraces the study of wear and friction, is a rather complex discipline. Wear and friction characteristics depend on many different parameters like material bulk properties, surface characteristics, type of contact between two surfaces, kinematics and environmental conditions. This implies that wear and friction characteristics are highly dependent on the system rather than being intrinsic properties of the material¹². Due to the complexity of the system, and its parameters (solid body, counter body, interfacial medium and environment), wear and friction characteristics of a material can vary in different type of application¹³.

Wear is defined as “the progressive loss of material from the surface of a solid body due to mechanical action”¹⁴. In general, when discussing the wear behaviour of a system, three different mechanisms are usually distinguished¹⁵. The most common wear mechanism found in polymers is *adhesion wear* which may act when two solid surfaces slide against each other. Usually, when a polymer surface is in sliding contact with a metal (or ceramic) surface, a thin polymer film is formed on the hard counter surface, which in the course of sliding can be fully detached and act as a loose wear particle¹⁶. This phenomenon is only possible if lubrication is poor. Adhesion wear has been found in both, the acetabular cup of the hip joint as well as in the tibial plateau of the knee joint. This implies that in the current design of prostheses, specially in the hip joints, lubrication is rather poor¹³. *Abrasive wear* occurs when material is removed, or displaced from a surface, by hard particles or by hard protuberances on a counter surface. The type of wear where hard particles are introduced between two

surfaces in the contact, is usually addressed as three body abrasion wear while the wear type induced by the protuberances on the counter surface is referred to as two body abrasion wear¹⁵. Abrasion is always found in artificial joints, both hip and knee¹³. It has been recognised, however, that this mechanism solely does not lead to fatal failure of the UHMW-PE component within the artificial joint. *Fatigue wear* can occur under cyclic loading and manifests itself in the formation of surface and subsurface cracks, which consequently lead to macroscopic delamination and pitting^{9,17}. It has been recognised that the motion within the knee joint includes continuous rolling and sliding of the convex metal against the polyethylene tibial component¹⁸. Due to such loading/unloading cycles, surface fatigue becomes rather prominent, which has been shown to lead to macroscopic fracture¹⁰. From this discussion it is rather obvious that the wear mechanisms act together and affect each other, which makes identification of the acting wear mechanisms in certain applications a rather tedious and complex problem. All attempts to improve polyethylene wear in artificial joints have been hindered due to the lack of fundamental understanding of wear mechanisms related to the complicated kinematics of the human joint. Recently, considerable progress has been made in the systematic development of models which successfully explain wear rates and wear modes found *in vivo* and *in vitro* (i.e. joint simulators)¹⁹. The motion-dependent friction characteristics of linear semicrystalline polymers have been reported long time ago in the pioneering work of Pooley and Tabor²⁰. However, only recently it has been confirmed that the wear resistance of UHMW-PE is also rather sensitive to the mode of relative motion^{21,22}. The experiments showed that linear motion results in very low wear rates for UHMW-PE. Contrarily, in multidirectional motion, wear rates of UHMW-PE reach very high values. These results have been associated with the molecular orientation found on the polyethylene surface after wear experiments²³. Such molecular orientation exhibits an anisotropic behaviour at the surface, which results in a structure being stronger in the orientation direction and weaker in the transverse direction²³. The sensitivity of UHMW-PE wear behaviour on the direction of motion is extremely important in its applications in artificial joints. Simulations of shear stress distributions on articulating surfaces of the hip joint, showed that the stress pattern developed during normal gait is multidirectional. Such pattern is usually referred to as a “cross-shear”²⁴ or “butterfly”²³ pattern. It has been shown further that the stress magnitude in one direction (main direction) is 20% larger than in the transverse direction. Similarly, the frequency at which the shear stress occurs is five times higher in the main direction. Due to such distributions of stress magnitudes and frequencies, polymer molecules are able to orient in the maximum stress direction. Consequently the material becomes stronger in the main direction where the strength is determined by the covalent bonds. However, in the transverse direction only weak van der Waals forces are present between molecules which leads to the orientational softening. Accordingly,

detachment of the fibrous debris from the surface will occur, if the motion of the counter surface is in the transverse direction. The shape of wear debris found within the blood stream is fibrous like^{25,26}, which confirms the suggested model. From this, it follows that the most important material property for wear resistance in applications which involve multidirectional motion is the resistance of the material to orientational softening¹³. Since molecular orientation is related to linear polymers rather than the branched or crosslinked ones, a way to improve wear resistance of the UHMW-PE is to convert the linear structure into the crosslinked one^{13,27,28}. If the chains are chemically bonded (by gamma irradiation or electron beam radiation), they are not able to orient and the material will consequently exhibit no significant wear upon multidirectional motion. An extensive amount of work has been performed in this direction and it is now generally accepted that crosslinked UHMW-PE exhibits practically no wear under multidirectional contact²⁸. Therefore, such modified crosslinked UHMW-PE is believed to be the ultimate improvement of a UHMW-PE part in artificial hip joints.

The kinematics of the knee joint is, however, much more linear¹³. The cross-shear motion is still present but the maximum transverse angle is not higher than 10°, which is much lower than in the hip joints where possible crossing are up to 90°. That means that the orientation softening does not play such a dominant role in wear behavior of knee joints, as it does in the case of the hip joints. The amount of wear debris found for the knee joint is also substantially less than in the case of the hip joints²⁶. However, as already mentioned, the contact stresses experienced by tibial component of the knee joint are much higher than in the hip cup. The motion experienced by tibial polyethylene component is identified as cyclic rolling and sliding, which causes fatigue, causing itself failure due to the formation of surface- and subsurface- microcrackings and, finally, delamination¹⁸.

The role of grain boundaries, in the different wear mechanisms responsible for insufficient lifetime of artificial joints, will be discussed in this chapter.

6.2 Experimental section

6.2.1 Materials

In this chapter, different types of polyethylene have been used. The main investigation has been performed on *grain boundary free* UHMW-PE that has been processed via the novel route presented in the Chapter 5. For this purpose, a special cylinder has been constructed in order to be able to process sufficiently big samples at pressures above 1000 bar. The laboratory scale Ziegler-Natta powder was compacted at 1500 bar and subsequently heated at 2°C/min up to the melt. After reaching the melt, the pressure was released and the sample has

been left to cool. Due to the lack of the proper cooling system the resulting material is shown to possess a somewhat higher crystallinity, as shown in Table 6.1.

As a reference material, an industrially processed (via ram extrusion) commercial UHMW-PE (GUR 4150) has been used. This material is a standard material used for investigations of UHMW-PE in artificial joints. It has been confirmed, with the help of optical microscopy, that it still exhibits residues of the original powder particles.

Further, wear investigations were performed on *crosslinked* UHMW-PE that is nowadays considered the alternative for the applications in artificial joints^{27,28}. It is generally accepted that this material exhibits no substantial surface wear under multidirectional motion^{2,13}. However, crosslinking does not affect the homogeneity of the sample in the sense of fusion of the original powder particles and, consequently, the material exhibits the same type of the fusion defects as observed in conventional products of UHMW-PE. The crosslinked material used in this study is Durasul[®], kindly provided by SulzerMedica. The material is crosslinked with the help of electron beam radiation at elevated temperatures. Subsequently, the material is melted in order to eliminate the trapped free radicals. This step is rather important to prevent oxidation of the sample²⁹.

Table 6.1: Physical properties of different polyethylene samples used in this study.

Properties	grain boundary free UHMW-PE	reference (GUR 4150)	Durasul (crosslinked)	high pressure (UH410)
M_w [g/mol]	$3.6 \cdot 10^6$	$3-6 \cdot 10^6$	$M_c=5500 \pm 300$	$3 \cdot 10^6$
Crystallinity [%]	55 ± 1	49.5 ± 1	50 ± 1	55 ± 1
Yield stress [MPa]	26 ± 0.5	20 ± 0.5	20 ± 1	23 ± 1
E-modulus [GPa]	1.0 ± 0.1	0.9 ± 0.5	1.0 ± 0.5	0.98 ± 0.1
Stress at break [MPa]	50 ± 2.0	37 ± 2.0	30 ± 2.0	43 ± 2.0
Strain at break [%]	327 ± 10	302 ± 10	274 ± 10	300 ± 10
Lamellae thickness [nm]	20-50	10-35	10-20	20-50
Density [kg/dm^3]	0.95	0.94	0.94	0.95
Grain boundaries	no	yes	yes	yes

In fatigue experiments two extra materials have been used. In order to eliminate the influence of crystallinity on crack propagation measurements, a commercial grade of UHMW-PE (UH410, DSM) was processed in the same way as the grain boundary free material. The product thus obtained possesses, approximately, the same crystallinity as the grain boundary free material, but, due to the insufficient residence time in the hexagonal phase, the grain boundaries still remain. The physical properties of these materials are given in Table 6.1.

6.2.2 Pin on ball wear machine

In order to quantify wear resistance of the UHMW-PE component within a total hip joint, a wear machine which follows the multidirectional kinematics of the joint has to be used. Due to the scarce availability of real hip simulators, an alternative wear machine has been used in this study. This specially designed wear machine, further referred to as the pin on ball, was shown to be able to reproduce a multidirectional motion, similar to the one found in hip joints during a normal gait³⁰. This machine is available at AO Research Institute in Davos (Switzerland) where all the experiments have been performed.

The pin on ball machine consists of a concave pin (made of UHMW-PE) sliding against a conforming ball, which is usually made of commercially available femoral head (CoCrMo). In the setup, which has been used in this work, two polyethylene pins were pressed orthogonally against one femoral head. Such construction has the advantage of generation of equivalent normal load on both pins, as pictured in Figure 6.1a.

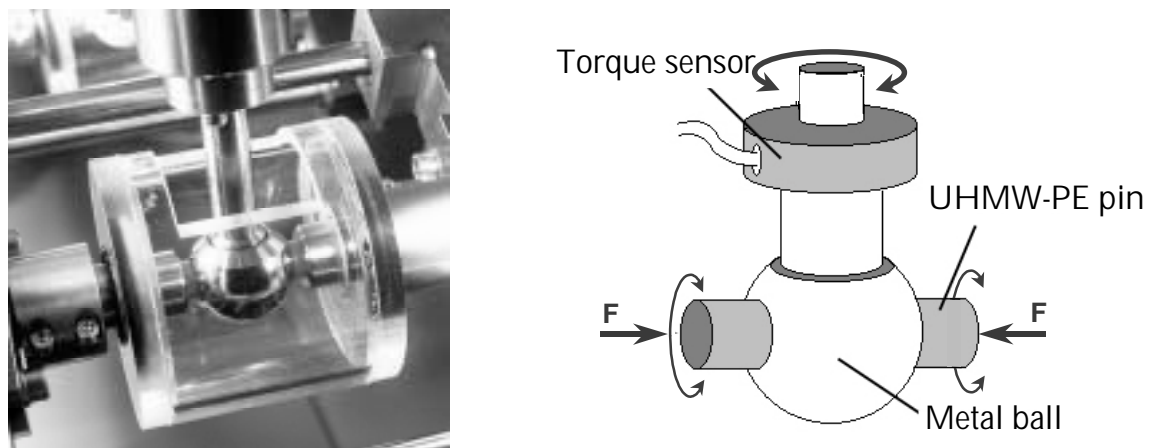


Figure 6.1: (a) Photograph of the Pin on Ball machine. (b) Schematic drawing of the main principle of the Pin on Ball wear machine for multidirectional motion.

A two-dimensional motion is generated by independent axial oscillation of pin and ball. By adjusting the proper phase shift of the oscillation of the pin with respect to the ball, multidirectional motion can be achieved where the trajectories of the adjacent points cross each other during a cycle (Figure 6.1b).

In the current setup, a six-station pin-on-ball testing device has been used, which allowed testing of 12 samples at the time. All the experiments were performed in diluted calf serum (33%), which was placed in Plexiglas container tempered at 37°C. Each test station consisted of a commercially available CoCrMo-ball (Ø28 mm), fitted between two concave UHMW-PE-pins. The clearance between those components resembled the one found within a real

artificial joint. A constant compressive load of 1000 N (nominal contact pressure is 8.8 MPa) was applied for 5 million cycles. In order to reduce the influence of fluid uptake (soak) and creep of UHMW-PE special preconditioning has been performed prior to wear experiments. First, UHMW-PE pins were soaked in the serum for 48 hours without any load. After cleaning in the distilled water and subsequent drying in the flowbox, the pins were weighed and the weight loss was taken as a starting zero. Subsequently, the pins were placed in the pin on ball machine and loaded with 1000N within the serum. After 48 hours of preloading wear measurements started by axial oscillations of pin and ball at frequency of 1.8 Hz. Every 500.000 cycles, the motion of the systems was stopped for weight loss measurements. The pins were weighed together with the metal holder on which they were glued with the help of PMMA. In total three series of experiments have been performed, which means that six samples of each material were tested.

Due to the ability of the polyethylene pins to absorb some fluid, the presence of the lubricant during wear measurements can influence the gravimetric measurements of the wear. Therefore, a separate set up, similar to the pin on ball machine, has been build to monitor the fluid uptake during the experimental time. The soak station is displayed in Figure 6.2. Pins were statically loaded with the same force as in the wear testing machine and left within the serum for the same period of time as in the wear machine, i.e. at the time it took for each 500.000 cycles, the samples were weighed. Prior to each next step of time it took for 500.000 cycles, pins were preconditioned in the same manner as for the wear testing.

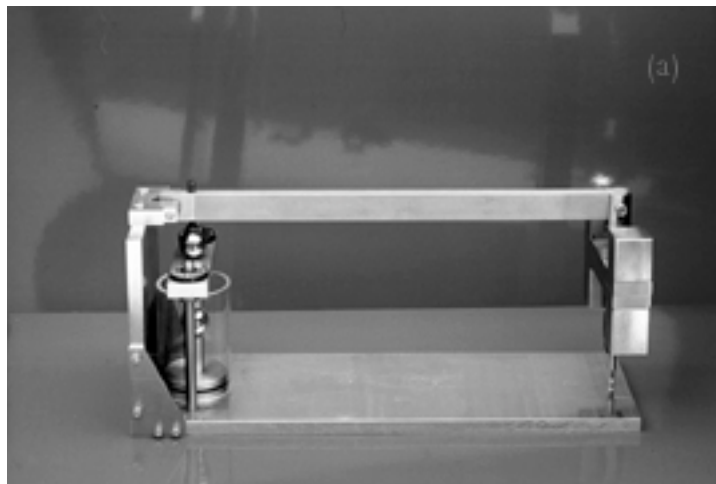


Figure 6.2: *Photograph of the soak station.*

After the time it took for 500.000 cycles the lubricant was changed and the used one was kept apart (at -18°C) for the particle analysis. The separation procedure of Scott³¹ has been followed. Prior to filtering the suspension was shaken within the ultrasonic bath. Filtering has been performed with the help of a polycarbonate filter membrane, having a pore diameter of $0.1\ \mu\text{m}$. Wear particles (debris) were determined with the help of Scanning Electron

Microscopy. The quantification of the particle size distribution has been done by using Equivalent Circle Diameter (ECD) which is for model shape as shown in Figure 6.3 defined as follows (according ASTM F1877):

$$ECD = \sqrt{\frac{4 \cdot A}{\pi}}, \quad (6.1)$$

where

$$A = l_0 \cdot w + w^2 \cdot \frac{\pi}{4} \quad (6.2)$$

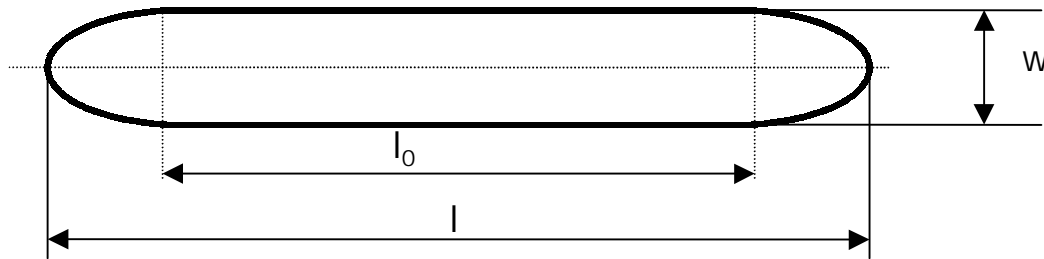


Figure 6.3: Model shape used for the particle size analysis.

6.2.3 Crack propagation measurements

Crack propagation measurements were performed according to the ASTM E 647-93. The most prominent requirement for standard measurements of crack propagation is to keep the ratio between minimum (K_{min}) and maximum stress intensity (K_{max}), i.e. $R=K_{min}/K_{max}$, the same for all different samples, while ΔK keeps increasing as the crack starts to grow. This has been fulfilled in two different ways. In the first set of the experiments, the maximum force (F_{max}) during cycling loading was kept constant for all different samples, which means that all the parameters ($\Delta F=F_{max}-F_{min}$, R and frequency) were kept constant. In the second set of the experiments, F_{max} has been adjusted so that the crack propagation rate becomes approximately the same for each sample. The later experimental approach is usually used in literature when discussing crack propagation results on UHMW-PE³²⁻³⁵.

Compact tension (CT) specimens, like the one shown in Figure 6.4 were used for the crack propagation measurements.

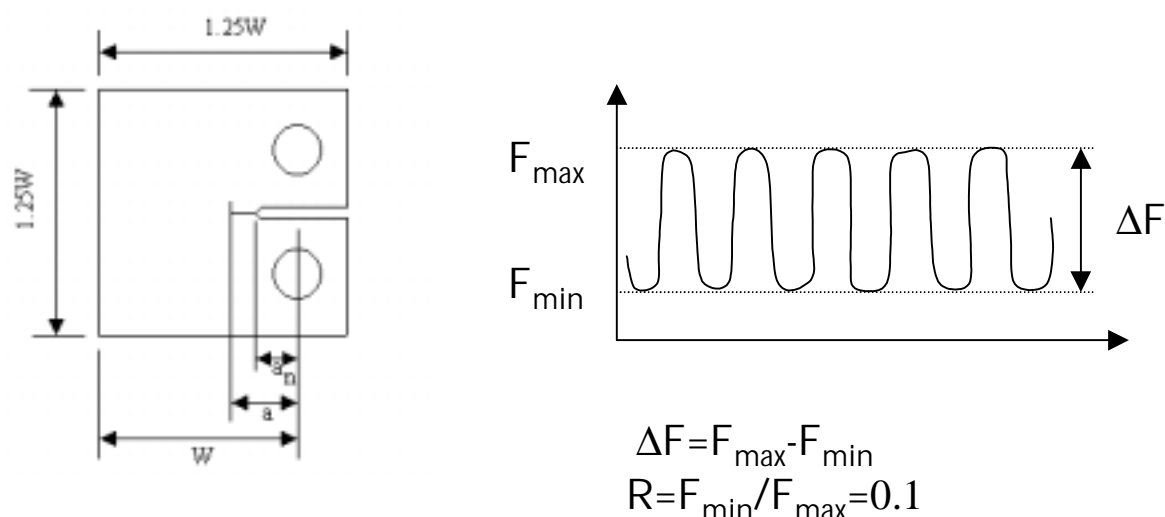


Figure 6.4: Schematic diagram of the compact tension specimen and definition of the stress ratio for fatigue testing.

The dimensions of the specimen were as follows: $W=32$ mm, $a_n=6.4$ mm and thickness (B) was 6 ± 0.5 mm. Each sample has been pre-cracked using a sharp razor blade just before testing ($a-a_n=1\pm 0.2$ mm).

The experiments were performed on a MTS 810 Elastomer test system, using a sinusoidal wave function at a frequency of 5Hz. Crack propagation has been followed using an optical objective (10x) on the digital Pixera camera.

The relation between the far-field loading and near-tip stress intensity is derived from fracture mechanics fundamentals³⁶, which for the compact tension geometry reads as:

$$\Delta K = \Delta F \cdot \frac{F(\alpha)}{(B \cdot \sqrt{W})} \quad (6.3)$$

where ΔF is the load amplitude of the fatigue cycle, $F(\alpha)$ is a geometric factor and α is defined as a/W . The geometric factor for the compact tension geometry, as calculated from the elastic theory, is³⁶:

$$F(\alpha) = \frac{(2 + \alpha)}{(1 - \alpha)^{1.5}} (0.886 + 4.64\alpha - 13.32\alpha^2 + 14.72\alpha^3 - 5.6\alpha^4) \quad (6.4)$$

Once the crack starts to propagate, the fatigue crack propagation can be presented with the help of the Paris-Erdogan equation³⁶, which implies that the crack propagation rate (da/dN) is only determined by the stress intensity range (ΔK) as given in the Equation 6.5

$$da/dN = C \cdot \Delta K^m \quad (6.5)$$

where C and m are material constants.

6.3 Results and Discussion

6.3.1 Wear results from pin on ball machine

In this experiment, the wear behaviour of grain boundary free material processed, via transient hexagonal phase, as explained in Chapter 5, has been compared with a standard reference material, as well as crosslinked UHMW-PE.

The results of weight loss for all three samples displayed as function of number of cycles is given in Figure 6.5. These results are raw data measured in the course of the experiment.

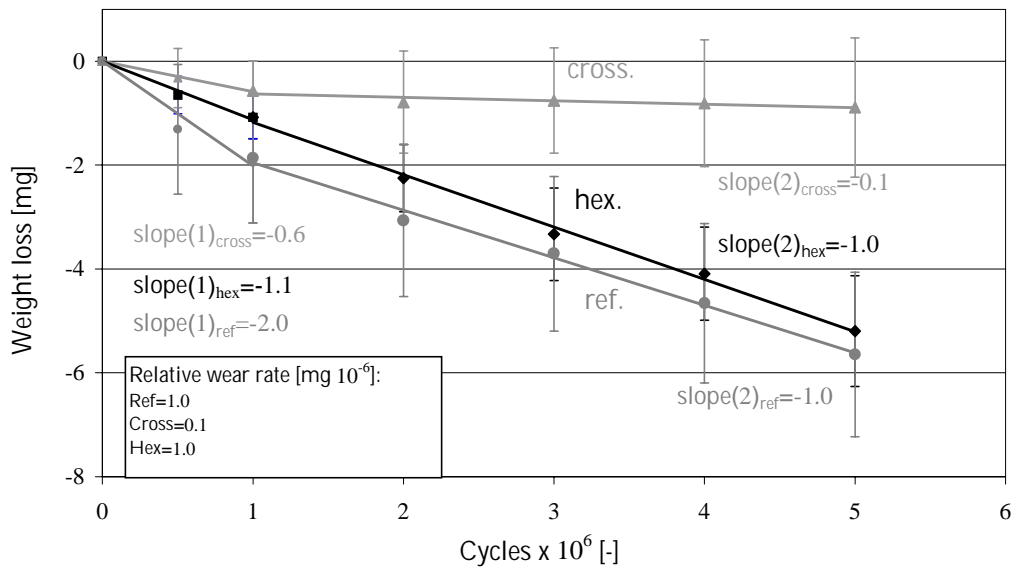


Figure 6.5: Weight loss during wear cycles. “Cross.” refers to the crosslinked sample, “ref” refers to the reference and “hex” refers to the grain boundary free material, processed via the hexagonal phase. The slopes indicated in the figure refer to linear fit of data for running-in period ($0-1 \cdot 10^6$; indicated as slope(1)) and steady wear region ($1 \cdot 10^6-5 \cdot 10^6$; indicated as slope(2)).

A linear fit has been performed for the steady wear region ($1 \cdot 10^6-5 \cdot 10^6$) as well as for the running-in period ($0-1 \cdot 10^6$). The wear rate is defined as the slope of the weight loss curves, as indicated in Figure 6.5. The results show that for the steady wear region ($1 \cdot 10^6-5 \cdot 10^6$) there is no considerable difference in wear rate between the reference and grain boundary free material, suggesting that the presence of grain boundaries does not affect the total surface wear of the material. However, considerable difference in the wear rate between these two materials could be observed for the running-in period. The wear rate of the grain boundary free material is considerably lower than for the reference. Additionally, it can be seen that the grain boundary free material does not exhibit an obvious running-in period as the wear rate stays almost the same for all $5 \cdot 10^6$ cycles (slope(1) and slope(2) in Figure 6.5 do not differ for this material). The first stage of the wear process is related to the presence of the machining

marks, created at the surface by machining the samples in the desired shape of the pin. It can be anticipated that the wear rate within the running-in period might be affected by the fusion of the original powder particles, as the improved fusion would prevent particles of being removed from the “hills” (peaks) created by machining. Once the machining marks are removed, the wear acts exclusively on a molecular level, which means that fusion of the particles with the size in the range of 50-200 μm does not affect the measured wear rate. The results in Figure 6.5 show that the wear rate of the crosslinked sample is approximately an order of magnitude lower than for the reference and grain boundary free materials, which confirms the literature data on superior multidirectional wear resistance of crosslinked material²⁸.

However, one has to be careful with the absolute interpretation of such weight loss data. All the experiments are performed within the lubricant (calf serum) and the fluid uptake (soak) will significantly influence the gravimetric measurements. Therefore the special set-up was constructed, to measure fluid uptake in the same time intervals as the wear measurements have been performed. The set-up is described in the experimental section. The results obtained from the soak measurements are given in Figure 6.6.

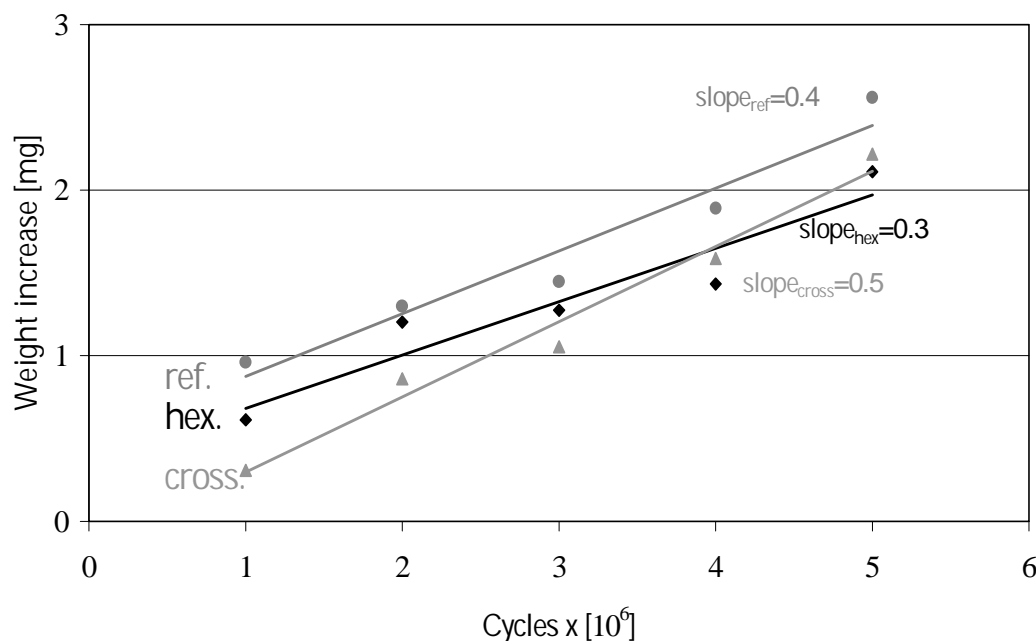


Figure 6.6: Weight increase due to the soak of the fluid as a function of the number of cycles. The slopes indicated in the figure refer to linear fit of data. “ref.” refers to the reference, “cross” refers to the crosslinked sample and “hex” refers to the grain boundary free material.

In this figure, the rate of the fluid uptake is plotted against number of cycles. For this discussion only the region related to the steady wear measurements ($1 \cdot 10^6$ - $5 \cdot 10^6$ cycles) is plotted. According to these results, the fluid uptake of each pin is about 0.55‰ per 1 million

cycles which is about an order of magnitude higher than found in a polyethylene cup during a hip simulator test³⁷. This can be related to the difference between the relative surface/volume ratio between the small pins, used in this study, and real hip cups. Additionally, the PMMA which has been used to glue the pins onto the metal holder, can also be responsible for some extra fluid uptake during measurements. In order to account for this artefact, the average fluid uptake of all the samples has been taken for correction, which is simply a line having average slope of all the three different samples shown in Figure 6.6. If the raw data of wear measurements (Figure 6.5) are now corrected by the average fluid uptake the results as shown in Figure 6.7 are obtained.

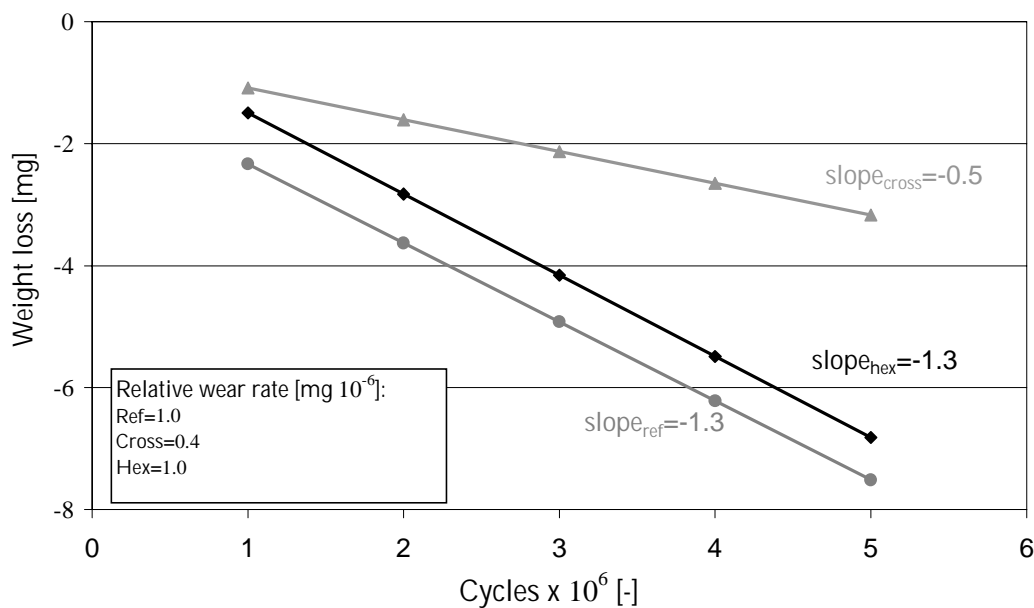


Figure 6.7: Corrected weight loss measurements (Figure 6.5) for the average fluid uptake (Figure 6.6). The slopes indicated in the figure refer to linear fit of data. “ref.” refers to the reference, “cross” refers to the crosslinked sample and “hex” refers to the grain boundary free material.

An interesting feature that can be retrieved from such corrected data (Figure 6.6), is the comparison of the obtained relative wear rate with the values obtained for uncorrected data (Figure 6.5). The difference between the grain boundary free and reference material stays approximately the same, however the relative wear rate of the crosslinked material becomes much less, once the data are corrected for the fluid uptake. For the corrected data, the wear rate of the crosslinked material is not any more orders of magnitude lower than the reference, as often stated in literature³⁸, but its superiority drops only to the factor of 2.8. These results suggest that the fluid uptake plays a rather important role in the wear measurements and should be taken into account when discussing wear results.

The results of pin on ball wear measurements suggest that the grain boundaries do not affect the surface wear during multidirectional motion. The wear mechanism during multidirectional sliding motion, typical for the hip joints, is governed on a molecular level and is primarily determined by orientational softening as explained in the introduction¹³. In that sense no substantial difference can be anticipated between the reference and the fully fused material because the fusion of the particles of a few 100 μm size does not induce any substantial difference on the molecular level. Crosslinking, however, introduces chemical constraints, which hinder the orientation of the chains and subsequently lead to different response upon multidirectional sliding motion¹³.

From the corrected weight loss data, shown in Figure 6.7, the volume of the lost material can be calculated, knowing the density of each sample. Subsequently, the volume loss can be converted in the linear wear for the particular geometry. The results of these calculations for steady wear region are given in the Figure 6.8.

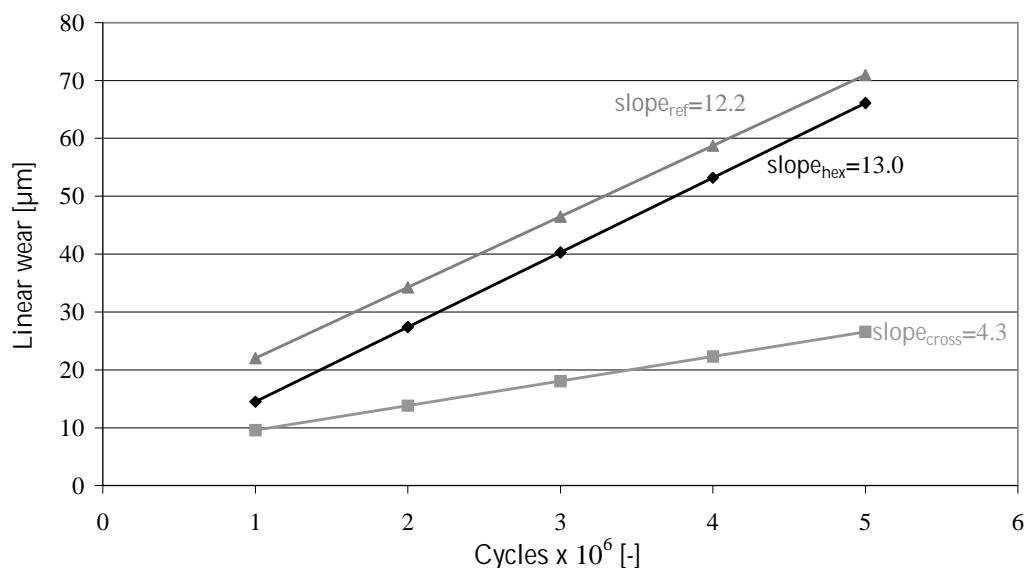


Figure 6.8: Calculated linear wear. The slopes indicated in the figure refer to linear fit of data. “ref.” refers to the reference, “cross” refers to the crosslinked sample and “hex” refers to the grain boundary free material.

These results represent the true linear wear, because they only take into account the linear displacement related to the loss of the material. It can be seen that after $5 \cdot 10^6$ cycles, approximately 28-70 μm is worn down from the surface. Again an interesting feature has been found for the crosslinked sample. From the calculated values of linear displacement, related to the weight loss of the material, it follows that approximately 28 μm of the material is worn down. On the other hand, even after $5 \cdot 10^6$ cycles, the surface of the crosslinked sample is still characterised by residues of the machining marks (as shown in Figure 6.9).

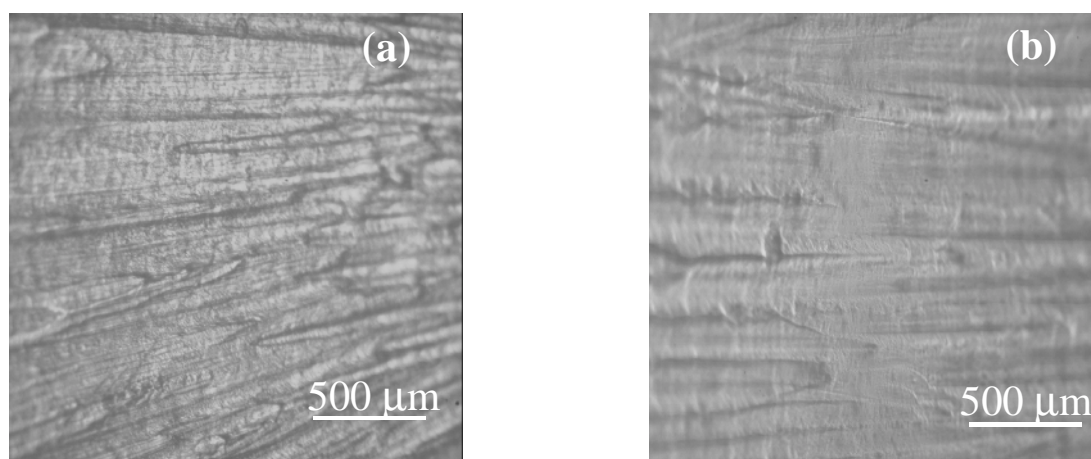


Figure 6.9: Reflection light microscopy of the machined pin of the crosslinked sample (a) before and (b) after wear test (5×10^6 cycles).

Surface roughness of the pins before wear testing was measured with help of laser profilometry. The maximum peak-to-valley height within the samples was in the range 6-8 μm , suggesting that the initial size of machining marks is not higher than this value. The similar results have been also reported in literature¹⁸. This discrepancy between the optical observations of still visible machining marks after wear testing (Figure 6.9b), and calculated linear wear for the crosslinked sample (Figure 6.8) can be bridged by the possibility of accumulation of the stress residues just below the surface of the sample. In order to assess the presence of the stress residues under the surface of the pins (before wear test) thin slices perpendicular to the pin surface, were microtomed under liquid nitrogen. The observations between crossed polarises strongly suggest that the stress residues after machining could be observed down to about 75 μm under the surface (Figure 6.10). Such thin birefringent layer has been observed only under the surface of the machined pins indicating that the stress residues in the material were induced by the machining process. The presence of such stress residues might suggest that the topography of the original machining marks might reappear on the surface after removal of the material belonging to the original marks.



Figure 6.10: Polarising light micrographs of birefringent layer under the surface of the machined pin of the crosslinked UHMW-PE.

Careful microscopical analysis of wear particles, found in the serum after wear measurements was performed. Figure 6.11 shows the ESEM micrographs of the retrieved particles originating from three different samples.

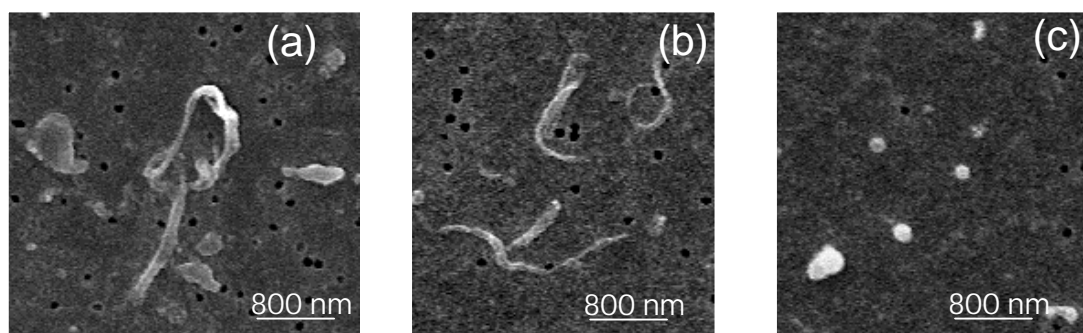


Figure 6.11: Particles found in the serum after wear tests. (a) reference, (b) grain boundary free (hex) and (c) crosslinked sample.

It can be seen that the generated wear debris of the fully fused and reference material do not differ significantly in size and shape. The particles are elongated and resemble as far as size and shape is concerned, the particles found *in vivo*^{25,26}. For crosslinked UHMW-PE rather different particles have been observed. The histogram in the Figure 6.12 shows the particle size distribution expressed with the size parameter ECD, discussed in the experimental section. The results show quantitatively that the particle size distribution of the reference material and fully fused one resemble very much, while the crosslinked sample generates much smaller particles.

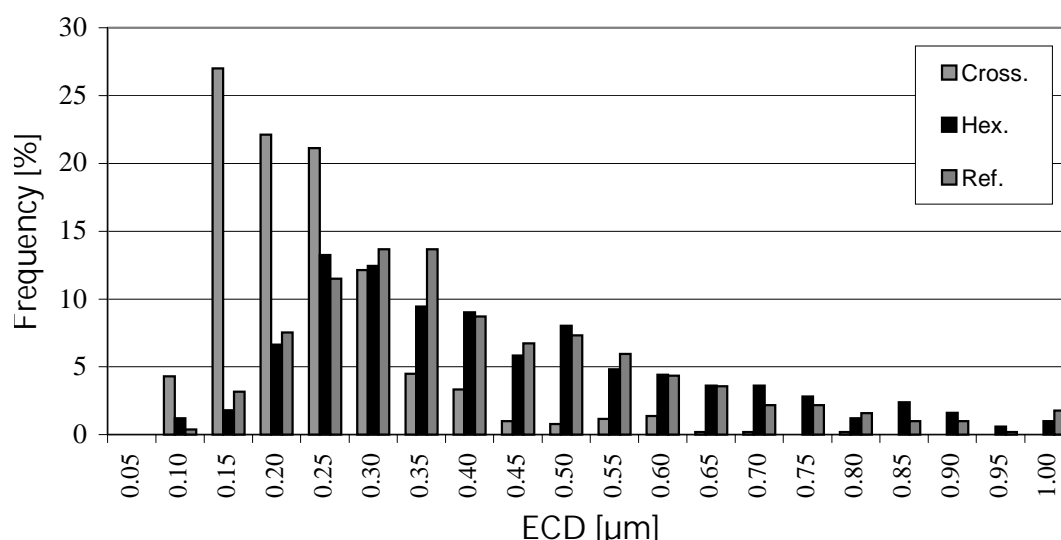


Figure 6.12: Histogram of the generated particles of three different samples used in this study. The parameter used to quantify the size is Equivalent Circle Diameter (ECD) defined in the experimental section.

It can be seen from the ESEM micrographs that the debris found in the crosslinked sample have a much more circular shape. These results suggest that the wear mechanisms in fully linear and crosslinked samples are rather different. The generation of smaller particles also implies that the number of the particles formed in the vicinity of the joint is relatively higher. It is still unclear what the response of the human body to different size and shape of the particles will be. On the other hand, it is well established that the cellular response on polyethylene particles is highly dependent upon particle number, size and surface area^{39,40}.

6.3.2 Tension fatigue resistance of different types of polyethylene: influence of the grain boundaries

It has already been mentioned that, due to the complex nature of the cyclic loading in a total knee replacement, the subsurface crack formation, and subsequent crack propagation, plays a dominant role in the failure of the polyethylene part. The fusion defects within the material have always been considered one of the major reasons for this mechanism. However, due to unavailability of the fusion defect free material, an extensive study in this direction has never been performed. Fracture mechanics assumes that all fractures result from the presence of the one or more defects^{36,41}. In that respect the grain boundaries can be considered as such defects and it is rather trivial to anticipate that the removal of such defects would lead to an improved fatigue resistance. The problem of standard crack propagation measurements is that it assumes that the sample behaves linear elastically up to the point of fracture³⁶. Due to their viscoelastic and plastic nature polymers only obey this criterion for samples that are much larger than the dimension of the plastic zone at the propagating crack tip and, therefore, treatment of the crack propagation becomes rather delicate. Though it is fundamentally not fully correct, Paris plots have been used extensively to evaluate the crack propagation resistance of different polymer materials^{41,35}. The Paris-Erdogan equation⁴² suggest that the governing parameter controlling the crack growth, is the range of stress intensity (ΔK), which is a measure of the stress distribution at the crack tip. Due to the plastic nature of polyethylene and the accompanying insufficient sample size, the derived values of the stress intensity range do not represent the intrinsic values for the material under investigation, but they are codetermined by the geometry of the compact tension test bar. Consequently, when discussing the results, ΔK as calculated from the experimental data will be denominated as ΔK^* . It should be noticed that this definition, in a systematic way, is always larger than the intrinsic ΔK value and hence can still be used for comparative purposes, as long as the geometry remains unchanged.

In order to determine the role of the grain boundaries in the crack propagation resistance of UHMW-PE, conventionally compressed (200 bar and 180°C) commercial powder of

UHMW-PE has been compared with the grain boundary free material processed via transient hexagonal phase, as already discussed before.

Crack propagation is measured by keeping the ratio between minimum (K_{\min}) and maximum stress intensity (K_{\max}), i.e. $R=K_{\min}/K_{\max}$, constant for all different samples, while ΔK keeps increasing as the crack starts to grow³⁶. As discussed in the experimental section, these experimental requirements can be met in two different ways, either by keeping the maximum force during cycling loading constant for all different samples, or by adjusting the force so that the crack propagation rate becomes approximately the same for each sample. Both types of the experiments have been performed and will be discussed separately.

The crack length versus number of cycles up to total failure is plotted in Figure 6.11.

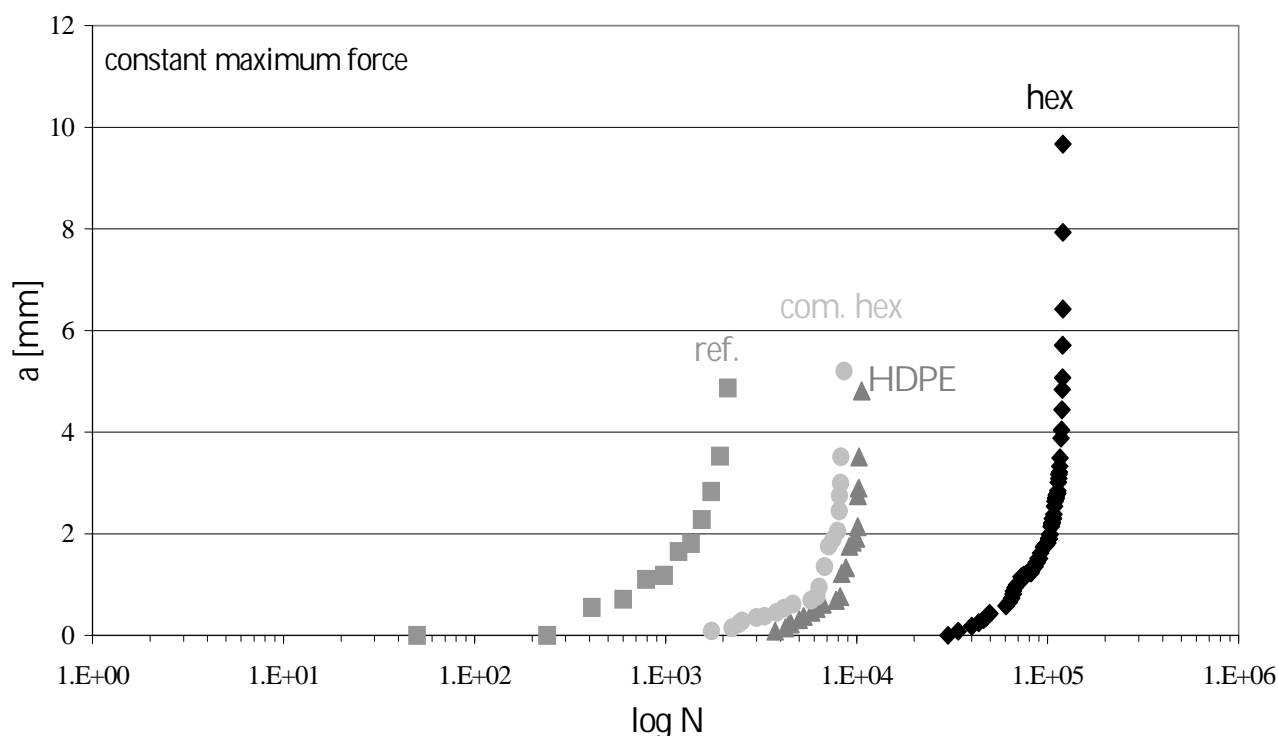


Figure 6.13: Crack length (a) versus number of cycles (logarithmic scale, N) for different samples. These results are measured under a constant force. “ref.” refers to the reference material, “com. hex” is the commercial grade processed via the metastable hexagonal phase at 1500 bar, “HDPE” is high density polyethylene and “hex” is the grain boundary free material.

These results were obtained in the experiment where the maximum force during cyclic loading has been kept constant for all different samples. It is obvious that the crack growth in the reference sample is the fastest, under the chosen loading conditions. This indicates that the fully fused material is more resistant to crack propagation. Hence these results support the hypothesis that the presence of grain boundaries plays an important role in the fatigue resistance of UHMW-PE products. In order to strengthen this argumentation, the same type

of measurements were performed on a high density polyethylene sample (HDPE) which of course does not feature any grain boundaries or any other fusion related defects. An interesting observation from this measurement is that HDPE features a higher fatigue resistance than the unfused UHMW-PE sample. At first glance, this result is rather striking because it is normally expected that the mechanical properties of higher molecular weight polymers will always exceed the properties of lower molecular weight species. However, these results confirm the fundamental postulate of fracture mechanics, that the fracture of the material is governed by the presence of internal defects. Therefore the UHMW-PE possessing intrinsic defects will fail easier than the defect free HDPE.

When discussing the response of semicrystalline materials to low deformations, one should not forget the strong influence of crystallinity on the elastic modulus and the yield stress. It has already been explained in the experimental section that, due to insufficient cooling in the current setup the crystallinity of the grain boundary free material is somewhat higher than that of the conventionally compression moulded material. In order to exclude the influence of the crystallinity on the results, the commercial powder has been processed under the same conditions as the material free of grain boundaries. Due to the same processing conditions (notably cooling rate) the samples were characterised to have approximately the same crystallinity (Table 6.1). However, the commercial powder processed via transient hexagonal phase at 1500 bar still exhibited residues of the original powder particles, as discussed in detail in Chapter 5. From the results shown in Figure 6.13 it can be seen that the results of crack propagation are influenced by the crystallinity. A more crystalline material needs a higher number of cycles to fail than its low crystallinity counterpart, which also possesses grain boundaries. However, the most significant difference in crack propagation behaviour remains between the commercial sample processed via the transient hexagonal phase (still featuring grain boundaries) and the fully fused sample. This indicates again that the influence of internal discontinuities (grain boundaries) on crack propagation is much stronger than the effect of crystallinity. For the present set experiments the Paris plot (da/dN vs. ΔK), as displayed in Figure 6.14, reveals that for the same stress intensity range (ΔK) the crack propagation rate is the fastest for the reference and slowest for the grain boundary free material, while the values for both the HDPE and the commercial grade, processed via transient hexagonal phase, lay in between.

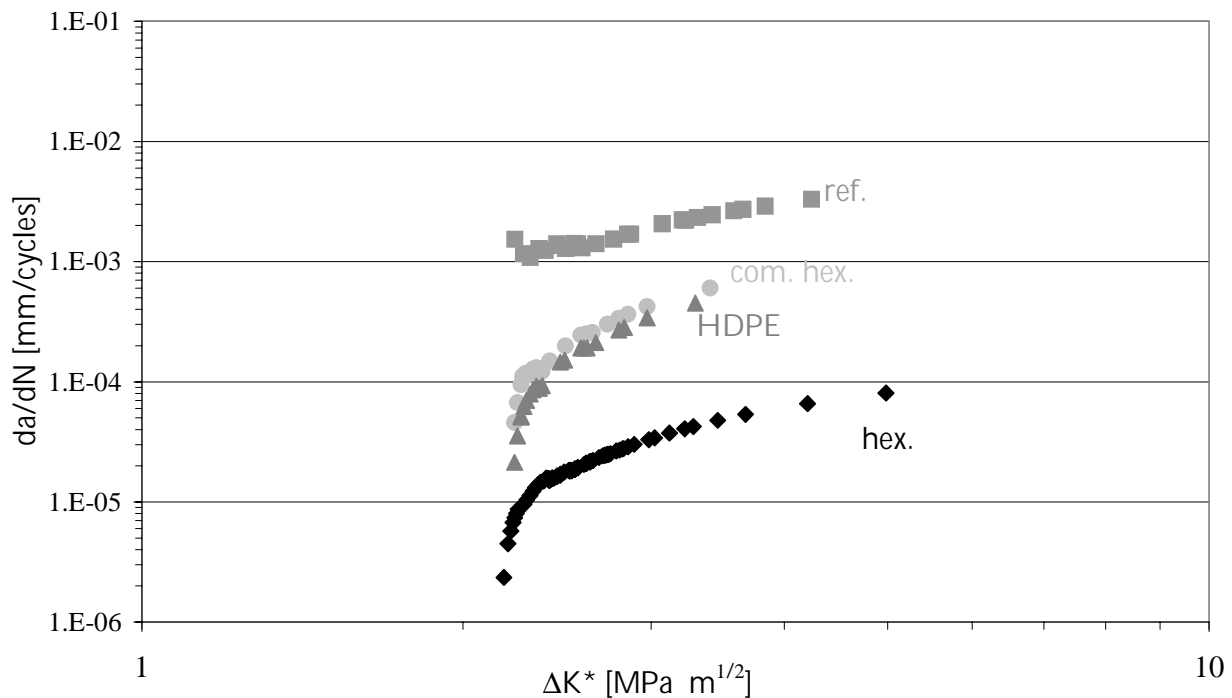


Figure 6.14: Paris plots calculated from the crack propagation data obtained by measurements under constant force. “ref.” refers to the reference material, “com. hex” is the commercial grade processed via the metastable hexagonal phase at 1500 bar, “HDPE” is high density polyethylene and “hex” is the grain boundary free material.

As already mentioned, these results have been obtained by keeping all experimental conditions, like F_{\max} , R and frequency constant for all three samples. However, one might argue that choosing one value of the maximum force during cyclic loading for all the samples is not fully correct. The impact response of these materials is rather different and by choosing one maximum force for all the samples the influence of plasticity, which is anyway very critical, might play a dominant role during fatigue measurements³⁵. This has been tested by measuring the response of different polyethylene samples on monotonous tensile displacement, which can be regarded as a slow impact test. The measurements were performed using the compaction tension test geometry, the same as used for the fatigue measurements. The typical force displacement curve for the different polyethylene samples under investigation is given in Figure 6.15.

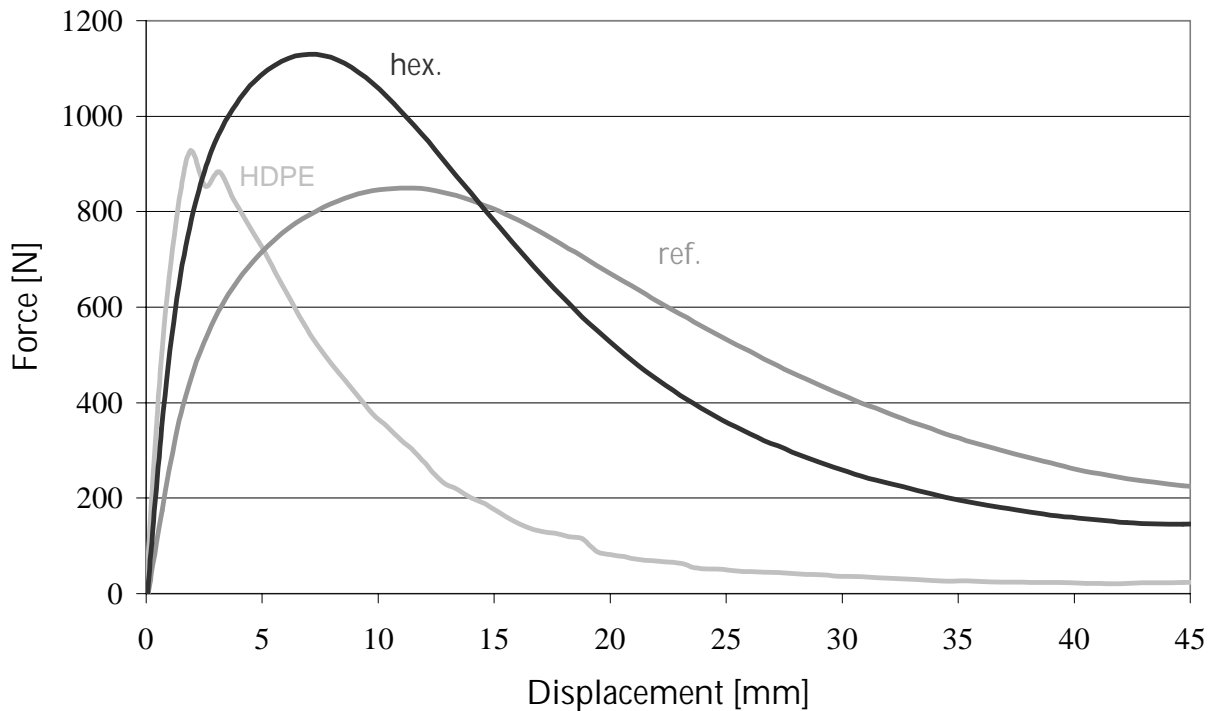


Figure 6.15: Force displacement curve for different samples of UHMW-PE performed on the compaction tension specimen. “ref.” refers to the reference material, “HDPE” is high density polyethylene and “hex” is the grain boundary free material.

It is generally accepted that at the maximum load, initiation of the crack occurs, which is followed by a catastrophic reduction in the load due to subsequent crack propagation⁴¹. Since we are dealing with polyethylene, which is very ductile material, plastic deformation will have a very strong influence on the response of the sample to monotonous tension and, therefore, the maximum load of the curve is not only related to the crack initiation but mostly to conventional yielding. This plot is not meant to characterise the different samples, but rather to emphasise that the fatigue measurements performed at one constant maximum force are fundamentally not fully correct due to the different plasticity when the selected maximum force is close to, or much below, the “yield point”. In order to avoid this, measurements have been performed in such a way that for each sample the maximum force during cyclic loading has been 50 % of the maximum load as observed in a monotonous run. By choosing the parameters in this way, the crack propagation rate for each sample was also approximately the same. Most of the work on crack propagation in UHMW-PE reported in literature has been performed in this way^{32,33-35}. The Paris plots obtained from the experimental results thus obtained are given in Figure 6.16.

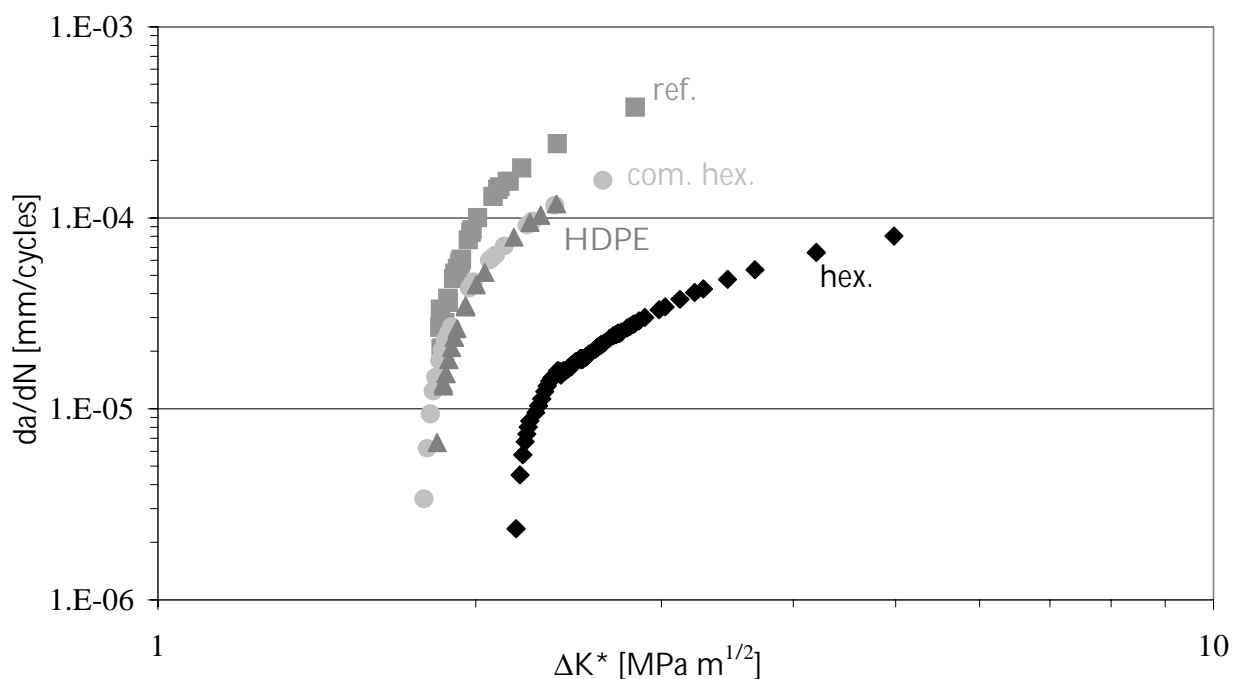


Figure 6.16: Paris plots calculated from the crack propagation data obtained by measurements performed under the same crack propagation rate. “ref.” refers to the reference material, “com. hex.” is the commercial grade processed via the metastable hexagonal phase at 1500 bar, “HDPE” is high density polyethylene and “hex.” is the grain boundary free material.

The parameters related to the Paris regime are given in the Table 6.2.

Table 6.2: The parameters of the Paris regime calculated from the plots expressed in Figure 6.16.

Material	$\Delta K_{\text{int.}}$ [MPa·m ^{1/2}]	Slope, m
Grain boundary free	2.18	3.2
Reference	1.85	16.6
Commercial grade pressed via hex.	1.79	5.7
HDPE	1.84	6.1

Because the crack started to propagate at approximately the same values of da/dN for all different samples, ΔK intercept (ΔK_{int}) has also been determined. ΔK_{int} is related to the stress at the tip needed for the crack to start to propagate. The results obtained on the reference material match the results obtained by Backer et al^{33,34}. Again, if the results for the different polyethylene samples are compared, the grain boundary free material exhibits the highest fatigue resistance. Table 6.2 shows that the ΔK_{int} for grain boundary free material is 2.18, which is much higher than the values obtained for the reference material. Again HDPE and the commercial grade sample processed via the hexagonal phase exhibit ΔK_{int} values that are

in between the values of the reference and grain boundary free sample. Taking these results into account, one can say with rather high confidence that the removal of the grain boundaries highly improves the fatigue resistance of the UHMW-PE. The superior fatigue behaviour of this material implies that the newly processed UHMW-PE should be a good alternative in the use of knee joints.

As already mentioned, crosslinked UHMW-PE is shown to possess superior wear properties and it has been considered to be the adequate alternative of UHMW-PE in the artificial prostheses. However, it has been extensively reported in the literature that the crosslinking causes poor fatigue resistance of UHMW-PE^{33,43}. The results presented in this study suggest that the fatigue resistance is mainly governed by the presence of internal defects i.e. grain boundaries. The irradiation of UHMW-PE does not affect the grain boundaries and it has been confirmed that the crosslinked material still features the residues of the original powder particles, which makes this material a bad alternative for applications where cyclic loading is concerned.

6.4 Conclusions

In this chapter the mechanical properties, notably wear and fatigue, of fully fused UHMW-PE products have been discussed. These properties are important for the high demanding applications of UHMW-PE, like bearing surfaces in the hip and knee artificial joints.

Wear experiments were performed on pin on ball wearing tester, which simulates the multidirectional motion typical for the hip joint during normal gait. It has been shown that the fusion of powder particles, with a size of few hundreds micrometers, does not effect the surface wear of UHMW-PE. Wear of UHMW-PE hip cup is determined at the molecular level and it is generally believed that its wear resistance under multidirectional motion is determined by the ability of the molecular chains to orient. Due to this reason the crosslinked material has been considered to offer sufficient improvement in wear characteristics of UHMW-PE where multidirectional motion plays an important role.

The wear resistance of crosslinked material has also been investigated. Some interesting features, which are often disregarded in literature, have been found. It is usually claimed that crosslinked material features a wear rate that is a few orders of magnitude lower than the wear rate of conventional UHMW-PE. However, it is often overlooked that wear measurements within hip simulators are performed in bovine serum and the soaking of the polyethylene sample strongly affects the gravimetric measurements during these wear tests. Therefore, a soak station has been built up and the fluid uptake has been monitored for all different polyethylene samples in the same time interval as the wear measurements. It has

been shown that, after subtraction of the soak data from the original weight loss measurements, the wear resistance of the crosslinked sample with respect to the conventional UHMW-PE, is only about three times higher, instead of a few orders of magnitude as usually reported in literature.

Another interesting phenomenon found in the present study is that the wear particles of crosslinked samples differ in size and shape from the debris particles found for linear UHMW-PE products. The particles are smaller in size and much more circular than the usual particles of the conventional UHMW-PE, which feature a characteristic fibrillar shape. The fact that the particles are smaller means that the number of generated particles is higher. Also the cellular reaction of the human body tissue might be different for different debris morphologies.

The influence of grain boundaries on the fatigue resistance of UHMW-PE has been established. It is well known that the failure of the UHMW-PE tibial component is mostly affected by cyclic loading which results in crack initiation and subsequent propagation leading to macroscopic failure. In order to approach this problem crack propagation measurements were performed. The usual experimental requirement of keeping R ($R=K_{\min}/K_{\max}$) constant has been achieved in two ways. In the first set of experiments all the parameters (R , frequency and F_{\max}) were kept constant for all different samples while in the second set of the experiments F_{\max} has been adjusted for each sample so that a constant propagation rate was achieved for all different samples. Both sets of experiments strongly suggest that the presence of the grain boundaries affects the fatigue resistance. It is shown that UHMW-PE possessing grain boundaries (i.e. internal defects) is more prone to fail than defect free low molecular weight HDPE upon cyclic loading, in spite of the huge difference in the molecular weight. UHMW-PE sample free of grain boundaries, however, exhibits superior fatigue resistance meeting the ultimate properties, which are anticipated for high molecular weight polymer. The superior fatigue resistance of this material opens the wide area of applications where severe conditions of cyclic loading have to be met.

6.5 References

1. Li, S.; Burstein, A.H. *J. Bone Joint Surg.* **1994**, *76A*, 1080
2. Kurtz, S.M.; Muratoglu, O.K.; Evans, M.; Edidin, A.A. *Biomaterials* **1999**, *20*, 1659
3. Amstutz, H.C.; Campbell, P.; Kossovsky, N.; Clarke, I.C. *Clin. Orthop. Rel. Res.* **1992**, *276*, 7
4. Harris, W.H. *Clin. Orthop. Rel. Res.* **1995**, *311*, 46

5. McKellop, H.A.; Campbell, P.; Park, S.; Schmalzried, T.P.; Grigoris, P.; Amstutz, H.C.; Sarmiento, A. *Clin Orthop.* **1995**, 311, 3
6. McGee, M.A.; Howie, D.W.; Neale, S.D.; Haynes, D.R.; Pearcy M.J. *Proc. Inst. Engrs. PartH* **1997**, 211, 65
7. Schmalzried, T.P.; Callaghan, J.J. *J. Bone Joint Surg.* **1999**, 81A, 115
8. Hood, R.W.; Wright, T.W.; Burstein, A.H. *J. Biomed. Mater. Res.* **1983**, 17, 829
9. Landy, M.M.; Walker, P.A. *J. Arthroplasty* **1988**, 3, S73
10. Lewis, G. *J. Biomed. Mater. Res.* **1997**, 38, 55
11. Wrona, M.; Mayor, M.B.; Collier, J.D.; Jensen, R.E. *Clin. Orthop.* **1994**, 299, 92
12. Czichos, H. *Tribology-A Systems Approach to the Science and Technology of Friction, Lubrication and Wear*, Elsevier: Amsterdam, **1978**
13. Wang, A.; Essner, A.; Polineni, V.K.; Stark, C.; Dumbleton, J.H. *Tribol. Int.* **1998**, 31, 17
14. DIN 50 320, *Deutsche Normen* **1979**
15. Hutchings, I.M. *Tribology: Friction and Wear of Engineering Materials*, Edward Arnold: London, **1992**
16. Lancaster, J.K. *Plastics and Polymers* **1973**, Dec, 297
17. Bartel, D.L.; Burstein, A.H.; Toda, M.D.; Edwards, D.L. *J. Biomech. Enging.* **1985**, 107, 113
18. Wimmer, M.A. *Ph.D. thesis*, Technical University of Hamburg, **1999**
19. Wang, A.; Stark, C.; Dumbleton, J.H. *Proc. Instn. Mech. Engrs.* **1996**, 210, 141
20. Pooley, C.M.; Tabor, D. *Proc. Royal Soc. London* **1972**, 329A, 251
21. Wang, A.; Sun, D.C.; Stark, C.; Dumbleton, J.H. *Proceedings of the 5th World Biomaterials Congress* **1996**, I-583
22. Bragdon, C.R.; O'Connor, D.O.; Lowenstein, J.D.; Jasty, M.; Syniuta, W.D. *Proc. Inst. Mech. Engrs., PartH* **1996**, 210, 157
23. Wang, A.; Sun, C.C.; Yau, S.-S.; Edwards, B.; Sokol, M.; Essner, A.; Polineni, V.K.; Stark, C.; Dumbleton, J.H. *Wear* **1997**, 203-204, 230
24. Ramamurti, B.S.; Bragdon, C.R.; Harris, W.H. *Trans. of the 21st Ann. Meet. of the Society for Biomaterials* **1995**, 347
25. Kobayashi, A.; Bonfield, W.; Kadoya, Y.; Yamac, T.; Freeman, M.A.R.; Scott, G.; Revell, P.A. *Proc. Instn. Mech. Engrs. Part H* **1997**, 211, 11
26. Schmalzried, T.P.; Campbell, P.; Schmitt, A.K.; Brown, I.C.; Amstutz, H.C. *J. Biomed. Mater. Res.* **1997**, 38, 203
27. McKellop, H.; Shen, F.W.; Salovey, R. *Trans of the 44th Orthop. Soc.* **1998**, 23, 98
28. McKellop, H.; Shen, F.W.; Lu, B.; Campbell, P.; Salovey, R. *J. Orthop. Res.* **1999**, 17, 157
29. www.sulzer.ch
30. Wimmer, M.A.; Nassutt, R.; Lampe, F.; Schneider, E.; Morlock, M.M. In *Alternative Bearing Surfaces in Total Joint Replacement*, ASTM STP1346, **1998**
31. Scott, M.; Forster, H.; Vadodaria, K.; Sauer, W.; Anthony, M. *Trans. of the 6th World Biomaterials Congress* **2000**, 177
32. Pruitt, L.; Bailey, L. *Polymer* **1998**, 39, 1545

33. Baker, D.A.; Hastings, R.S.; Pruitt, L. *J. Biomed. Mater. Res.* **1999**, *46*, 573
34. Baker, D.A.; Hastings, R.S.; Pruitt, L. *Polymer* **2000**, *41*, 795
35. Riemsdag, A.C. *Ph.D. thesis*, Technical University of Delft, **1997**
36. Anderson, T.L. *Fracture Mechanics-Fundamentals and Applications*, CRC Press Inc.: Boston, **1991**
37. Kaddick, C.; Wimmer, M.A. *Proc. Instn. Mech. Engrs. Part H* **2001** (in press)
38. Essner, A.; Schmidig, G.; Wang, A. *Trans. of the 6th World Biomaterials Congress* **2000**, 854
39. Green, T.R.; Fisher, J.; Stone, M.; Wroblewski, B.M.; Ingham, E. *Biomaterials* **1998**, *19*, 2297
40. Scott, M.; Widding, K.; Ries, M.; Shanbhag, A. *Proceedings of the 47th Annual Meeting of the Orthopaedic Research Society* **2001**, 1
41. Brostow, W.; Corneliussen, R.D. *Failure of Plastics*, Hanser Publishers: Munich, **1986**
42. Paris, P.; Erdogan, F. *Trans. ASME* **1963**, 528
43. Baker, D.A.; Bellare, A.; Pruitt, L. *Trans. of the 11th Inter. Conference on Deformation, Yield and Fracture of Polymers* **2000**, 69

Chapter 7

High melting temperature of nascent powders, a kinetic approach

7.1 Introduction

A detailed study on the structural and morphological features of nascent powders of UHMW-PE (Chapter 3) revealed that the morphology created during synthesis differs significantly from the one obtained by crystallisation from the melt or solution. Accordingly, not all the phenomena found for nascent materials can be explained by the classical approach, postulated on the basis of the experimental results obtained for melt and solution-crystallised materials. An example of such a discrepancy between the classical approach and the specificity of the nascent morphology, is the paradox of the very high melting point of the nascent powders of UHMW-PE. It has been shown in Chapter 3 that nascent powders consist of folded chain crystals, having both the thickness and the lateral dimensions in the order of 10-30 nm. According to the classical thermodynamic approach, which relates melting temperature of folded chain crystals to lamellae thickness (Gibbs-Thompson eq.; eq. 2.1), the measured melting point of such small crystals would be much lower. It is, however, well known that nascent powders exhibit a first melting point in order of 141-142°C, which corresponds to the equilibrium melting temperature for polyethylene ($T_m^0 = 141.5^\circ\text{C}^1$). Engelen et al.² proposed a model in which the high melting temperature of the nascent powders has been related to successive thickening of the small metastable crystals upon heating, which ultimately leads to lamella thickness of fully extended chains. In the part of this work presented in Chapter 3, it has been shown with the help of WAXS and TEM that the crystals within the nascent powders do not thicken to such high lamellar thickness even after annealing at 120°C for 24 hours. Even more striking findings concerning ability of the nascent powders to thicken were shown in Chapter 5 (Figure 5.6). Here it has been shown that even in the hexagonal phase, where the chains possess enhanced chain mobility in the chain direction, thickening of the crystals within the nascent powder is restricted and it highly depends on the initial entanglement density. Even for the less entangled system (laboratory scale Ziegler-Natta grade) crystal thickness does not exceed a value of 100 nm, which is for UHMW-PE still far below the full chain extension. These results strongly suggest that

thickening of the crystals during heating of the nascent powders can not cause such a high increase in the melting point, as usually measured by DSC. So what is the reason for such high melting point found for small folded chain crystals within the nascent UHMW-PE powders? Since the thermodynamics alone (Gibbs- Thomson equation; eq. 2.1, Chapter 2) fails to explain this feature, the idea has been raised to invoke the role of the kinetics in the melting behaviour of the nascent powders, which will be discussed in this chapter.

7.2 Experimental Section

7.2.1 Materials

The three grades of nascent powders as described in Chapter 3 (Section 3.2) have been investigated. Additionally, a metallocene grade possessing lower molecular weight has also been used ($M_w=800\,000\text{ g mol}^{-1}$; $M_w/M_n=1.8$). This grade was synthesised under the same conditions, using the same type of catalyst as the high molecular weight metallocene grade introduced in Chapter 3.

Prior to further experimentation all nascent powders were soaked in acetone with 1-2 wt% (based on polymer) antioxidant, for 1 day at room temperature, followed by ambient evaporation of the acetone to provide an homogeneous distribution of the antioxidant within the sample. The powders compacted at 50°C were wrapped in aluminium foil and placed in an oil bath, heated to 136°C. After appropriate annealing time the samples were removed from the oil bath and carefully cleaned with acetone. Infra red spectra of the samples showed that no oxidation occurred after annealing at 136°C.

7.2.2 Differential Scanning Calorimetry (DSC)

DSC measurements of the annealed samples were performed using heating rates from 0.1-10°C min⁻¹. Samples of 2.0 – 3.0 mg mass were weighted with a precision balance and encapsulated in standard (crimped) Al-pans. Almost identical empty pans were used in the reference side and for the baseline run.

The empty pan run (taking the same measuring parameters and phase position) was subtracted from the DSC curves related to the sample runs in order to reduce surroundings and apparatus influences.

7.3 Results and Discussion

In order to confirm the hypothesis that kinetics influences the melting behaviour of the nascent crystals, the annealing experiments at 136°C (around the onset of the conventional melting point) have been performed on different grades of nascent UHMW-PE. DSC run has been performed on samples that were annealed for different times and, subsequently cooled to room temperature. The DSC results on metallocene grade ($M_w=3.6 \cdot 10^6 \text{ g mol}^{-1}$) are shown in Figure 7.1. From these curves it is obvious that after annealing at 136°C two different populations of crystals exist; one associated to the melt-crystallised material (peak at 135°C) and the other related to the original nascent morphology (peak at 141°C).

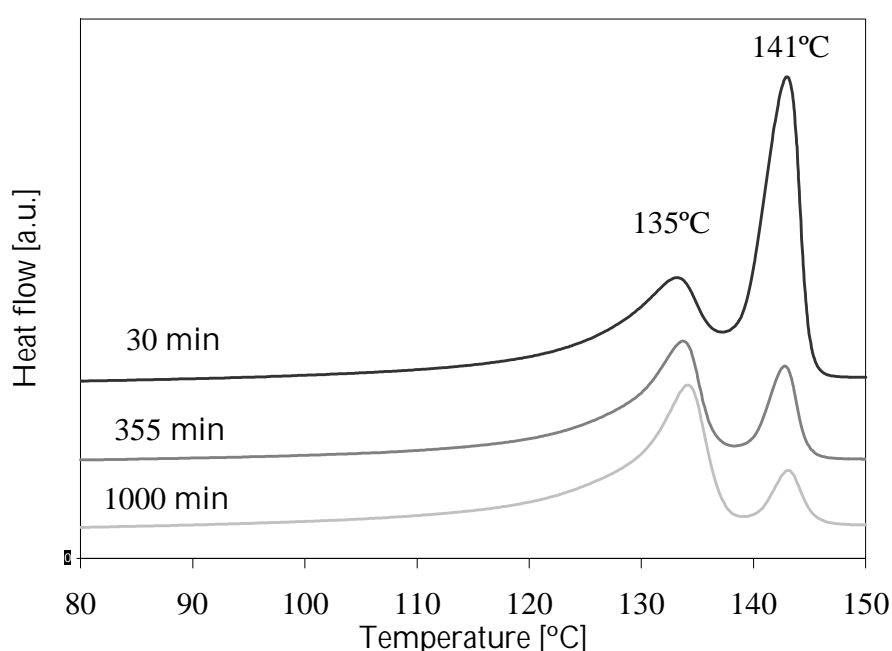


Figure 7.1: DSC heating runs at $10 \text{ }^\circ\text{C min}^{-1}$ for metallocene grade ($M_w=3.6 \cdot 10^6 \text{ g mol}^{-1}$) after different annealing times, as indicated on the curves.

It is obvious from this figure that the ratio between two peaks changes with increasing annealing time. The longer the annealing time, the more of the nascent morphology is lost. Similar DSC curves have been obtained for different grades after annealing at 136°C. In order to quantify this change the percentage of the area under peak at 135°C relative to the total area has been calculated ($\Delta H_{(135^\circ\text{C})}/(\Delta H_{(135^\circ\text{C})}+\Delta H_{(142^\circ\text{C})})$). The results obtained for different nascent grades are plotted as a function of the annealing time in Figure 7.2.

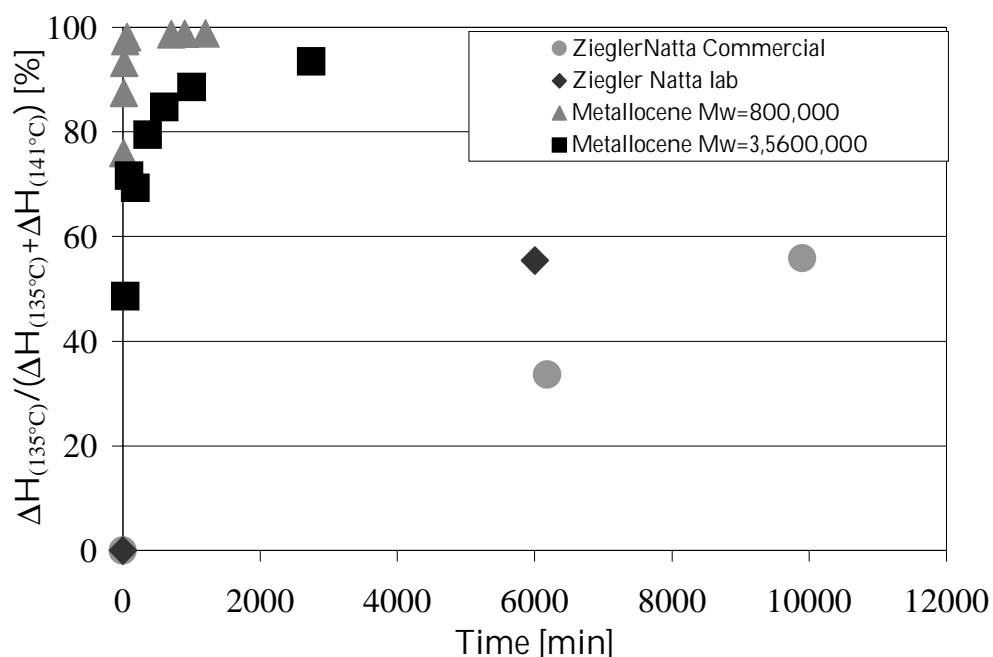


Figure 7.2: Influence of annealing time on melting after annealing at 136°C for different grades of nascent UHMW-PE.

The morphological differences of these grades are discussed in detail in Chapter 3. From Figure 7.2 it can be seen that the kinetics of melting highly depends on these morphological differences. For initially entangled powders, like the Ziegler-Natta based grades, the time needed to melt the sample at 136°C is much longer than for the highly disentangled metallocene grades. The two metallocene based grades used in this study were synthesised with help of the same catalyst. The only difference was the molecular weight. From the results displayed in Figure 7.2 it can be seen that the kinetics of the melting process also highly depends on the molecular weight. The observations were that on annealing at 136°C, lower molecular weight material requires less time for melting.

These results confirm that kinetic factors play an important role in the melting process of nascent powders. If nascent UHMW-PE is annealed at 136°C (i.e. at the onset of the melting peak during a standard heating run) for sufficiently long time, it will eventually melt. The fact that the crystals melt upon annealing at much lower temperatures than usually observed by DSC measurements suggests that the real melting point of the nascent powders is much lower than generally anticipated. The measured high melting point (141±1°C) upon “fast” heating in DSC, even at heating rate of 1 to 100°C/min, implies that the chains are simply not able to follow the temperature changes and therefore the high melting temperature is the result of superheating³. When the molecular chains are given time to follow the temperature changes the material is able to melt far below 141±1°C. This can be achieved by annealing for long times at an appropriate temperature or by heating extremely slowly. It has been observed that the melting temperature decreases on heating a nascent powder at rates below

0.1°C min⁻¹), The amount of time necessary for crystals to melt upon annealing is highly dependent on the initial crystal topology. For a highly disentangled state the process of melting upon annealing is relatively faster than that of an entangled state. If melting during annealing is a very slow process it can be anticipated that the material melts by detachment of chains from a crystal lattice.

This phenomenon is comparable with melting of extended chain single crystals of polyethylene obtained upon crystallisation via the hexagonal phase⁴. It has been shown with the help of in-situ light microscopy that at temperatures around melting point, the single crystals start to shrink, both in lateral and thickness direction, suggesting that the chains are slowly detaching from the surface of the crystal, which is actually a reverse process of crystallisation. A similar phenomenon is anticipated for the nascent crystals because of their unique morphological characteristics determined by the specific crystallisation conditions. Such process is highly dependent on the initial topology of the nascent crystals as well as the length of a chain.

7.4 Conclusions

The experimental results presented in this chapter suggest that kinetics plays an important role in melting of the nascent crystals. It has been shown that upon annealing nascent powders for sufficiently long time at 136°C, (i.e. at the onset of the melting peak during standard heating run) the nascent crystals melt. The melting of crystals at temperatures below the usually measured melting point suggest that the high melting point of the nascent powders is an effect of superheating. Heating rates in the range of 1-100°C min⁻¹ are too fast to realise the superheating effect, which becomes visible when heating rates below 0.1°C min⁻¹ are used. These results suggest the melting process of nascent crystals is kinetically controlled and strongly depends on crystal topology generated during polymerisation.

7.5 References

1. Wunderlich, B. et al. *ATHAS databank*. <http://web.utk.edu/~athas>
2. Tervoort-Engelen, Y.M.T.; Lemstra, P.J. *Polym. Comm.* **1991**, 32, 343
3. Wunderlich, B.; Czornyj, G. *Macromolecules* **1977**, 10, 906
4. Hikosaka, M.; Rastogi, S.; Keller, A.; Kawabata, H. *J. Macromol. Sci. Phys.* **1992**, B31, 87

Technology Assessment

In this thesis, it has been shown that understanding of the initial morphology of the nascent powders, created during synthesis, is a precursor for improvement of the processability of UHMW-PE, usually intractable via conventional processing routes. Though it is generally accepted that the mechanical properties increase with the molecular mass, performance of the products can be deficient due to difficulties that these materials encounter during processing. The most illustrative examples, which have been treated in detail in this work, are the UHMW-PE components in the artificial joints, where the insufficient lifetime of the products is related, at least partially, to the intractability of UHMW-PE^{1,2}. Due to very high melt viscosity and long reptation times, which are consequence of highly entangled state of the melt, the products made of UHMW-PE possess residues of the initial powder particles which were strongly believed to influence their ultimate performance. In this work a novel route to process UHMW-PE into fully homogeneous products has been developed. This route utilises the phenomenon of “chain explosion”³ upon melting in order to enable chains to traverse from one powder particle to another, which ultimately results in fully fused products.

Such products, free of fusion defects, have been extensively tested for the mechanical properties, relevant in applications of UHMW-PE in artificial joints, notably wear and fatigue. It has been discussed in detail in Chapter 6 that the major reason for the failure of *artificial hip joint* is a release of hundreds thousand submicron particles per step, which leads to severe body reaction and, subsequently loosening of the joint¹. The occurrence of such submicron particles in the blood stream is associated to a complex joint kinematics⁴. Due to rather complicated multidirectional motion of the countersurface (metal pin) against the UHMW-PE cup, polyethylene chains are able to orient in the preferential direction (direction of the maximum contact stress) which makes the material stronger in the orientation direction and weaker in the transverse direction. Accordingly, if the countersurface slides in the transverse direction, a detachment of fibrous debris occurs. This model suggests that the most important property for wear resistance of polymer material in applications that involve multidirectional sliding contact, is the resistance of the material to orient. Guided by this reasoning a material, which has been chosen as a solution for the wear problems in hip joints is the crosslinked UHMW-PE. Many studies using hip simulators, which follow multidirectional motion of the joint, showed that the crosslinked material indeed exhibits almost no measurable wear^{2,5}. Such superior performance of the crosslinked material in high

demanding application, like hip joint, is rather surprising. Normally, crosslinking of linear polyethylene deteriorates its mechanical properties, like stiffness and strength⁶. Moreover, it has been also reported that the crosslinked material possesses rather poor wear resistance in the classical (unidirectional) wear machines, like pin on plate or pin on disc, as well as in the abrasion wear machines⁴. If the superiority of this material in multidirectional sliding wear is only related to the formation of a three-dimensional network (which prevents molecular orientation), it can be anticipated that the similar effects might be achieved by crosslinking of high density polyethylene. In that case, tedious processing via sintering and machining could be avoided by simple conventional processes like injection moulding or extrusion.

Another possibility, which might affect performance of UHMW-PE in applications where multidirectional motion is required, could be an incorporation of branches in UHMW-PE. The branched systems would be more difficult to orient and therefore more resistant to the undesirable orientational softening. In this case irradiation step could be overcome which makes the whole process much easier and cheaper.

Though the incomplete fusion of the powder particles has been often referred to as one of the possible reasons for insufficient lifetime of the hip joint, the results presented in this thesis suggest that the fusion of the particles (having dimensions 50-200 μm) does not lead to substantial improvement of multidirectional wear resistance of UHMW-PE. If one assumes that the wear in such multidirectional kinematics is governed on the molecular level, it can be easily anticipated that fusion of powder particles having dimensions of 50-100 μm would not affect wear resistance of this material. It should be, however, mentioned that the powder grade used in this study (laboratory Ziegler-Natta grade) possesses molecular weight much lower ($M_w=3.6 \cdot 10^6 \text{ g mol}^{-1}$) than conventionally used grades ($M_w \sim 6 \cdot 10^6 \text{ g mol}^{-1}$). This might affect the final results of the wear measurements obtained in Chapter 6.

In the case of *knee joint*, completely different wear mechanism causes a failure of a tibial plateau of UHMW-PE. In this case the material is subjected to a cyclic loading which ultimately leads to macroscopic failure by delamination and pitting. If fusion defects are considered as internal defects within the material it can be anticipated that they will highly affect the ultimate fatigue resistance of the material. It has been shown in Chapter 6, that a fully fused material exhibits superior fatigue resistance, where expectations of realising the intrinsic properties anticipated for high molar mass materials, become feasible. This makes the fused UHMW-PE products the best alternative for the applications in which the resistance to cyclic loading is required.

References

1. Li, S.; Burstein, A.H. *J. Bone Joint Surg.* **1994**, *76A*, 1080
2. Kurtz, S.M.; Muratoglu, O.K.; Evans, M.; Edidin, A.A. *Biomaterials* **1999**, *20*, 1659
3. Barham, P.; Sadler, D.M. *Polymer* **1991**, *32*, 393
4. Wang, A.; Essner, A.; Polineni, V.K.; Stark, C.; Dumbleton, J.H. *Tribology Int.* **1998**, *31*, 17
5. McKellop, H.; Shen, F.; Lu, B.; Campbell, P.; Salovey, R. *J. Orth. Res.* **1999**, *17*, 157
6. Bajaria, S.H.; Bellare, A. *Medical Plastics and Biomaterials Magazine*, **1998**
(<http://www.devicelink.com/mpb>)

Appendix 1

Determination of Crystallite Size of Polymers from WAXS

A1.1 Theory

For relatively perfect crystalline particles the mean crystallite size can be determined with the familiar Scherrer equation^{1,2}:

$$L_{hkl} = \frac{K \cdot \lambda}{\beta_0 \cdot \cos\Theta}, \quad (\text{A1.1})$$

where L_{hkl} is the mean dimension of the crystallites perpendicular to the planes (hkl), β_0 is the integral width of the pure reflection profile in radians and K is a constant. This equation has been often used in literature for determination of the crystal size in semi crystalline polymers. However due to prevalence of lattice distortions in semi-crystalline materials, which also contribute to broadening of the reflections, such numerical results are rather unreliable. It is therefore necessary to separate two contributions, crystal size and lattice distortions, in evaluation of the line width of X-ray pattern in order to assess precise and reliable values for the mean crystal size of polymeric systems. Evaluation method of Wilke et al.^{3,4,5} which is based on concept of paracrystal⁶ allows this separation and it has been used for evaluation of the data presented in this work.

In this treatment integral width of reflection is given as:

$$\delta\beta_{hkl} = \delta\beta_{hkl}(S^2) \oplus \delta\beta_{hkl}(Z) \quad (\text{A1.2})$$

where $\delta\beta_{hkl}(S^2)$ indicates the reflection broadening from the finite crystallite size and $\delta\beta_{hkl}(Z)$ the reflection broadening from the lattice distortions.

The mean shape of crystallites is represented by ellipsoid whose principal axes are of reciprocal length³. For our purpose this is quite good approximation if we assume that nascent powder possesses rather irregularly stacked prismatic crystals, which once rotated three dimensionally in different directions lead to the mean shape of the ellipsoid. For the orthorhombic crystals the principal axis \bar{D}_3 is parallel to the crystallographic axis c (the chain direction), whereas the \bar{D}_1 and \bar{D}_2 are rotated for angle ϕ between the \bar{D}_1 and the [100] reflection as shown in Figure 1.

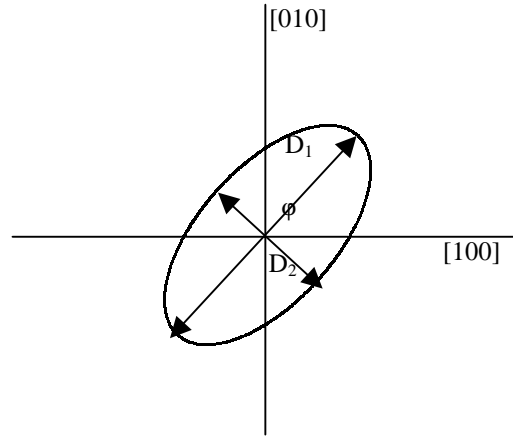


Figure A1. Shape ellipsoid (sectional drawing of the $a - b$ plane); according ref. 4

For powder sample the average size of the crystallite contributes to the integral width of a reflection hkl with³:

$$\delta\beta_{hkl}(S^2) = \frac{2}{\overline{D_{hkl}} + \overline{D_{\bar{h}kl}}} = \frac{1}{\overline{D_{\{hkl\}}}} \quad (\text{A1.3})$$

with $\overline{D_{hkl}}$ average crystallite size perpendicular to the net plane (hkl) . From this equation reciprocal of the integral width $\delta\beta_{hkl}(S^2)$ of a line profile hkl does not in general yield the average crystallite size perpendicular to the net plane (hkl) but the average over both directions hkl and $\bar{h}kl$.

Contribution of the paracrystalline distortions to the integral width of the reflection (having order m) increases with the square of the reflection order⁷:

$$\delta\beta_{hkl}(Z) = \frac{\pi^2 g_s^2}{d_{\bar{h}kl}} \cdot m^2 \quad (\text{A1.4})$$

where

$$g_s^2 = \frac{\sum_{i=1}^3 \sum_{k=1}^3 \hat{h}_i^2 \cdot \frac{\hat{h}_k}{a_k} \cdot g_{ik}^2}{\sum_{i=1}^3 \frac{\hat{h}_i^2}{a_k}} \quad (\text{A1.5})$$

is the distortion parameter with the relative fluctuations g_{ik}^2 of the components of the cell edge vectors \mathbf{a}_k in direction i ⁶.

$$g_{ik}^2 = \frac{\Delta_k^2 x_i}{a_k} \quad (\text{A1.6})$$

$d_{\widehat{hkl}}$ is the net plane spacing with Miller indices without common measure ($h = m \cdot \widehat{h}_i$; $i=h,k,l$), a_k is the lattice constant of the unit cell, $\Delta_{x_k}^2$ is the mean square fluctuation of the cell edge vector a_k in direction x_k (Figure A2).

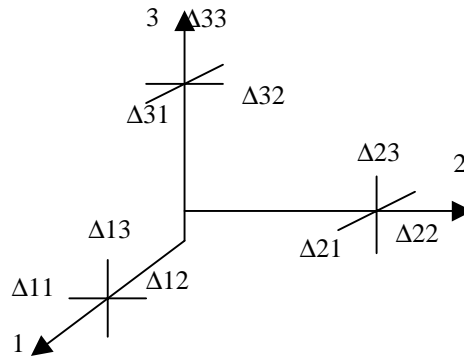


Figure A2. *The relative fluctuations of the lattice cell vectors*

Taking both contributions (eq. A1.3 and eq. A1.4) into account it is possible to express the integral width as follows:

$$\delta\beta_{hkl} = \frac{1}{D_{\{hkl\}}} + \frac{\pi^2 g_s^2}{d_{\widehat{hkl}}} \cdot m^2 \quad (\text{A1.7})$$

A1.2 Data evaluation

The width of the reflections obtained from the raw data using the fit program Grams is influenced by four parameters which have to be taken into account before determining the precise value for the mean crystal size. The experimentally obtained values for the peak width can be expressed as follows⁵:

$$\delta\beta_{\text{exp}} = \delta\beta_S \oplus \delta\beta_Z \oplus \delta\beta_A \oplus \delta\beta_D = \delta\beta_{hkl} \oplus \delta\beta_A \oplus \delta\beta_D \quad (\text{A1.8})$$

$\delta\beta_S$ and $\delta\beta_Z$ refer to reflection broadening caused by the crystal size and lattice distortions as discussed above (eq. A1.3 and eq. A1.4). $\delta\beta_A$ is line broadening component which is caused by apparatus and it includes lattice distortions as well as particle size deviations of the monochromator. However by the good adjustment of Guinier camera and monochromator this influence is rather negligible in comparison with the influence of sample thickness to line width ($\delta\beta_D$). Sample thickness has rather big influence on line broadening and it depends on scattering angle (θ) as well as incident angle of the beam to the sample (ψ). Influence of the sample thickness to the width of the reflection peak is given by the following eq.

$$\delta\beta_D = \frac{2 \cdot (D + \Delta D)}{\sin(2\psi) + (\cos(2\psi) + 1) \cdot \cot(2\Theta)} \quad (\text{A1.9})$$

This equation contains correction ΔD which takes into account that the sample is placed tangential to the focus circle and not bended. This value is dependent on diameter of the film storage ring as well as opening angle of the monocromator to the sample (ϵ).

$$\Delta D = 2r \sin^2\left(\frac{\epsilon}{2}\right) \quad (\text{A1.10})$$

The camera used in this study has diameter 100.3mm and ϵ is 3.5° which means that $\Delta D=0.093$.

For the angle of the incident beam $\Psi=45$

$$\delta\beta_{\text{hkl,exp}} = \sqrt{\delta\beta_{\text{exp}}^2 - \delta\beta_D^2} = \sqrt{\delta\beta_{\text{exp}}^2 - \left(\frac{2 \cdot (D + \Delta D)}{1 + \cot(2\Theta)}\right)^2} \quad (\text{A1.11})$$

This integral width ($\delta\beta_{\text{hkl,exp}}$) is originally given in “film millimetres”. In order to convert this value in the angle (degrees) correction for camera resolution has to be applied ($\Delta\Theta=1^\circ$ is 3.5 mm on the film strip). Finally the angle values can be converted into scattering number given in nm^{-1} by applying the differential form of Bragg eq.

$$\delta\beta_{\text{hkl,exp}}(b) = \frac{2 \cdot \cos \Theta}{\lambda} \cdot \delta\beta_{\text{hkl,exp}}(\Theta) \quad [\text{nm}^{-1}] \quad (\text{A1.12})$$

After obtaining line width value which only consists of two contributions, crystal size and lattice distortions, $\delta\beta_{\text{hkl,exp}}(b)$ has been plotted against m^2 (according to eq. A1.6).

Further calculations have been performed by fitting the experimental results by hand until the best fit has been obtained.

References

1. Scherrer, P. *Goettinger Nachrichten* **1918**, 2, 98
2. Alexander, L. E., *X-ray Diffraction Methods in Polymer Science*, Willey-Interscience: New York, **1969**
3. Wilke, W.; Martis, K.W. *Colloid Polym. Sci.* **1974**, 252, 718
4. Bodor, G.; Gall, S.; Haeberle, K.D.; Lode, U., Wilke, W. *J. Polym. Sci: Part B: Polym. Phys. Edn.* **1996**, 34, 485
5. Gerum, W. *Ph.D. thesis*, University of Ulm, **1996**
6. Hoseman, R.; Bagchi, S.N. *Direct Analysis of Diffraction by Matter*, North Holland: Amsterdam, **1962**, p.239
7. Wilke, W.; Vogel, V.; Hosemann, R. *Colloid Polym. Sci.* **1970**, 237, 317

Appendix 2

Temperature Modulated Differential Scanning Calorimetry

A2.1 Introduction

Calorimetry offers the possibility to get information about processes taking place in materials if heat is exchanged with the surroundings. Conventional differential scanning calorimetry (DSC) measures the heat flow rate into a sample on heating it at a given rate¹:

$$\Phi(T, t) = C_p(T) \frac{dT}{dt} + \Phi^{\text{ex.}}(T, t) \quad (\text{A2.1})$$

The first term on the right side characterises the heat flow connected with the heat capacity of the sample. It is usually referred to static heat capacity and it is always greater than zero. The separation of the static heat capacity from the total signal is rather straightforward. Due to the fact that C_p does not change very much with temperature, this contribution can be approximated by a straight line (the baseline), which can easily be subtracted from the total signal. The second term, the excess heat flow rate ($\Phi^{\text{ex.}}$), contains all heat flow from processes possibly occurring in the sample (melting, crystallisation, chemical reactions etc.). Such processes are usually combined with enthalpy changes which require the exchange of “latent heat” with the surroundings. If there are different processes occurring in the sample at the same time, the DSC measures the **net** heat flow rate of all processes. That means that if for example exothermic and endothermic processes (e.g. crystallisation and melting) occur in the same moment they can not be visible in the measured curve which in that case shows heat flow rate about zero.

The method of temperature-modulated DSC (TMDSC) offers the possibility to separate time dependent processes (with a non-zero complex excess heat capacity) from static heat capacity and latent heat signals which are time-independent but very fast compared to the time scale of modulation.

A2.2 The TMDSC method

TMDSC method uses modification of the DSC by (small) sinusoidal (or other periodic) term having amplitude T_A and angular frequency ω^2 . In our set-up a standard Perkin Elmer DSC-7 modified by a precision function generator was used to enable a sinusoidal temperature modulation:

$$T(t) = T_0 + \beta_0 t + T_A \sin(\omega t) \quad (\text{A2.2})$$

with a certain “underlying” heating rate β_0 , a temperature amplitude T_A and the angular frequency, $\omega = 2\pi f$ (f frequency).

The measured (modulated) heat flow signal $\Phi(t)$ consists of underlying ($\Phi_0(t)$) and periodic ($\Phi_{\text{per}}(t)$) part. The “underlying” part $\Phi_0(t)$ is obtained by “gliding integration” over one period and represents the signal which is identical to the signal which would be obtained from conventional DSC under the same measuring conditions. The periodic part is obtained by subtracting the underlying signal from the measured one:

$$\Phi_{\text{per}}(t) = \Phi(t) - \Phi_0(t) \quad (\text{A2.3})$$

The periodic part, which can be written as follows

$$\Phi_{\text{per}}(t) = \Phi_A(t) \cdot \cos(\omega t + \varphi), \quad (\text{A2.3})$$

was evaluated further, using the mathematical method deduced from lock-in amplification techniques[3], in order to get the amplitude Φ_A and the phase shift φ (relative to the temperature change) of that function.

From the amplitude Φ_A the magnitude (modulus, absolute value) of the apparent (related to the modulation) complex heat capacity could be obtained:

$$|C_p^*| = \frac{\Phi_A}{(T_A \cdot \omega)}, \quad (\text{A2.4})$$

which together with the phase φ reads:

$$C_p^*(\omega) = |C_p^*| \cdot e^{i\varphi} \quad (\text{A2.5})$$

*[Remark: Complex quantities are marked with a *, whereas the real valued magnitude (absolute value) is referred without the upper star.]*

The phase of the complex heat capacity is disregarded at this point, because the precise calibration of this quantity makes still problems.

The magnitude $|C_p^*|$ of the apparent heat capacity can again be considered to have two components:

$$|C_p(T, t)| = c_p(T) \cdot m + |C_p^{\text{ex}}(T, t)| \quad (\text{A2.6})$$

The first term on the right side, is related to the conventional (static) specific heat capacity $c_p(T)$ (> 0) of the sample which always causes a heat flow in phase with the temperature change dT/dt . The excess heat capacity ($C_p^{\text{ex}}(T, t)$), contains the heat flow from all processes

which react significantly on the small temperature changes of the modulation. Such processes are normally time dependent as well. There is a non-zero contribution to the magnitude only if the time constant is not too slow compared to the time scale of the modulation (the period). If the time constant is within the same order of magnitude, the heat flow connected with the excess heat capacity is shifted in phase which causes a non-zero imaginary part of the (complex) heat capacity.

The apparent heat capacity determined from the modulated part of the signal is also called “reversing heat capacity”, because it is determined from that part of the heat flow signal which is caused by the periodical changing (reversing) temperature. *[Remark: the term “reversing” must not be mixed up with “reversible” in the thermodynamic sense, in fact the reversing heat capacity contains in its excess part often irreversible components.]*

It should be emphasised that the excess heat capacity from Eq. A2.6 does not contain all of $\Phi^{\text{ex}}(T,t)$ from Eq. A1.1 but only a certain fraction related to the changes with temperature modulation having the proper time constant. The fraction may change if we change the period (frequency) of the experiment [Remark: A time dependent apparent heat capacity is equivalent to a frequency dependence in Fourier space.] The contribution from processes with no or only very weak temperature dependence to $\Phi^{\text{ex}}(T,t)$ is found in the underlying signal (for instance from processes like crystallisation or chemical reactions). Unfortunately the separation of the contributions into temperature and time dependent components is neither complete nor linear (additive) and depends, in addition, on the period (frequency) used in the experiment.

Generally the deconvolution of the excess heat flow into the different time and temperature dependent processes is a tricky and not so easy task. However, the method of TMDSC offers the possibility to separate processes with different temperature and time dependence from one another and determine characteristic quantities (like the time constant) from their frequency dependence. The evaluation of the TMDSC measurements done with nascent UHMMPE may serve as an example.

References

1. Höhne, G.W.H.; Hemminger, W.; Flammersheim, H.J. *Differential Scanning Calorimetry: An Introduction for Practitioners*, Springer: Berlin, **1996**
2. Wunderlich, B. et al. *ATHAS databank*, <http://web.utk.edu/~athas>

Samenvatting

Eigenschappen van polymere materialen hangen niet alleen af van de chemische samenstelling maar ook van de structuur en morfologie ontwikkeling tijdens de verwerking. Daarnaast zijn polymeren met intrinsiek goede eigenschappen soms moeilijk bruikbaar door hun slechte verwerkbaarheid. Een karakteristiek voorbeeld van zo'n polymeer is Ultra Hoog Moleculair Polyetheen (UHMW-PE), een lineair polyetheen met een hoog moleculair gewicht (vanaf $3 \cdot 10^3$ kg/mol). Het hoge moleculair gewicht geeft het polymeer uitstekende intrinsieke mechanische eigenschappen, zoals een extreme (specifieke) sterkte en stijfheid in high performance vezels, maar ook een goede slijtage- en vermoeiingsbestendigheid in de ongeoriënteerde toestand. Deze laatste eigenschappen maken UHMW-PE geschikt voor veeleisende toepassingen zoals lageroppervlakken in heup- en knieprothesen. In deze kunstgewrichten wordt UHMW-PE gebruikt als inlegstuk tussen een metaal of keramisch oppervlak en het menselijk bot. De levensduur van het gewricht is echter beperkt en in de meeste gevallen bezwijkt het UHMW-PE onderdeel.

Dit probleem wordt gedeeltelijk veroorzaakt doordat de hoge moleculaire massa van het polymeer een hoge smeltviscositeit en lange reptatietijden impliceert, hetgeen het materiaal moeilijk verwerkbaar maakt via conventionele processen. UHMW-PE wordt voor deze toepassingen eerst geperst en vervolgens gesinterd (door de hoge viscositeit zijn andere verwerkingsmethoden onmogelijk) tot een soort halffabrikaat dat later machinaal wordt bewerkt via draaien en frezen tot de uiteindelijk gewenste vorm. Tijdens sinteren kunnen ketens in de smelt slecht van het ene poederdeel naar het andere migreren door hun extreem lange relaxietijd en bevat het eindproduct dus nog resten van de oorspronkelijke poederdeeltjes. Deze korrelgrenzen worden in het algemeen beschouwd als een van de belangrijkste redenen voor een onvoldoende levensduur van de polyetheencomponenten in kunstgewrichten. Gezien het feit dat wereldwijd ongeveer 1 miljoen UHMW-PE componenten geïmplanteerd worden per jaar, lijkt het belangrijk nieuwe routes te exploreren voor het verwerken van UHMW-PE poeder tot producten met betere eigenschappen.

In dit proefschrift wordt zo'n nieuwe route ontwikkeld, gebruikmakend van het merkwaardige fenomeen "ketenexplosie" dat plaatsvindt tijdens het opsmelten van *gedisentangelde* ("ontwarde"), gevouwen-ketenkristallen. Ketenexplosie gaat gepaard met een plotselinge toename van de gyrationstraal van de moleculen en kan helpen een volledige

fusie over de oorspronkelijke korrelgrenzen te bereiken. De enige voorwaarde om gebruik te kunnen maken van dit interessante verschijnsel is een volledig gedisentangelde staat vóór opsmelten.

Vermindering van het aantal entanglements in hoog moleculaire polymeren kan direkt in de reaktor worden bereikt door een synthesetemperatuur te kiezen die lager is dan de kristallisatietemperatuur in het polymerisatiemedium. Hierdoor kunnen ketens niet de nagestreefde *random coil* configuratie innemen, aangezien ze direkt na ontstaan moeten kristalliseren, hetgeen leidt tot een unieke morfologie in het *nascent* poeder. Dit wordt in dit proefschrift gedetailleerd onderzocht teneinde de ontstane morfologie en de karakteristieke structuren in deze *nascent* poeders te ontrafelen, als functie van de synthesetemperatuur en het type katalysator. Momenteel worden de meeste commerciële UHMW-PE grades gemaakt met Ziegler-Natta katalysatoren, die niet in staat zijn een ontwarde morfologie op te leveren, doordat de actieve plaatsen op het katalysatoroppervak te dicht bij elkaar liggen (gewenst ook vanwege hoge produktiesnelheden). Willen we deze (commerciële) polymeren effectief sinteren via het “*chain explosion*” mechanisme, dan dienen ze eerst te worden ontward. Een mogelijkheid daartoe is gebruik te maken van de toegenomen ketenmobiliteit in de hexagonale fase (die voor polyethyleen thermodynamisch stabiel is bij drukken > 4000 bar en temperaturen > 250 °C). Door deze hoge mobiliteit in de hexagonale kunnen kristallen groeien (verdikken) door ketens uit de omgeving te trekken, hetgeen gepaard gaat met ontwarren: disentangling. Om dit te onderzoeken zijn de fase-transformaties van oplossingsgekristalliseerd polyethyleen onder hoge druk en hoge temperatuur onderzocht met behulp van in-situ WAXS experimenten bij de ESRF (European Synchrotron Radiation Facilities) in Grenoble. Gebleken is dat de stabiliteit van de onderzochte fases afhangt van de kristal grootte en, door een geschikte keuze van de uitgangsmorfologie, bleek het mogelijk een stabiele hexagonale fase te bereiken bij drukken van de orde van grootte van 1000 bar, een waarde die binnen het bereik van verwerkingsprocessen komt.

Vervolgens werd onderzocht of de tussenkomst van de hexagonale fase, bij een druk die veel lager is dan het evenwichts-triple-punt, het sintergedrag van UHMW-PE positief kon beïnvloeden. Daartoe werden de fase-transformaties tijdens het proces gevolgd met in-situ Raman spectroscopie en dit bleek een uitermate geschikte en krachtige methode. Experimenten met verschillende monsters toonden aan dat, afhankelijk van de initiële entanglementdichtheid, kortere of langere verblijftijden in de hexagonale fase noodzakelijk waren om uiteindelijk een volledige fusie over de korrelgrenzen heen te bereiken. In dit nieuwe proces wordt de hexagonale fase dus gebruikt om UHMW-PE zonder tussenkomst van een oplosmiddel in de vaste, maar mobiele, fase te disentanglen om, vervolgens, gebruikmakend van ketenexplosie bij opsmelten tot volledige fusie te komen tijdens het

sinterproces. Nog interessanter bleek dat, ook zonder tussenkomst van een verwerkingsstap in de hexagonale fase, *volledig* gedisentangeld poeder kan worden verkregen door optimalisatie van de polymerisatiecondities in de reaktor, specifiek voor dit doel, en gebruik te maken van *single-side* metalloceen katalysatoren, met maar één actieve plaats op het katoppervlak. Bij deze katalysatoren groeien nieuwe ketens, tijdens polymerisatie, zover van elkaar, dat ze elkaar niet *kunnen* ontmoeten. Het bleek dat dit soort nascent poeders, zonder verdere tussenkomst van de hexagonale fase, volledig konden fuseren tijdens het sinterproces via het ketenexplosieproces tijdens opsmelten.

De nieuwe verwerkingsroute voor UHMW-PE is opgeschaald. De daarmee verkregen korrelgrensvrije produkten zijn getest op mechanische eigenschappen met de nadruk op slijtage en vermoeiingsgedrag. Vooral in het laatste, het vermoeiingsgedrag, vertoonde het volledig gefuseerde materiaal *superieure* eigenschappen ten opzichte van de standaard materialen die tot nu toe worden gebruikt (gecrosslinkt of niet). In het slijtageonderzoek bleek het materiaal beter dan het standaardmateriaal, waarin nog altijd korrelgrenzen aanwezig zijn, maar scoorde het duidelijk slechter dan het gecrosslinkte standaardmateriaal. Mogelijke redenen hiervoor worden aangegeven.

Acknowledgements

Before ending this thesis I would like to dedicate the last two pages to all people who directly or indirectly contributed to this work and its completion.

First, I would like to thank my first promotor prof.dr. P.J. Lemstra for giving me the opportunity to perform my Ph.D. in his group. His support and engagement in the project contributed to its realisation.

Secondly, I would like to thank my coach dr. S. Rastogi with whom I worked and discussed the subject on a daily basis. Thank you, Sanjay, for your enthusiasm, which surely worked contagious and helped in transforming “downs” into “ups”.

Further, I would also like to thank my second promotor prof.dr.ir. H.E.H. Meijer for his interest in the subject and for the time he spent in correcting articles in my thesis as well as writing the Dutch version of the summary.

Next to my promotors and co-promotor, I would like to acknowledge the other two members of the reading committee, dr. E. Nies and prof.dr. J. Vancso, who read this thesis in its initial version and whose comments helped me in bringing it to its final stage.

My involvement in this project started with extensive measuring times in Grenoble, in the European Synchrotron Radiation Facilities, at beamline ID2/BL11, where thanks to the enthusiastic help of beamline scientists (Ann Terry and Gavin Vaughan), we managed to generate huge amount of data which helped further developments in this project. Here, I would also like to thank all the SKT members who lost their nights in waiting for the hexagonal phase to appear. Sanjay, Tosca, Ankur, Frank, Hans and Anne thank you all.

The work presented in this thesis has been performed in close collaboration with DSM Research. I would like to thank dr. Martin Jacobs for the first kilogram of special vergin powder. Further, I would like to acknowledge the groups of dr. F. Nooyen and dr. G. Evens who provided us with the powder grades that we intensively used in this study. I am also grateful to ir. J.M. Migchels for performing first preliminary tests on our samples. Dr. Rudy Deblieck I would like to thank for the extensive discussions related to mechanical properties of the novel materials.

Up-scaling of the processing route was not an easy task. However, thanks to the devoted involvement of the central workshop of the University (GTD) sufficiently big samples could be obtained. Bij deze, wil ik graag bedanken Meneer Theo Maas van GTD en zijn team voor hun inzet en geduld met het ontwerpen van onze cylinder. Ook wil ik hen bedanken dat ze altijd tijd voor mij hadden om alle reparaties uit te voeren. Sorry dat alles “gisteren” klaar moest zijn.

Meneer Ceelen van de Faculteit Bouwkunde wil ik bedanken voor het ter beschikking stellen van zijn pers.

Extensive wear measurements relevant for applications of UHMW-PE in the hip joints were performed in AO Research Institute in Davos (Switzerland). Here, I would like to thank dr. M. Wimmer for setting up a one year project which involved a detailed wear study of grain boundary free materials. I would like to express my thanks to his team of students (Dirk, Artelt, Katrin Engel and Volker Hausam) and technical staff (Christoph Sprecher) for performing the measurements and processing the obtained data. This was an immense piece of work.

Further, I would like to thank dr. Leon Govaert from the Faculty of Mechanical Engineering for helping me with the fatigue measurements.

The morphological studies of nascent powders were highly enriched by close collaboration with prof. G.W.H. Höhne. Thank you very much for your help, understanding and support.

All my colleagues from SKT, I would like to thank for providing a nice and inspiring atmosphere to work in. Some of you I would like to address separately. Tosca, dank voor jouw vriendschap gedurende de vier jaren van onze promotie. Je was er altijd, van het begin tot het einde. Jouw gevoel voor realiteit zorgde voor een goede balans met mijn zuidelijk temperament. Ankur and Tilo it was really fun sharing the room with you. Michael and Peter bedankt voor de gezelligheid. Ik kon altijd op jullie rekenen. Pauline en Anne bedankt voor jullie hulp met microscopie en interesse in het onderwerp.

Studenten Juul Cuijpers, Mark van de Mee en Bob van de Gender wil ik bedanken voor hun inzet in dit project.

Ik wil ook graag alle vrienden bedanken voor hun belangstelling en steun. Soms was het moeilijk te begrijpen dat ik zo veel uren aan het werk kon besteden maar nu kunnen wij samen het resultaat vieren. Ik beloof dat ik vanaf nu vaker ga bellen.

Takoder bih se zeljela zahvaliti svim mojim hrvatskim prijateljima na razumijevanju i podrsci koju ste mi pruzili u ove cetiri godine. Obecajem, da cu od sada cesce pisati i cesce dolaziti.

Mijn paranimfen wil ik bedanken voor het terzijde staan in de “langste” uur van mijn leven.

Een speciaal woord van dank gaat aan familie Corbeij die er altijd voor mij was. Jullie steun en hulp betekenden ontzettend veel voor mij.

Na kraju, zeljela bih se zahvaliti mojim roditeljima na podrsci koju su mi uvijek pruzali. Vas optimizam i vjera u mene zaslužni su za postojanje ove knjige.

René, jij was mijn steun en toeverlaat door de jaren heen. Door jou geduld, rust en betrokkenheid heb ik mijn promotie tot een goede einde kunnen brengen. Dit boek is net zo veel van jou als van mij.

Curriculum Vitae

The author of this thesis was born in Zagreb, Croatia, on 3rd January 1970. After completing secondary education she studied Chemical Engineering at the University of Zagreb, Croatia. In 1994 she completed her studies by obtaining the Bachelor degree. In 1995 she started the Master program at the University of Zagreb. The experimental part for her Master thesis she performed in Eindhoven Polymer Laboratories at the Eindhoven University of Technology, under supervision of prof.dr. P.J. Lemstra. The title of her Master thesis was “Processing of UHMW-PE in the solid state”.

After obtaining her Master degree in 1997 she started the Ph.D. study within the same group. Her project concerning nascent morphology and processing of UHMW-PE was financially supported by Dutch Polymer Institute (DPI). During the last four years the author has completed five modules of the course “Registered Polymer Technologist“ (“Register Polymeerkundige”, RPK) organised by the “National Graduate School of Polymer Science and Technology” (“Polymeertechnologie Nederland”, PTN).

From November 2001, the author will join DSM Research in Geleen, The Netherlands.